UNIVERSITY OF OKLAHOMA
GRADUATE COLLEGE

MICROPHYSICAL STUDIES OF MELTING HAIL USING IN SITU AIRCRAFT MEASUREMENTS, CLOUD MODELING, AND POLARIMETRIC RADAR DATA

A THESIS
SUBMITTED TO THE GRADUATE FACULTY
in partial fulfillment of the requirements for the
Degree of
MASTER OF SCIENCE

by SAVANNAH J SOUTHWARD
Norman, Oklahoma
2026

Downloaded from SHAREOK. Persistent Handle URL: https://hdl.handle.net/11244/342911

MICROPHYSICAL STUDIES OF MELTING HAIL USING IN SITU AIRCRAFT MEASUREMENTS, CLOUD MODELING, AND POLARIMETRIC RADAR DATA

A THESIS APPROVED FOR THE
SCHOOL OF METEOROLOGY

BY THE COMMITTEE CONSISTING OF

Dr. David Bodine (Chair)

Dr. Alexander Ryzhkov (Co-Chair)

Dr. Jacob Carlin

Dr. Zachary Lebo

Dr. Greg McFarquhar

©Copyright by SAVANNAH J SOUTHWARD 2026

All Rights Reserved.

Acknowledgments

This research would not have been possible without the support of the National Science Foundation. I extend my sincerest gratitude towards my advisor, Dr. Alexander Ryzhkov, for his guidance, patience, and wealth of knowledge he has provided me. Furthermore, I would also like to thank Dr. Jacob Carlin for his efforts in aiding not only my understanding of not only the model he created, but also furthering my understanding of this complex science. Both of these individuals excelled in providing unwavering support that has challenged me to grow as a young scientist and gain confidence in my abilities.

I also would like to extend thanks to Dr. Andrew Heymsfield, Dr. Aaron Bansemer, and John Krause whose efforts alongside this work fueled discussions, clarifications, and new avenues to travel down. Their expertise and willingness to share their knowledge have been greatly appreciated.

Before I took on this research, I will admit that I had not truly dove into this realm of meteorology and with that came many days of reading relevant literature, drawing schematics, and dabbling with doubts of whether or not I was capable of doing this at all. Thankfully, on one hand, I had the support of my colleagues in the Doppler Radar and Remote Sensing Research team at CIWRO/NSSL, but I also had my parents, Hal and Vanita Southward, as well as my best friend in the whole word: My cat, Swayze. My family is my pillar, and without their endless love and support, I genuinely do not know where I would be. They have pushed me to always follow my heart and chase my dreams. Hence why I made that decision six years ago to move ten hours away from my home in Mississippi to study here at The University of Oklahoma.

It has been a long journey, but I am optimistic as to what the future holds. I look

forward to taking my meteorological toolbox into a career where I can serve others. My passion for this field starts with inspiration from the skies and is driven by a desire to protect people. And that is my why. If you read this far, thank you! Although, there are many more pages ahead...

Table of Contents

Acknowledgments iv

List of Tables viii

List of Figures ix

Abstract xii

1 Introduction 1
- 1.1 Background Literature 3
- 1.2 Observations of Hail and Hail Particle Size Distributions 11
  - 1.2.1 Uncertainty in Hail Particle Size Distributions 20
- 1.3 Modern Observational Studies of Hail Populations 22
- 1.4 Radar Observations and Hail Detection 25
  - 1.4.1 Polarimetric Radar Variables 28
  - 1.4.2 Derived Products for Hail Detection 41
- 1.5 Numerical Modeling of Hail and Radar Signatures 43

2 T-28 Dataset and Observations 47
- 2.1 Dataset Reprocessing 49
- 2.2 T-28 PSDs 51
  - 2.2.1 Comparison with Previous PSD Parameterizations 54
- 2.3 Maximum Hail Size Estimation 56
  - 2.3.1 Fitted Maximum Diameter 56
  - 2.3.2 Maximum Observed Diameter 57
  - 2.3.3 Ulbrich Maximum Diameter 57

3 Description of 1D Cloud Model 60
- 3.1 Model Overview and Physical Basis 61
- 3.2 Numerical Framework 64
  - 3.2.1 Radar Forward Operator 65
  - 3.2.2 Representation of Hail Microphysics 67
  - 3.2.3 Model Assumptions and Limitations 70
- 3.3 Adaptations for the Present Study 73

3.3.1 Environmental Ingest Using ERA5 . . . 73
3.4 Simulation Configuration . . . 75

4 Analysis of the PSD Data and Simulated Profiles . . . 76
4.1 Simulated Radar Profiles from the Full T-28 Dataset . . . 77
4.1.1 Closer Examination of $D_{\max}$ Estimations . . . 84
4.2 Environmental Controls on Vertical Velocity . . . 87
4.3 Influence of Vertical Velocity Field Updates . . . 89
4.3.1 Implications for Polarimetric Rainfall Estimation . . . 93
4.4 Discussion . . . 98

5 29 June 2000 Case Study . . . 102
5.1 Case Overview . . . 102
5.2 Comparison of Simulated and Observed Radar Profiles . . . 104

6 Summary and Conclusions . . . 114
6.1 Closing Thoughts . . . 118

Reference List . . . 121

List of Tables

2.1 Summary of the T-28 hail dataset used in this study. 48

2.2 T-28 research flights included in this study. Flight start and end times correspond to the first and last observations contained within the processed dataset. 49

List of Figures

2.1 Photo of the T-28 Armored plane in 2001, courtesy of the Digital Library of South Dakota. 47

2.2 Examples of observed hail PSDs obtained from the reprocessed T-28 dataset. The observed particle concentrations are shown together with the corresponding exponential fits used to characterize each distribution. 52

2.3 (a) Mean observed hail particle size distribution (PSD) computed by averaging all 257 T-28 PSD observations. (b) Frequency of occurrence of each diameter bin, expressed as the percentage of observed PSDs containing at least one particle within that size class. 53

2.4 Comparison of exponential particle size distribution (PSD) parameters derived from the reprocessed T-28 dataset with the median N_0–Λ relationship reported by Heymsfield et al. (2023b). Open diamonds denote the fitted exponential intercept (N_0) and slope (Λ) parameters for individual PSDs obtained from the reprocessed observations. The blue line represents the median relationship, $N_0 = 125\Lambda^{3.68}$, derived from the original T-28 dataset, while the black line shows the median of the reprocessed observations computed within bins of Λ. 55

2.5 Visual representation of fitted $D_{\max}$ assessed from the raw PSDs in the T-28 Dataset. 57

2.6 Example of the maximum observed $D_{\max}$ value obtained from the raw PSDs of the T-28 Dataset. 58

2.7 Histograms of the fitted $D_{\max}$, maximum observed $D_{\max}$, and Ulbrich $D_{\max}$ estimates computed from all reprocessed T-28 PSDs included in this study. 59

3.1 Evolution of simulated microphysical variables (top) and corresponding polarimetric radar variables (bottom) during the melting of hail in a one-dimensional downdraft model. The left panel shows the evolution of ice mass content, liquid mass content, relative humidity with respect to water, and vertical velocity, while the right panel shows simulated Z_H, Z_{DR}, K_{DP}, and copolar correlation coefficient (ρ_{hv}). Figures adapted from *Carlin and Ryzhkov (2025)* with permission. 62

4.1 Mean vertical profiles of simulated horizontal reflectivity (Z_H), differential reflectivity (Z_{DR}), and specific differential phase (K_{DP}) after 600 s of model integration for all T-28 simulations. Profiles are shown for the three $D_{\max}$ estimation methods together with simulations performed with and without vertical velocity field updates. 78

4.2 Mean simulated vertical profiles of Z_H, Z_{DR}, and K_{DP} after 600 s together with the variability among all modeled T-28 simulations. Shaded regions denote the spread among individual simulations for each experiment. 82

4.3 Median simulated vertical profiles of horizontal reflectivity (Z_H), differential reflectivity (Z_{DR}), and specific differential phase (K_{DP}) after 600 s of model integration, grouped by 5-mm $D_{\max}$ bins for each $D_{\max}$ estimation method. Rows correspond to the fitted, maximum observed, and Ulbrich–Atlas $D_{\max}$ definitions, respectively. Solid curves denote median profiles within each bin, and shaded regions indicate the interquartile range across simulations. 84

4.4 Relationship between the environmental lapse rate and the maximum modeled downdraft velocity for all simulations. The dashed line denotes the least-squares linear regression. 88

4.5 Comparison of simulated radar profiles after 600 s for simulations performed with and without vertical velocity field updates for the 29 June 200 case. Profiles are shown for horizontal reflectivity (Z_H), differential reflectivity (Z_{DR}), and specific differential phase (K_{DP}). 90

4.6 Illustration of the influence of downdraft velocity on K_{DP}-based rainfall estimation. The solid curve represents the particle size distribution and corresponding K_{DP} in the absence of vertical air motion ($w = 0$ m s^{-1}), while the thin line represents the same particle flux in the presence of a 20 m s^{-1} downdraft. Figure provided by Dr. Alexander Ryzhkov in tandem with this research avenue. 96

4.7 Mean vertical profiles of (a) reflectivity (Z_H) specific differential phase (K_{DP}), and (c) differential reflectivity (Z_{DR}) for four hail-size classes derived from the WSR-88D hail climatology provided with permission by Krause et al. 99

5.1 S-Pol 1.5° elevation reflectivity PPI collected at 23:37:52Z on 29 June 2000 during the STEPS field campaign. The blue line denotes the T-28 aircraft flight transect through the storm, while the marker indicates the approximate aircraft sampling location used to initialize the numerical simulations for the comparison in this chapter. 104

5.2 Comparison between observed S-Pol vertical profiles and the simulated radar variables from the one-dimensional downburst model for the 29 June 2000 STEPS supercell. Colored curves represent four successive S-Pol volume scans spanning the aircraft sampling period, while the bold navy curve denotes the model simulation initialized using the T-28 PSD measured at 23:34:53 UTC. Profiles are shown for horizontal reflectivity (Z_H), differential reflectivity (Z_{DR}), and specific differential phase (K_{DP}). The comparison emphasizes the overall vertical structure and magnitude of the radar variables rather than exact point-by-point agreement. 105

Abstract

Hail is a highly destructive severe weather hazard, causing over $10 billion USD in insured losses annually. Beyond impacts to personal and commercial property, industries such as agriculture and aviation are also highly vulnerable to the damaging nature of hail. Advanced polarimetric weather radars provide the primary means for remotely detecting hail, estimating its size, and issuing timely warnings. However, existing methodologies for quantifying and forecasting large hail remain limited, particularly due to uncertainties in relating radar signatures to hail microphysics and storm dynamics.

This research leverages unique in situ observations from the armored T-28 aircraft, which has sampled hail-bearing storms across multiple field campaigns, to better constrain these relationships. Throughout this work, I investigate the sensitivity of polarimetric radar variables to hail size aloft and the role of downdraft dynamics in shaping radar signatures in hail-producing storms. Using a one-dimensional downdraft model with spectral bin microphysics initialized from T-28 aircraft observations, I examine how different definitions of maximum hail size (D_{max}) influence simulated vertical profiles of reflectivity (Z_H), differential reflectivity (Z_{DR}), and specific differential phase (K_{DP}).

The model framework enables controlled exploration of how microphysical assumptions and environmental conditions influence both radar presentation and downdraft evolution. By linking in situ measurements, modeling, and radar observations, this work aims to improve understanding of hail microphysics and support the development of more optimized radar-based hail detection and prediction methodologies.

The results demonstrate that uncertainty in the assumed maximum hail size prop-

agates directly into simulated polarimetric radar signatures. While the inclusion of modeled downdrafts produced measurable reductions in hydrometeor concentration and corresponding decreases in radar variables, these effects were secondary to the influence of the particle size distribution and environmental thermodynamic structure.

Comparison with S-Pol observations from the 29 June 2000 STEPS field campaign showed that the model successfully reproduced the primary characteristics of the observed vertical profiles of Z_H, Z_{DR}, and K_{DP}, providing confidence that the coupled aircraft-model-radar framework captures the dominant physical processes governing melting hail. These findings improve understanding of how particle size distribution uncertainty and vertical transport influence polarimetric radar observations and provide guidance for the continued development of radar-based hail detection and quantitative precipitation estimation algorithms.

Chapter 1

Introduction

Hail-producing thunderstorms are among the most destructive forms of severe weather, capable of producing widespread damage to property, agriculture, and even disruptions to aviation. The accurate detection and prediction of hail size is essential for issuing timely warnings and understanding storm severity. Central to this challenge is the need to better understand the microphysical evolution of hailstones as they fall through the atmosphere. As hail falls through a warmer column of air, it begins to melt. This process not only alters the hailstones' own characteristics but also profoundly affects the surrounding air and further influences storm dynamics (Ludlam, 1958; Mason, 1971). Melting hail cools and moistens the surrounding air, enhancing negative buoyancy that can contribute to damaging wet microbursts and ground-level hazards (Srivastava, 1987; Rasmussen and Heymsfield, 1987).

Dual-polarization radar provides information about hydrometeor size, shape, orientation, and phase, especially during melting (Doviak and Zrnić, 1993; Zrnić and Ryzhkov, 1999; Bringi and Chandrasekar, 2001; Ryzhkov and Zrnić, 2019). However, interpreting these radar signatures requires a deeper understanding of how hail particles evolve as they descend through varying thermodynamic profiles. By understanding the microphysical evolution of melting hail and its corresponding radar signatures, we can look towards improving severe storm forecasts and developing more reliable radar-based hail detection and sizing algorithms (Ortega et al., 2016). This motivates the integration of in situ aircraft observations, physics based modeling, and radar analysis

to explore the link between hail microphysics and radar-detectable signatures.

The overarching objective of this research is to use direct aircraft observations of hail particle size distributions (PSDs), one-dimensional bin-microphysics modeling, and polarimetric radar interpretation to better understand the connection between hail aloft and what we expect down at the surface. This work primarily focuses on investigating the sensitivity of simulated radar variables to different estimates of maximum hail size aloft. Additionally, I aim to better understand how downdraft velocities influence the radar presentation of hail and if downdraft intensity depend on environmental characteristics such as lapse rate and humidity.

The first point of research addresses an important ambiguity in hail studies: the maximum hail size within a measured particle size distribution (PSD) is not always known with certainty. One may define maximum hail size, or $D_{\max}$, as the largest observed particle bin. However, it can also be assessed as a fitted distribution cutoff, or through a relationship involving the slope parameter of an exponential hail PSD. These definitions may differ substantially, especially when the observed spectrum is sparse or when a few large particles appear in the tail of the distribution. Because reflectivity (Z_H) is strongly weighted toward the largest particles, these differences can alter simulated Z_H (Doviak and Zrnić, 1993; Bringi and Chandrasekar, 2001). Other polarimetric variables may respond differently. Differential Reflectivity (Z_{DR}) depends on relative horizontal and vertical scattering and is tied to shape, orientation, melting state, and composition (Zrnić and Ryzhkov, 1999; Bringi and Chandrasekar, 2001; Kumjian, 2013a). Specific Differential Phase (K_{DP}) is more closely related to the integrated differential phase contribution of populations of anisotropic hydrometeors and can be sensitive to concentrations of melting particles (Bringi and Chandrasekar, 2001; Ryzhkov et al., 2013a,b). Thus, comparing $D_{\max}$ definitions tests how uncertainty in the upper tail of the hail PSD propagates into radar observables.

The second point of research addresses the dynamical evolution of the particle population during descent. A downdraft changes the effective fall speed of hydrometeors relative to the ground and therefore changes the residence time of particles within a given layer. Through flux conservation, a stronger downward air motion can reduce the local number concentration for a given downward particle flux, particularly for smaller or medium-sized hydrometeors whose terminal velocities are comparable to the downdraft (Srivastava, 1987; Carlin and Ryzhkov, 2022). This effect has direct implications for K_{DP} and precipitation estimation because K_{DP} is concentration-sensitive. At the same time, downdraft strength is linked to environmental lapse rate, relative humidity, melting, evaporation, and precipitation loading. The 1D model utilized in this work provides a controlled framework for isolating these effects while retaining physically based microphysics.

This research seeks to clarify the physical pathways by which hail size distributions aloft affect radar signatures and how those signatures may be modified by descent, melting, and vertical motion. The findings are intended to inform future radar-based algorithms and model evaluation.

1.1 Background Literature

Hail is among the most complex forms of precipitation produced by convective storms. Unlike rainfall, which is generated primarily through liquid-phase collision and coalescence, hail formation requires the interaction of ice particles, supercooled liquid water, and sustained vertical motion within a mixed-phase cloud (Ludlam, 1958; Mason, 1971; Pruppacher and Klett, 1997). Therefore, the production of large hail cannot be understood from microphysics or storm dynamics alone. It requires favorable thermodynamic conditions, sufficient liquid water, strong and persistent vertical motions, along with

particle trajectories that allow embryos to remain within regions of growth long enough to become hailstones (Browning, 1964; Foote, 1984). Scientific understanding of these processes developed gradually, as observations moved from hailstones at the surface to radar studies of storm structure, aircraft penetrations of hail-bearing clouds, laboratory studies of freezing and melting, and numerical models capable of simulating hail growth and fallout.

Early scientific interest in hail was motivated by the striking physical character of hailstones themselves. Hailstones are often much larger than most atmospheric ice particles, and many contain alternating layers of transparent and opaque ice. These internal layers provided some of the earliest evidence that hailstones experience changing environmental conditions during their growth. Transparent layers are generally associated with wet growth, in which liquid water spreads across the particle surface before freezing, whereas opaque layers often indicate rapid freezing and the trapping of air bubbles. Even before the details of cloud microphysics were solidified, the internal structure of hailstones suggested that hail growth is not a single-step process. Rather, hailstones appear to record a sequence of environmental encounters as they move through a storm.

One of the earliest influential attempts to explain hail formation was offered by Wegener (1911). Wegener recognized a central dynamical problem in which large hailstones have substantial terminal fall speeds, so they should fall quickly out of a cloud unless supported by strong upward air motion. This insight connected hail growth to thunderstorm dynamics at a time when direct measurements of convective updrafts were not available. The basic idea remains correct. A growing hailstone must remain within regions of supercooled liquid water for a sufficient period of time, and strong vertical air motion is one mechanism that can prolong that residence time. However, later work showed that updraft strength by itself is not enough to explain hail size.

Wegener correctly identified the importance of sustained updrafts, but his conceptual framework could not explain why storms with apparently similar updraft strengths often produce dramatically different hail populations. Resolving this discrepancy required a more complete understanding of cloud microphysics, particularly the role of supercooled liquid water and particle growth history.

During the middle of the twentieth century, the emergence of cloud physics transformed hail research from a descriptive field into a quantitative one. Studies by Ludlam (1958), Mason (1971), Macklin (1963), and others established many thermodynamic and microphysical concepts still used in modern hail-growth theory. Ludlam (1958) distinguished between dry and wet hail growth according to whether collected supercooled water freezes completely upon impact. During dry growth, efficient heat removal allows rapid freezing, often producing relatively opaque, porous ice. During wet growth, collection exceeds the rate at which latent heat can be removed, leaving liquid water on the hailstone surface and producing denser, clearer ice. Because growth regime influences hailstone density, shape, liquid-water distribution, fall speed, and melting behavior, it also affects polarimetric radar scattering. A central advance was recognition of the importance of supercooled liquid water. In deep convective clouds, liquid water can persist at temperatures well below 0°C because droplets do not necessarily freeze immediately in the absence of efficient ice nuclei. When an ice particle or graupel embryo encounters these droplets, the droplets may freeze upon impact and contribute mass to the growing particle. This collection of supercooled droplets through riming and accretion is the foundation of hail growth.

Following classical cloud microphysical theory, the growth rate of a hailstone may be written conceptually as (Mason, 1971; Pruppacher and Klett, 1997)

$$\frac{dm}{dt} = E w_{\mathrm{L}} A v_{\mathrm{r}} \tag{1.1}$$

where E is the collection efficiency,w_L is liquid water content, A is the cross-sectional area, and v_r is the relative terminal velocity. This expression is simple, but it captures several ideas that recur throughout hail research. Growth is favored when liquid water content is large, when collection efficiency is high, when the particle has a large collection area, and when the particle remains in the growth region long enough for substantial accretion to occur.

Laboratory and theoretical studies during the same period refined the understanding of heat and mass transfer at the hailstone surface. Macklin (1963) quantified how droplets freeze on ice particles and how particle temperature evolves during accretion. Mason (1971) connected these processes to the broader thermodynamic environment of mixed-phase clouds. These studies made it possible to represent hail growth through energy-balance arguments rather than through purely qualitative descriptions. The surface of a growing hailstone can be viewed as a boundary where latent heat release, sensible heat transfer, evaporative or sublimative cooling, and conductive heat exchange must balance. In simplified form, the heat balance may be written conceptually as (Mason, 1971)

$$Q_{\mathrm{s}} + Q_{\mathrm{l}} + Q_{\mathrm{v}} + Q_{\mathrm{c}} = 0 \tag{1.2}$$

where the subscripts represent sensible (s), latent (l), ventilation (v), and conductive (c) heat exchanges.

This equation is not intended here as a complete predictive model, but it illustrates why hail growth is sensitive to environmental temperature, humidity, ventilation, and liquid water content. A hailstone in a cold, relatively dry environment may lose heat efficiently and grow in a dry regime, whereas a hailstone in a warmer and liquid-rich region may enter wet growth. These processes also influence melting once hailstones descend below the freezing level, linking growth aloft to subsequent fallout and radar

signatures. Although these studies established the physical principles governing hail growth, they largely described the evolution of an individual hailstone. They did not address how entire hail populations evolve within a storm or how variability among those populations might influence observations.

While cloud physicists were developing this microphysical framework, radar meteorologists were revealing the storm-scale structures that support hail growth. Early radar observations showed that hail-producing storms often contain intense Z_H cores and strong vertical development. The presence of high Z_H at altitudes well above the freezing level suggested that large particles were being supported aloft by vigorous updrafts. This finding reinforced the importance of storm dynamics and helped shift hail research away from isolated particle growth toward a coupled view of particles moving through organized convective storms.

Browning (1962) and Browning (1964) were especially influential in connecting hail growth to organized storm-scale airflow. Through radar analysis and conceptual modeling, Browning showed that severe convective storms possess organized flow structures capable of sustaining long-lived updrafts and transporting hydrometeors through different storm regions. This framework explained why storms with similar thermodynamic environments may produce substantially different hail characteristics as growth depends not only on buoyancy, but also on the organization of storm-scale airflow, the distribution of supercooled liquid water, and the trajectories followed by individual particles (Browning, 1964; Foote, 1984). Browning's conceptual model continues to serve as the foundation for modern interpretations of supercell structure and hail growth.

The recognition of organized storm-scale flow led naturally to the concept of hail embryo trajectories. A hail embryo may originate as a frozen drop, graupel particle, or small ice particle. Its subsequent growth depends on where it travels within the storm. If it passes quickly through a growth region and falls out, it may remain small. If it

is carried through regions of high liquid water content for an extended time, it may grow into large hail(Browning, 1964; Foote, 1984). Some conceptual models proposed that embryos may recycle through the updraft, experiencing multiple growth episodes before eventually falling out. This embryo-recycling concept became one of the most influential, yet heavily debated, ideas in the realm of hail research.

The National Hail Research Experiment (NHRE) and related field programs in the 1970s further advanced understanding by combining radar, aircraft, surface networks, and environmental observations (Foote, 1984). These programs demonstrated that hail production varies substantially within storms and among storms, even when large-scale environments appear broadly favorable. They also highlighted the importance of storm organization, updraft intensity, liquid water content, and particle trajectories. Hail was increasingly understood as a population-level problem rather than simply a question of how one stone grows. Storms contain distributions of embryos and hailstones, and the shape of that distribution reflects the integrated effects of microphysics and dynamics. Even so, the available observations remained relatively sparse. Radar documented storm structure, hailpads sampled hail after it reached the surface, and aircraft penetrations were necessarily limited in space and time. Quantifying the complete PSD within hail-producing storms therefore remained a major observational challenge.

Numerical modeling studies during the late twentieth century provided a way to investigate these sensitivities systematically. Early hail-growth models tracked particles through prescribed or simulated storm flows and calculated changes in mass as particles encountered varying liquid water contents and temperatures (Foote, 1984; Mason, 1971). These models showed that small changes in the assumed trajectory, liquid water distribution, or thermal structure can lead to large differences in final hail size. This sensitivity helps explain why hail forecasts remain difficult and why storms in seemingly similar environments can produce different hail outcomes.

At the same time, models revealed that hail is not a passive product of the storm environment. Hail growth and fallout can influence the storm through precipitation loading, melting, evaporation, and downdraft production. When hailstones descend into warmer air and melt, they consume latent heat and cool the surrounding air. Evaporation of meltwater or rain produced by shedding can further enhance cooling (Srivastava, 1987; Rasmussen and Heymsfield, 1987). These processes contribute to negative buoyancy and can help generate downdrafts or downbursts. Thus, hail microphysics can feed back into storm dynamics, especially in the lower portions of storms where melting and evaporation are active. The late twentieth- and early twenty-first-century view of hail growth therefore became increasingly integrated. Large hail requires favorable microphysical ingredients, including embryos and supercooled liquid water, but these ingredients must be embedded within a storm structure that provides appropriate trajectories and residence time. Environmental temperature and humidity influence both growth and melting. Particle density, shape, and liquid water fraction affect terminal velocity and radar scattering. Maximum hail size is therefore not controlled by any single variable. It is the outcome of a coupled system involving storm dynamics, microphysics, and thermodynamics.

Modern research has continued to refine this framework. High-resolution numerical simulations have challenged overly simple interpretations of embryo recycling, showing that trajectories can be highly variable and that some large hailstones may grow rapidly along relatively direct paths through intense liquid water regions (Brook et al., 2021; Fischer et al., 2025). Other studies have emphasized the role of storm-relative flow, updraft width, mesocyclone structure, and hydrometeor sorting in controlling hail growth. This has led to a more nuanced view in which recycling may be important in some storms but not necessarily universal. The production of giant hail may occur through multiple pathways depending on storm mode, environmental shear, liquid

water availability, and the spatial organization of growth regions.

Polarimetric radar studies have added another dimension to this evolving understanding by providing indirect observations of hydrometeor type, shape, and phase within storms (Zrnić and Ryzhkov, 1999; Bringi and Chandrasekar, 2001; Kumjian, 2013a,b). Radar signatures associated with hail growth, melting, and fallout have helped connect storm-scale structure to microphysical interpretation (Ryzhkov et al., 2013b; Ryzhkov and Zrnić, 2019). However, radar observations remain indirect. They do not measure hail size distributions directly, and the same radar signature can sometimes arise from different particle populations. The primary reasoning being that for ice particles and quasi spherical hail stones, the dual-polarization signatures go to zero, which leaves us with very few constraints for retrievals. This limitation has kept direct microphysical observations central to hail research.

One of the major lessons from more than a century of hail research is that progress depends on linking observations across scales. Surface reports document the hail that survives to the ground. Radar observations reveal storm structure and hydrometeor signatures aloft. Aircraft and in situ measurements provide direct samples of particle populations within storms. Numerical models connect these perspectives by simulating the evolution of hail under controlled physical assumptions (Ryzhkov et al., 2013a). The present state of hail science reflects the gradual integration of these approaches, but important gaps remain, particularly in connecting observed hail PSDs aloft to the radar signatures observed during descent.

These gaps motivate continued investigation of hail microphysics using direct observations and physically based modeling. The historical development of hail research shows that the field has repeatedly advanced when new observations made it possible to test previously conceptual ideas. Modern reanalysis of aircraft-based hail observations, combined with radar forward modeling and environmental data, provides a sim-

ilar opportunity (Field et al., 2019; Heymsfield et al., 2023b; Bansemer, 2022; Ryzhkov et al., 2011). It allows questions about hail size distributions, melting, downdraft development, and radar signatures to be addressed using observationally constrained microphysical inputs rather than purely idealized assumptions.

1.2 Observations of Hail and Hail Particle Size Distributions

A fundamental challenge in hail research is that the hail observed at the surface may differ substantially from the hail population that existed aloft. Once hailstones leave the primary growth region and begin descending through warmer portions of the atmosphere, they undergo melting, sublimation, fragmentation, and shedding. The extent of these modifications depends on environmental temperature, humidity, hailstone size, and residence time below the freezing level. Thus, measurements obtained at the surface provide information regarding the final stage of hail evolution rather than the conditions that existed during active growth.

Surface-Based Hail Observations

Historically speaking, most information regarding hail has originated from observations at the Earth's surface (Foote, 1984). Prior to the development of weather radar and specialized aircraft instrumentation, investigators relied primarily upon eyewitness reports, damage assessments, and direct measurements of hailstones collected following storms. These observations formed the foundation of early hail climatologies and provided the first systematic descriptions of hail occurrence across many regions of the world.

Surface hail reports remain one of the most widely used sources of hail information. In the United States, severe weather databases maintained by the National Weather Service contain thousands of hail reports submitted by trained spotters, emergency managers, law enforcement personnel, and members of the public. Similar reporting systems exist in many other countries. These datasets have been used extensively to investigate hail climatology, seasonal variability, geographic distributions of hail occurrence, and long-term trends in severe weather (Cintineo et al., 2012).

Although hail reports provide valuable information regarding hail occurrence, they possess important limitations. Reported hail sizes are often estimated visually using common reference objects such as coins, golf balls, baseballs, or softballs. Such estimates introduce uncertainty because different observers may assign different sizes to the same hailstone. Furthermore, reports tend to emphasize unusually large hail while providing relatively little information regarding the complete PSD present within a storm (Allen et al., 2015).

Reporting biases also influence the spatial distribution of hail observations. Storms occurring over urban areas typically generate more reports than storms affecting sparsely populated regions. Additionally, observational datasets may reflect population density as much as actual hail frequency. Allen et al. (2015) and Cintineo et al. (2012) have documented these biases and emphasized the need for caution when interpreting climatological hail datasets derived solely from public reports.

To address some of these limitations, researchers developed hailpad networks capable of providing more objective measurements of hail occurrence and size (Foote, 1984). Hailpads consist of soft recording surfaces designed to preserve impact marks produced by falling hailstones. By examining the size and distribution of these impact signatures, investigators can estimate hailstone size distributions and spatial patterns of hailfall across relatively large regions.

Hailpads played a central role in several major field programs, including the National Hail Research Experiment and the Alberta Hail Project (Foote, 1984). These networks provided valuable information regarding hail swaths, spatial variability, and storm-scale hail production. Compared to isolated point observations, hailpad networks offered a more comprehensive view of hailfall distribution and significantly improved understanding of the geographic variability associated with severe hailstorms.

Agricultural damage surveys have also contributed substantially to hail research (Changnon, 1999). Because hail frequently produces significant crop damage, agricultural observations have long been used to document hail occurrence and severity. These records provided some of the earliest large-scale datasets available for hail climatology and continue to serve as important indicators of hail impacts. More recently, insurance claims databases have emerged as an additional source of information regarding hail occurrence, particularly in regions where severe hail produces substantial economic losses (Allen et al., 2015).

Despite their value, all surface-based observing systems share a common limitation: they observe hail only after it has completed its descent through the atmosphere. Furthermore, they cannot directly characterize the hail populations responsible for radar signatures aloft or reveal the microphysical processes occurring within active growth regions. These limitations motivated the development of observational approaches capable of directly sampling hail-producing storms.

Aircraft Observations of Hail

Aircraft observations represented a major turning point in hail research because they provided the first opportunity to directly sample hydrometeor populations within convective storms. Unlike surface observations, which record hail after growth has ceased and melting has begun, aircraft measurements can observe particles while growth pro-

cesses are actively occurring. As a result, airborne observations have provided some of the most valuable information available regarding hail microphysics.

Early aircraft studies focused primarily on cloud structure, liquid water content, and thermodynamic conditions within convective storms. However, advances in instrumentation soon made it possible to directly measure cloud particle populations. The development of optical array probes during the latter half of the twentieth century revolutionized airborne cloud physics by enabling investigators to record images of individual hydrometeors encountered during flight (Knollenberg, 1970).

Optical array probes operate by measuring the shadow cast by a particle as it passes through a laser beam. The resulting images provide information regarding particle size and shape and can be used to construct PSDs. Instruments such as the Particle Measuring Systems, Inc. (PMS) Two-Dimensional Cloud (2D-C) and Two-Dimensional Precipitation (2D-P) probes became widely used in cloud physics research and contributed significantly to understanding precipitation microphysics.

Subsequent developments extended observational capabilities toward increasingly large particles. The High Volume Particle Spectrometer (HVPS) provided improved sampling of large hydrometeors and helped address limitations associated with earlier cloud probes. Because large hailstones occur at relatively low concentrations, obtaining representative measurements requires instruments capable of sampling large volumes of air. The HVPS represented an important advance in this regard and became a valuable tool for studying hail-producing storms (Lawson et al., 1993).

Aircraft observations offered several advantages over both surface observations and radar measurements (Field et al., 2019; Heymsfield et al., 2023b). Most importantly, they provided direct information regarding particle populations. Radar observations infer particle characteristics indirectly through electromagnetic scattering, whereas aircraft instruments directly sample the particles themselves. This distinction allows

airborne observations to provide critical constraints on PSDs, concentrations, and microphysical evolution.

Nevertheless, aircraft observations also face important challenges. Severe thunderstorms contain strong turbulence, intense precipitation, lightning, and large hailstones capable of damaging research aircraft. These hazards restrict the environments that can be safely sampled and limit the number of direct observations available. Furthermore, aircraft measurements provide information only along the flight path and therefore represent a relatively small portion of the overall storm.

Despite these limitations, airborne observations remain among the most valuable tools available for investigating hail microphysics (Field et al., 2019). Measurements obtained through aircraft field programs have provided direct evidence regarding particle growth processes, PSDs, and the microphysical characteristics of hail-producing storms. These observations have played a critical role in evaluating numerical models, interpreting radar signatures, and improving understanding of hail formation.

Perhaps most importantly, aircraft observations demonstrated that hail populations exhibit substantial variability both within and among storms (Heymsfield et al., 2023b). This realization motivated increasing attention toward the statistical characterization of hydrometeor populations through PSDs, which have become one of the most important frameworks for describing hail microphysics.

Particle Size Distributions

A central objective of observational cloud physics is the characterization of hydrometeor populations within clouds and precipitation systems. Because individual particles vary continuously in size, shape, density, and concentration, it is often impractical to describe a precipitation population solely through measurements of individual particles. Instead, investigators typically employ PSDs, which provide a statistical representation

of the number concentration of particles as a function of diameter. PSDs have become one of the most fundamental tools in cloud physics, precipitation research, radar meteorology, and numerical weather prediction because they provide a compact framework for describing complex hydrometeor populations (Ulbrich, 1983).

PSDs provide a statistical description of the number of hydrometeors present as a function of particle size and represent one of the most fundamental quantities in cloud and precipitation physics. Rather than describing an individual hydrometeor, a PSD characterizes the complete spectrum of particle sizes occupying a unit volume of air and therefore governs the bulk microphysical properties of a cloud or precipitation shaft. Quantities including number concentration, water content, radar reflectivity, precipitation rate, and sedimentation are all derived from moments of the PSD. Consequently, an accurate representation of the PSD is essential for both numerical cloud models and radar forward operators.

The PSD, denoted $N(D)$, describes the number concentration of hydrometeors as a function of particle diameter. Specifically, N(D)dD represents the number of particles per unit volume with diameters between D and $D + dD$. The total number concentration is obtained by integrating the PSD over all particle sizes,

$$N_T = \int_0^\infty N(D)\, dD. \tag{1.3}$$

More generally, many bulk microphysical quantities correspond to moments of the PSD,

$$M_n = \int_0^\infty D^n N(D)\, dD, \tag{1.4}$$

where the zeroth moment represents total number concentration, higher moments are related to particle mass and liquid or ice water content, and the sixth moment

is proportional to radar reflectivity in the Rayleigh scattering regime. Because different physical processes preferentially modify different portions of the PSD, the complete distribution contains substantially more information than any single characteristic particle size. PSDs are commonly represented using analytical functions that describe the variation in particle concentration with diameter. Among these, the gamma distribution provides one of the most flexible formulations because it allows the shape of the distribution to vary while retaining a relatively simple mathematical form. The gamma PSD is expressed as

$$N(D) = N_0 D^{\mu} e^{-\Lambda D}, \tag{1.5}$$

where $N(D)$ is the particle concentration per unit diameter interval at diameter D, N_0 is the intercept parameter, Λ is the slope parameter, and μ is the dimensionless shape parameter (Ulbrich, 1983). The intercept parameter controls the overall magnitude of the distribution, while the slope parameter determines the rate at which particle concentration decreases with increasing diameter. The shape parameter provides additional flexibility by allowing the distribution to deviate from a purely exponential form, improving the representation of observed hydrometeor populations that exhibit curvature on semi-logarithmic plots. Positive values of μ generally produce narrower distributions with a more pronounced modal diameter, whereas negative values produce broader distributions with relatively greater concentrations of small particles.

The exponential PSD introduced by Marshall and Palmer (1948) is obtained as the special case of Eq. 1.5 by setting the shape parameter equal to zero ($\mu = 0$), yielding

$$N(D) = N_0 e^{-\Lambda D}. \tag{1.6}$$

The exponential distribution has historically been one of the most widely used

PSD formulations because only two parameters are required to characterize the distribution. Although originally developed for rainfall, the exponential distribution has been applied extensively to graupel and hail because of its mathematical simplicity and computational efficiency in radar retrieval algorithms and numerical cloud models (Marshall and Palmer, 1948; Ulbrich, 1983; Bringi and Chandrasekar, 2001). However, observations frequently show that hail PSDs deviate from a purely exponential form, particularly for small and intermediate particle sizes. The additional degree of freedom provided by the gamma distribution often produces improved agreement with observed PSDs and has therefore become increasingly common in cloud microphysics studies. Analytical PSD parameters are estimated by fitting the selected distribution to discrete particle concentrations measured across a finite set of diameter bins. For an observed PSD consisting of concentrations $N_{\text{obs}}(D_i)$ at bin-center diameters D_i, the fitted parameters are commonly obtained by minimizing an objective function that measures the difference between the observed and analytical distributions. For a gamma PSD, a general least-squares objective may be written as

$$J(N_0, \Lambda, \mu) = \sum_{i=1}^{n} w_i \left[N_{\text{obs}}(D_i) - N_0 D_i^{\mu} \exp(-\Lambda D_i) \right]^2 , \tag{1.7}$$

where n is the number of diameter bins included in the fit and w_i is an optional weighting factor assigned to the ith bin (Ulbrich, 1983; Testud et al., 2001). The fitted values of N_0, Λ, and μ are those that minimize Eq. 1.7. For an exponential PSD, μ is fixed at zero, and only N_0 and Λ are optimized. Weighting may be applied to account for differences in sampling uncertainty among diameter bins or to prevent bins containing the largest concentrations from dominating the fitting procedure.

Because hydrometeor concentrations commonly span several orders of magnitude, PSDs may also be fitted in logarithmic space. In this approach, the fitting objective

can be expressed as

$$J_{\log}(N_0, \Lambda, \mu) = \sum_{i=1}^{n} w_i \left[\log N_{\text{obs}}(D_i) - \log N_{\text{fit}}(D_i)\right]^2, \tag{1.8}$$

where $N_{\text{fit}}(D_i)$ is the concentration predicted by the selected analytical distribution (Ulbrich, 1983). Logarithmic fitting reduces the influence of high-concentration bins and gives greater relative weight to the lower-concentration tail of the distribution. However, bins with zero observed particles cannot be represented directly in logarithmic space and must therefore be excluded, assigned a detection-limit value, or treated using an alternative statistical method. The resulting fitted parameters can depend on whether the fit is performed in linear or logarithmic concentration space, which diameter range is included, and how empty or poorly sampled bins are handled.

Alternative fitting approaches estimate PSD parameters from integral moments of the observed distribution. The kth moment of a PSD is defined as

$$M_k = \int_0^{\infty} D^k N(D)\, dD, \tag{1.9}$$

or, for discrete observations,

$$M_k \approx \sum_{i=1}^{n} D_i^k N_{\text{obs}}(D_i) \Delta D_i, \tag{1.10}$$

where ΔD_i is the width of the ith diameter bin (Ulbrich, 1983; Bringi and Chandrasekar, 2001). Selected moments can then be used to constrain the analytical PSD parameters. Lower-order moments are more strongly influenced by the numerous small particles, whereas higher-order moments place progressively greater emphasis on the sparsely sampled large-particle tail. Because radar reflectivity is closely related to a high-order moment of the PSD, fitting methods that reproduce total number concen-

tration well do not necessarily reproduce the largest particles or the resulting radar variables with equal accuracy.

The fitted analytical distribution therefore represents a statistical approximation to the measured PSD rather than a unique reconstruction of the underlying hydrometeor population. The resulting parameters depend on the fitting method, bin resolution, selected diameter interval, weighting scheme, and number of particles detected within each bin. These dependencies are especially important for hail PSDs because large hailstones occur infrequently but exert a disproportionate influence on fitted distribution parameters, maximum-diameter estimates, and radar forward calculations. The finite sample volume and sparse population of the upper PSD tail introduce uncertainty that must be considered when interpreting both the fitted distributions and the modeled radar signatures derived from them.

Although analytical PSD functions provide a convenient mathematical representation, they are approximations to naturally occurring particle populations. Real hailstorms frequently exhibit multimodal distributions, localized maxima, or abrupt decreases in concentration that cannot be represented perfectly by a single exponential or gamma function. Consequently, fitted PSD parameters should be interpreted as statistical descriptions of the observed particle population rather than exact representations of every measured particle. This distinction becomes particularly important when fitted distributions are subsequently used to initialize numerical models, since small differences in the fitted parameters may propagate into substantially different simulated radar signatures after melting.

1.2.1 Uncertainty in Hail Particle Size Distributions

Unlike rainfall observations, hail PSDs are typically derived from relatively sparse in situ measurements obtained along an aircraft flight path. Consequently, the measured

PSD represents only a small sample of an inherently heterogeneous storm. Spatial variability within convective updrafts, temporal evolution during the sampling period, and the relatively low concentration of large hailstones all contribute to uncertainty in the fitted distribution. These sampling limitations become increasingly important near the upper tail of the PSD, where the largest particles may be represented by only a few observations. Additional uncertainty arises from the measurement process itself. Optical array probes estimate particle dimensions from two-dimensional shadow images obtained as particles pass through the sampling area. Instrument limitations, including finite sampling volume, partial particle images, depth-of-field effects, shattering, particle coincidence, and image reconstruction algorithms, introduce uncertainty into both the measured particle size and the derived concentration. These uncertainties cannot be eliminated completely and should be considered when interpreting fitted PSD parameters.

The maximum hail size in the population ($D_{\max}$) is commonly used as a convenient descriptor of hail size because it provides a single quantity that is readily measured and compared among observations. However, $D_{\max}$ alone provides only limited information regarding the complete particle population. Two storms may exhibit identical maximum hail sizes while possessing substantially different particle concentrations, water contents, or PSD shapes. Likewise, uncertainty in the largest observed particle may arise simply because the sampling volume did not intercept the largest hailstone present within the storm. Therefore, maximum particle dimension should be interpreted as one descriptor of the hail population rather than a complete characterization of the PSD. Despite these limitations, $D_{\max}$ remains an important parameter because the largest hailstones exert a disproportionate influence on storm impacts and radar observations. Large hailstones contribute strongly to high-order moments of the PSD that govern radar reflectivity, substantially increase hail kinetic energy and damage potential, and

provide a practical metric for communicating hail severity in both operational forecasting and post-storm assessments. As a result, accurate estimation of $D_{\max}$ remains essential even though it cannot uniquely define the underlying PSD. Moreover, because the largest particles dominate radar scattering and are often responsible for the greatest societal impacts, uncertainty in ($D_{\max}$) can propagate directly into simulated polarimetric radar variables and the interpretation of hail severity. The methodologies used to estimate maximum hail diameter in the present study will be later described in Chapter 3.

1.3 Modern Observational Studies of Hail Populations

Advances in airborne instrumentation, digital imaging, particle processing methodologies, and statistical analysis techniques have significantly improved observational understanding of hail populations during the past two decades. Modern studies have increasingly emphasized the characterization of complete PSDs rather than focusing exclusively on individual hailstones or maximum hail size (Field et al., 2019). This shift reflects growing recognition that many important meteorological quantities, including radar observables and precipitation fluxes, depend upon the collective properties of the entire hail population rather than upon a single representative particle (Heymsfield et al., 2023a).

Modern airborne observations demonstrate that hail PSDs can vary substantially both among storms and over short distances within the same storm. Differences in concentration, characteristic size, and distribution shape reflect variations in storm dynamics, environmental conditions, and particle growth histories (Heymsfield et al., 2023a). This heterogeneity makes a single representative hail distribution inadequate

and motivates the use of observationally constrained PSDs in numerical simulations.

Recent airborne investigations have provided important insight into these issues. Studies examining in situ measurements collected within severe convective storms have shown that hail populations frequently evolve rapidly over relatively short spatial and temporal scales. Regions separated by only a few kilometers may contain substantially different particle populations despite existing within the same storm. These observations emphasize the inherently heterogeneous nature of hail production and highlight the difficulty of characterizing hail using sparse observations alone.

Field et al. (2019) examined extensive aircraft observations of frozen hydrometeors and emphasized the importance of PSDs for understanding precipitation microphysics. Their work demonstrated that PSD characteristics vary substantially among convective systems and that this variability influences both observational interpretation and model representation of precipitation processes. The study further illustrated that assumptions regarding PSD structure can strongly affect derived quantities such as water content, precipitation flux, and radar observables.

Modern observational analyses have also highlighted the importance of sampling uncertainty. Because large hailstones occur at relatively low concentrations, estimates of PSD parameters and maximum hail size may depend strongly upon sampling volume and observational methodology (Heymsfield et al., 2023b). This issue becomes particularly important when comparing observations collected using different instruments or platforms. Differences in instrument design, sampling area, image-processing techniques, and particle identification procedures can influence derived PSD characteristics and complicate intercomparison among datasets (Bansemer, 2022).

These challenges have motivated increasing attention toward uncertainty quantification in hail observations. Rather than treating measured PSD parameters as exact values, many contemporary studies explicitly acknowledge the uncertainty associated

with sampling limitations, particle identification, and fitting methodologies. Such approaches provide a more realistic assessment of observational confidence and facilitate more meaningful comparisons between observations and model simulations.

Another important development has been the reanalysis of historical observational datasets using modern processing techniques. Improvements in digital imaging, computational power, and particle reconstruction algorithms have made it possible to revisit observations collected decades earlier and extract additional information regarding particle populations. These efforts have demonstrated that advances in processing methodology can sometimes alter interpretations of historical observations, particularly for large particles that are most sensitive to sizing uncertainties (Bansemer, 2022).

The increasing availability of high-quality observational datasets has also improved opportunities for evaluating radar-based hail retrievals. Because radar observations provide only indirect information regarding hydrometeor populations, direct measurements remain essential for assessing retrieval accuracy. Comparisons between observed PSDs and radar signatures have revealed both the strengths and limitations of existing hail detection methodologies and have helped identify areas where additional refinement is needed (Ryzhkov et al., 2013a,b; Dawson et al., 2010).

Despite these advances, significant observational challenges remain. Direct measurements of hail-producing regions are still relatively rare compared to observations of rainfall or snow. Addressing these uncertainties requires coordinated use of in situ observations, radar measurements, and numerical simulations. Aircraft observations constrain hail PSDs, radar provides broader spatial and temporal coverage, and physically based models connect the observed particle populations to their evolution and radar signatures.

Perhaps the most important lesson emerging from modern observational studies is that hail populations are considerably more complex than early conceptual models

suggested. Variability in PSDs, maximum hail size, concentration, and particle morphology indicates that hail production cannot be adequately described using a single characteristic distribution or growth pathway (Heymsfield et al., 2023a). Instead, observed hail populations reflect the integrated effects of storm dynamics, thermodynamic structure, liquid water availability, and microphysical evolution.

These findings have important implications for radar meteorology. Because radar observations are sensitive to the collective properties of hydrometeor populations, uncertainty in hail PSDs translates directly into uncertainty in radar interpretation (Ryzhkov et al., 2013a,b; Dawson et al., 2010). The ability to relate radar observables to hail characteristics therefore depends critically upon understanding the microphysical structure of hail populations and the variability that exists among storms.

As a result, modern hail research increasingly emphasizes the integration of direct observations, radar measurements, and numerical simulations. Observational datasets provide critical constraints on PSDs and hail characteristics, while radar observations offer continuous spatial and temporal coverage of storm evolution. Together, these approaches provide a more complete framework for understanding hail-producing storms than either could provide independently.

1.4 Radar Observations and Hail Detection

Weather radar has fundamentally transformed the study of hail-producing storms by providing continuous observations of storm structure and precipitation evolution over large spatial domains. Unlike aircraft observations, which sample only a limited portion of a storm, radar observations provide nearly continuous surveillance throughout the storm lifecycle. In operational settings, radar is the primary tool used in identifying hail-producing storms, estimating hail severity, and issuing severe weather warnings.

However, radar observations remain indirect measurements of precipitation and therefore require interpretation through the lens of cloud microphysics and electromagnetic scattering theory.

The earliest meteorological applications of radar emerged following World War II, when operators discovered that precipitation produced detectable echoes on military radar systems (Doviak and Zrnić, 1993). These observations revealed that hydrometeors scatter electromagnetic radiation and can therefore be monitored remotely. Throughout the following decades, radar became increasingly important in weather forecasting and atmospheric research, culminating in the development of dedicated weather radar networks such as the WSR-57, WSR-74, and eventually the WSR-88D Doppler radar system (Crum and Alberty, 1993). These networks provided unprecedented opportunities to observe thunderstorms and severe weather events in real time.

The primary radar variable used to characterize precipitation intensity is reflectivity factor, commonly denoted Z. Radar reflectivity is strongly weighted toward the largest particles within a precipitation population. Because diameter appears to the sixth power, relatively small numbers of large particles can dominate the radar return.

This size dependence makes radar particularly sensitive to hail. Storms containing large hailstones often exhibit Z_H values greater than approximately 55 dBZ, while exceptionally intense hail-producing storms may exceed 70 dBZ (Waldvogel et al., 1979). Early radar studies quickly recognized that large Z_H values frequently corresponded to hail occurrence and that regions of elevated high Z_H often existed above the environmental freezing level. These observations provided some of the earliest evidence linking storm dynamics to hail production and established radar as an important tool for severe hail detection.

Despite its utility, Z_H alone cannot uniquely determine hail size. Similar Z_H values may arise from different combinations of particle concentration and diameter, while

intense rainfall can sometimes produce Z_H values comparable to those associated with hail (Bringi and Chandrasekar, 2001). Due to this, researchers sought methods capable of relating radar observations more directly to hail occurrence and severity.

One of the most influential early developments was the work of Waldvogel (1979), who demonstrated that the vertical extent of high Z_H above the freezing level could be used as an indicator of hail potential. The underlying concept was physically intuitive. Hail growth occurs primarily within regions containing supercooled liquid water above the freezing level. Storms capable of maintaining intense Z_H well above this level likely contain strong updrafts and substantial populations of growing ice particles. Waldvogel's work showed that the height of the 45 dBZ echo above the freezing level correlated with severe hail occurrence and provided a practical framework for radar-based hail detection.

Subsequent studies expanded upon these concepts through the development of echo-top analyses, vertically integrated liquid (VIL), and hail growth zone diagnostics (Greene and Clark, 1972; Amburn and Wolf, 1997). VIL estimates the total quantity of liquid water implied by a Z_H profile and became widely used as an operational indicator of severe storm intensity. Although VIL does not directly measure hail, large values often indicate storms capable of producing substantial hail. Similarly, echo-top products provide information regarding storm depth and convective intensity, both of which are associated with severe hail production.

While these methods significantly improved operational hail detection, they remained fundamentally limited by their reliance on Z_H alone. Because Z_H does not uniquely determine particle type, size, or phase, considerable ambiguity remained regarding the interpretation of radar observations. The development of dual-polarization radar addressed many of these limitations and marked a major advancement in severe-storm meteorology.

1.4.1 Polarimetric Radar Variables

Dual-polarization weather radars simultaneously transmit and receive horizontally and vertically polarized electromagnetic waves, allowing the scattering characteristics of hydrometeors to be evaluated beyond conventional radar reflectivity alone. By comparing the returned signals in the horizontal and vertical polarization states, polarimetric radar provides additional information regarding particle size, shape, orientation, concentration, phase, and composition (Doviak and Zrnić, 1993; Bringi and Chandrasekar, 2001, e.g.,). These measurements have become fundamental to the identification of precipitation type, quantitative precipitation estimation, and the diagnosis of storm microphysical processes, particularly in severe convective storms containing hail (Ryzhkov et al., 2013a; Kumjian, 2013a, e.g.,).

Although all radar variables depend on the scattering properties of hydrometeors, polarimetric measurements provide additional constraints on particle size, shape, orientation, and dielectric properties by comparing the returned signals at horizontal and vertical polarizations. In comparison to conventional Z_H, which primarily provides information regarding the total backscattered power from hydrometeors, polarimetric variables respond differently to changes in particle geometry and dielectric properties. As a result, combinations of polarimetric variables are capable of distinguishing between rain, graupel, hail, melting ice, and mixed-phase hydrometeors that may exhibit similar Z_H values but possess substantially different scattering characteristics (Bringi and Chandrasekar, 2001; Kumjian, 2013b).

As hailstones descend below the melting level, their physical characteristics evolve continuously through melting, water accretion, shedding, evaporation, and, under sufficiently dry conditions, sublimation. These processes modify both the PSD and the electromagnetic scattering properties of the particles, producing characteristic signa-

tures in polarimetric radar observations (Ryzhkov et al., 2013b; Dawson et al., 2010).

The present study focuses on three polarimetric variables that are particularly sensitive to melting hail: (Z_H), (Z_{DR}), and (K_{DP}). Collectively, these variables provide complementary information regarding the hail population. Z_H is dominated by the largest particles because of its strong dependence on particle diameter, Z_{DR} primarily responds to particle shape and orientation, and K_{DP} is particularly sensitive to the concentration and liquid water content of oriented hydrometeors (Bringi and Chandrasekar, 2001; Ryzhkov et al., 2013a). Because each variable responds differently to the underlying microphysics, their combined interpretation provides substantially greater insight into hail evolution than any individual variable alone.

Radar Reflectivity (Z)

Radar reflectivity (Z) represents the total power returned to the radar from hydrometeors within a sampled volume and is the most commonly used variable for identifying regions of intense precipitation. Under the Rayleigh scattering approximation, where the particle diameter is substantially smaller than the radar wavelength, the equivalent radar reflectivity factor is proportional to the sixth moment of the PSD and may be expressed as

$$Z = \int_0^\infty D^6 N(D)\, dD, \tag{1.11}$$

where D is the particle diameter and $N(D)$ is the PSD expressed as the number concentration per unit diameter interval (Doviak and Zrnić, 1993; Bringi and Chandrasekar, 2001). Although operational weather radar reports reflectivity in logarithmic units (dBZ),

$$Z_{\mathrm{H}} = 10 \log_{10}(Z_h), \tag{1.12}$$

the underlying linear reflectivity remains proportional to the sixth power of particle diameter. Consequently, relatively few large hailstones can contribute more to the total radar reflectivity than a much larger population of smaller particles.

The strong diameter dependence of Eq. 1.11 makes reflectivity highly sensitive to the upper tail of the hail PSD. This sensitivity is particularly important for hail observations because the largest particles generally occur at much lower concentrations than smaller hailstones. As discussed in the previous section, the upper tail of aircraft-observed PSDs is often sparsely sampled, introducing uncertainty into estimates of the largest hail sizes while simultaneously exerting a disproportionate influence on the calculated radar reflectivity. Consequently, Z_H alone is generally insufficient to uniquely determine hail size or concentration because similar Z_H values may result from either a small number of large hailstones or a much larger population of smaller particles (Bringi and Chandrasekar, 2001; Kumjian, 2013a).

Although Eq. 1.11 is derived under the Rayleigh approximation, hailstones frequently approach or exceed the Rayleigh scattering limit at S-band wavelengths, particularly for diameters exceeding approximately 20–30 mm. In these cases, Mie scattering effects become increasingly important, producing resonances phenomena that alter the scattering efficiency of individual particles and complicate the relationship between particle diameter and radar reflectivity (Doviak and Zrnić, 1993; Ryzhkov et al., 2013a). Many operational radar algorithms and forward operators employ the Rayleigh approximation because it provides an accurate representation of scattering when particle diameters are small relative to the radar wavelength, particularly for rain at S-band. However, as particle sizes increase or radar wavelength decreases, the

assumptions underlying Rayleigh scattering become less valid.

More advanced forward operators therefore employ full electromagnetic scattering methods, such as the T-matrix method or other numerical scattering solutions, to account for particle size, shape, orientation, and dielectric properties. Neglecting these non-Rayleigh scattering effects can introduce biases in simulated radar variables, including an overestimation of Z_H for large hailstones, with the magnitude of the error increasing at shorter radar wavelengths (e.g., C- and X-band). Operational radar calculations and forward scattering models employ full electromagnetic scattering calculations rather than relying solely on the Rayleigh approximation. Nevertheless, the sixth-power dependence remains useful for understanding why Z_H is dominated by the largest particles within the observed PSD.

The dielectric properties of hailstones also evolve substantially as melting progresses. Dry hail possesses a much lower complex dielectric constant than liquid water, resulting in substantially weaker electromagnetic scattering than similarly sized water-coated particles. At S-band and 0°C, the complex dielectric constant of pure ice is approximately 3.18+0.000854i, whereas that of liquid water is approximately 81.0+23.2i (Ryzhkov et al., 2013a). This large dielectric contrast causes even a relatively thin liquid water coating on a hailstone to increase its radar backscatter considerably as melting progresses. As a result, partially melted hailstones often produce much stronger radar returns than dry hailstones of comparable size, despite only modest changes in particle diameter. Dry hail possesses a relatively low effective dielectric constant compared to liquid water, producing weaker backscatter than similarly sized water-coated particles.

As hailstones descend below the freezing level, meltwater accumulates on their surfaces, increasing the effective dielectric constant and enhancing the backscattered radar signal (Ryzhkov et al., 2013a; Dawson et al., 2010). During the early stages

of melting, this increase in dielectric contrast may partially offset reductions in Z_H associated with decreasing particle size. As melting continues, however, progressive mass loss, water shedding, and eventual breakup reduce particle size and scattering cross section, ultimately decreasing Z_H toward the surface.

Z_H is therefore controlled by the combined effects of particle size, concentration, and composition. Because radar reflectivity is approximately proportional to the sixth power of particle diameter, the largest hailstones dominate the returned power despite being relatively few in number. These large hailstones also undergo comparatively modest microphysical evolution during descent because their greater mass, higher fall velocities, and smaller surface-area-to-volume ratios reduce the relative effects of melting over a given distance.

As a result, Z_H often remains high throughout much of the melting layer even as numerous smaller hailstones melt rapidly or disappear. Melting nevertheless alters the dielectric properties of hailstones as low-dielectric ice becomes coated with high-dielectric liquid water, increasing their scattering efficiency and modifying the observed Z_H independently of changes in particle size. The net radar signature therefore reflects the competing influences of particle shrinkage, changes in dielectric properties, and the continued dominance of the largest hailstones. Z_H is therefore influenced simultaneously by particle diameter, particle concentration, and particle composition.

Large hailstones dominate the total returned power because of the sixth-power dependence on diameter, while changes in the dielectric properties associated with melting further modify the observed radar signature. These competing effects explain why Z_H often remains relatively high within the melting layer despite substantial changes in hail microphysics and why Z_H alone cannot uniquely characterize hail size or melting state. Instead, meaningful interpretation of hail evolution requires combining Z_H with additional polarimetric variables that provide independent information regarding

particle shape, orientation, and concentration.

Differential Reflectivity (Z_{DR})

Differential reflectivity (Z_{DR}) is defined as the logarithmic ratio of the horizontally and vertically polarized radar reflectivity factors,

$$Z_{DR} = 10 \log_{10} \left(\frac{Z_H}{Z_V} \right), \tag{1.13}$$

where Z_hH and Z_V represent the horizontally and vertically polarized reflectivities in linear units, respectively (Doviak and Zrnić, 1993; Bringi and Chandrasekar, 2001). Like all radar observables, Z_{DR} is influenced by particle size, shape, orientation, and dielectric properties. However, because it is defined as the logarithmic ratio of the horizontally and vertically polarized reflectivities, Z_{DR} provides direct information about particle anisotropy that cannot be inferred from Z_H alone.

With conventional reflectivity, which primarily depends on particle size and concentration, Z_{DR} provides information regarding hydrometeor shape, orientation, and phase. For oblate hydrometeors that preferentially orient with their major axes approximately horizontal, horizontally polarized electromagnetic waves generally experience greater backscatter than vertically polarized waves, producing positive values of Because most precipitation particles are not perfectly spherical, horizontally polarized electromagnetic waves generally experience greater backscatter than vertically polarized waves, producing positive values of Z_{DR}.

For nearly spherical particles, such as small hailstones or graupel, the horizontal and vertical backscattered powers are nearly identical, resulting in Z_{DR} values close to 0 dB. As particles become increasingly oblate, the projected horizontal dimension increases relative to the vertical dimension, producing larger horizontally polarized reflectivity

and increasing Z_{DR} (Bringi and Chandrasekar, 2001; Kumjian, 2013a). Raindrops provide a classic example of this behavior, becoming progressively more oblate with increasing diameter due to aerodynamic forces. Large raindrops therefore exhibit larger values of Z_{DR} than small raindrops, while dry hail generally remains near 0 dB because of its approximately spherical shape and random orientation.

The magnitude of this enhancement depends on the amount and distribution of liquid water on the hailstone, the resulting particle shape, and the orientation of the particle relative to the radar beam. While the effects of liquid water and particle shape on scattering are reasonably well understood, the orientation behavior of melting hailstones remains an area of active research. In particular, the extent to which melting alters hailstone orientation, tumbling, and preferred fall alignment is not yet well constrained, introducing uncertainty into both forward scattering calculations and the interpretation of polarimetric radar observations. Recent observational efforts, including the development of the HailCam stereoscopic imaging system, aim to directly quantify the fall behavior and orientation of natural hailstones to improve the representation of these processes in radar forward operators and numerical models (Ortega et al., 2025).

The melting of hailstones substantially alters their scattering characteristics. As hail descends through the melting layer, liquid water accumulates on the particle surface, producing a water-coated ice core whose shape becomes increasingly oblate under aerodynamic forces. The higher dielectric constant of liquid water enhances the asymmetry between the horizontal and vertical scattering components, often producing elevated values of Z_{DR} within and immediately below the melting layer (Ryzhkov et al., 2013a; Dawson et al., 2010). The magnitude of this enhancement depends on the amount of liquid water present, the degree of particle oblateness, and the orientation of the hydrometeors within the radar sampling volume.

Several additional microphysical processes modify differential reflectivity during hail descent. Continued melting reduces the size of the ice core while increasing the fraction of liquid water surrounding the particle. As liquid water accumulates, portions of the coating may be shed from the hailstone surface. This process alters the thickness and spatial distribution of the water layer, changes the particle's effective shape, and reduces the volume of high-dielectric liquid water contributing to electromagnetic scattering. Continued melting reduces the size of the ice core while increasing the fraction of liquid water surrounding the particle. Water shedding may remove portions of the liquid coating, altering both particle geometry and dielectric structure.

Evaporation reduces the size of shed raindrops and partially melted hailstones, while sublimation above the melting layer removes ice mass without producing liquid water. Each of these processes modifies the thickness and distribution of the liquid water coating, the size of the remaining ice core, and the particle geometry. These changes alter the relative horizontal and vertical scattering amplitudes by increasing or decreasing the particle's effective dielectric contrast and anisotropy, thereby modifying the simulated values of Z_H, Z_{DR}, and K_{DP}.

Each of these processes modifies particle shape and composition, producing corresponding changes in the horizontal and vertical scattering amplitudes. Because Z_{DR} responds primarily to particle geometry rather than particle concentration, it serves as a valuable complement to Z_H when identifying melting hail and distinguishing it from dry hail or heavy rain (Kumjian, 2013a; Ryzhkov et al., 2013a).

Although Z_{DR} is highly sensitive to particle shape, interpretation of Z_{DR} alone can be ambiguous because similar values may arise from different combinations of particle size, liquid water fraction, and orientation. For this reason, Z_{DR} is typically interpreted together with other polarimetric variables, particularly Z_H and K_{DP}, to better characterize the evolution of melting hail within convective storms.

Specific Differential Phase (K_{DP})

K_{DP} describes the range rate of change of the differential propagation phase shift between horizontally and vertically polarized electromagnetic waves as they traverse a population of hydrometeors. It is defined as

$$K_{DP} = \frac{1}{2}\frac{d\Phi_{DP}}{dr}, \tag{1.14}$$

where Φ_{DP} is the cumulative differential propagation phase and r is the distance along the radar beam (Bringi and Chandrasekar, 2001; Ryzhkov et al., 2013a). Unlike Z_H and Z_{DR}, which are derived from backscattered power, K_{DP} is a propagation variable that depends on the differential phase delay accumulated as the radar wave travels through precipitation. Because it is calculated from phase rather than power, K_{DP} is largely unaffected by radar calibration errors, partial beam blockage, or attenuation at S-band wavelengths, making it a particularly robust variable for quantitative precipitation and hail studies (Ryzhkov et al., 2013a).

K_{DP} is primarily controlled by the concentration, liquid water content, and orientation of anisotropic hydrometeors. Nearly spherical particles, including dry hail, produce little differential phase shift because horizontally and vertically polarized waves propagate at nearly identical speeds through the scattering medium. As hydrometeors become increasingly oblate or develop liquid water coatings during melting, the horizontal polarization experiences a larger phase delay than the vertical polarization, resulting in positive values of K_{DP} (Bringi and Chandrasekar, 2001; Kumjian, 2013a). Since the differential phase accumulates continuously along the radar beam, even modest asymmetry in individual particles can produce substantial values of K_{DP} when particle concentrations are sufficiently large.

Both Z_H and K_{DP} are influenced by particle concentration. However, Z_H is

weighted toward the largest hydrometeors because of its strong dependence on particle size, whereas K_{DP} responds to the integrated contribution of all oriented hydrometeors and liquid water along the radar propagation path. As a result, a relatively large population of moderately sized melting hailstones or raindrops may produce large values of K_{DP} despite contributing less to the total Z_H than a few very large hailstones (Ryzhkov et al., 2013a,a).

For example, storms producing large accumulations of small hail (SPLASH) have been observed to produce K_{DP} values exceeding 10° km^{-1}, with reprocessed S-band observations exceeding 17° km^{-1}, despite reflectivities that were not exceptionally large for severe hailstorms. Electromagnetic scattering calculations demonstrated that these extreme K_{DP} values resulted from high concentrations of small melting hailstones rather than a small number of large hailstones (Kumjian et al., 2018). This enhanced sensitivity makes K_{DP} particularly useful for diagnosing changes in hydrometeor concentration and liquid water content during melting.

The dependence of K_{DP} on particle concentration distinguishes it from Z_H. Z_H is heavily weighted toward the largest particles through its sixth-power dependence on diameter, whereas K_{DP} responds to the integrated contribution of all oriented hydrometeors along the radar path. A relatively large population of moderately sized melting hailstones or raindrops may therefore produce substantial values of K_{DP} despite contributing less to the total Z_H than a few very large hailstones (Ryzhkov et al., 2013a,a). This sensitivity makes K_{DP} particularly useful for diagnosing changes in hydrometeor concentration and liquid water content during the melting process.

Furthermore, subsequent microphysical processes influence the evolution of K_{DP} beneath the melting layer. As hailstones begin to melt, the accumulation of liquid water on the particle surface increases both the dielectric contrast and particle asymmetry, producing larger differential phase shifts. Continued melting generates increasing

numbers of raindrops through water shedding, further increasing the concentration of oblate liquid particles contributing to the total phase delay.

As melting progresses toward completion, evaporation reduces the size and liquid water content of raindrops, while sublimation above the melting level decreases ice mass before liquid water develops. These competing processes modify both particle concentration and liquid water content, producing vertical profiles in which K_{DP} generally increases through the melting layer, peaks near or just below it, and decreases toward the surface as hailstones continue to melt and particle concentrations evolve (Dawson et al., 2010; Ryzhkov et al., 2013a). These competing processes modify both particle concentration and liquid water content, producing characteristic vertical variations in K_{DP} that are commonly observed in convective storms containing melting hail (Dawson et al., 2010; Ryzhkov et al., 2013a).

Although K_{DP} provides valuable information regarding hydrometeor concentration and liquid water content, it does not uniquely determine hail size or particle shape. Similar values of K_{DP} may arise from different combinations of particle concentration, size distribution, and meltwater fraction. For this reason, K_{DP} is most effectively interpreted together with Z_H and Z_{DR}, allowing the combined polarimetric signatures to better constrain the underlying microphysical characteristics of hail-producing storms (Bringi and Chandrasekar, 2001; Kumjian, 2013a).

However, K_{DP} is not measured directly; it is estimated from the range derivative of differential propagation phase (Φ_{DP}). Because differentiation amplifies measurement noise, Φ_{DP} must typically be smoothed or filtered before calculating K_{DP}, introducing a tradeoff between noise reduction and spatial resolution. As a result, K_{DP} estimates may become noisy in regions of weak signal or short propagation paths, requiring careful quality control and interpretation despite their strong sensitivity to hydrometeor concentration and liquid water content.

Effects of Microphysical Processes on Polarimetric Radar Variables

The polarimetric signatures observed within hail-producing storms are governed by the continuous evolution of hydrometeor size, shape, phase, and concentration as particles descend through the atmosphere. Melting, evaporation, sublimation, and water shedding each modify these characteristics, producing predictable changes in (Z), (Z_{DR}), and (K_{DP}). Because these processes often occur simultaneously, the resulting radar signatures represent the combined effects of multiple microphysical mechanisms rather than the influence of a single process alone (Ryzhkov et al., 2013a; Dawson et al., 2010).

Melting is generally the dominant process controlling the polarimetric signatures of hail below the freezing level. As hailstones encounter temperatures above 0°C, liquid water accumulates on the particle surface while the ice core gradually decreases in size. The presence of liquid water substantially increases the effective dielectric constant of the particle because liquid water is a much stronger microwave scatterer than ice (Bringi and Chandrasekar, 2001).

During the initial stages of melting, this increase in dielectric contrast may partially offset reductions in particle size, allowing Z_H to remain relatively large despite ongoing mass loss. At the same time, the development of water-coated, increasingly oblate particles enhances both Z_{DR} and K_{DP} through stronger polarization-dependent scattering and propagation effects. As melting progresses further, continued reductions in particle size eventually outweigh the increased dielectric contribution, producing decreasing Z_H toward the surface.

Water shedding becomes increasingly important once the liquid coating surrounding a melting hailstone exceeds the amount that can be retained against aerodynamic forces (Rasmussen and Heymsfield, 1987). Excess meltwater is removed from the hailstone surface as raindrops, reducing the liquid water fraction of the parent particle while

increasing the concentration of liquid hydrometeors within the radar sampling volume (Ryzhkov et al., 2013a). The redistribution of liquid water modifies the scattering properties of the precipitation mixture and may alter all three polarimetric variables. Z_H depends on the balance between the loss of mass from large hailstones and the increased number of smaller liquid drops, while both Z_{DR} and K_{DP} often increase because oblate raindrops produce stronger polarization-dependent scattering than nearly spherical hailstones.

Evaporation primarily affects liquid hydrometeors after melting has occurred. The effects of evaporation are most easily understood for raindrops. As raindrops evaporate within relatively dry environmental air, both particle diameter and liquid water content decrease. These reductions diminish the total back-scattered power, resulting in lower Z_H. Z_{DR} may also decrease as drops become smaller and less oblate, while K_{DP} is reduced through the combined effects of decreasing liquid water content and lower concentrations of anisotropic particles along the radar beam (Bringi and Chandrasekar, 2001; Kumjian, 2013a). The magnitude of evaporation depends strongly on the ambient temperature and relative humidity, producing substantial variability among storms.

Above the melting layer, sublimation removes ice mass directly through the phase change from solid ice to water vapor. Although sublimation generally proceeds more slowly than melting, it removes ice mass from the particle surface, shifting the PSD toward smaller diameters and eliminating the smallest particles before melting begins. Although sublimation proceeds more slowly than melting under many atmospheric conditions, it gradually reduces particle size and concentration before liquid water develops on the particle surface. This process generally produces decreasing Z_H while having comparatively small effects on Z_{DR} because particle shape often remains approximately spherical . Additionally, the particles remain as ice such that their Z_{DR} is naturally suppressed. Since dry ice particles generate relatively little differential phase

shift, sublimation likewise produces only modest changes in K_{DP} until melting begins (Pruppacher and Klett, 1997; Ryzhkov et al., 2013a). The combined influence of these microphysical processes produces the characteristic vertical evolution of polarimetric radar variables observed within hail-producing storms.

1.4.2 Derived Products for Hail Detection

Together, these variables provide a much richer description of storm microphysics than Z_H alone. Research by Ryzhkov et al. (2013a) and numerous others demonstrated that combinations of polarimetric variables can reveal important aspects of hail growth, melting, and hydrometeor composition. Features such as hail cores, melting layers, and mixed-phase regions became increasingly identifiable through polarimetric analysis, significantly improving operational hail detection capabilities.

These advances led directly to the development of modern hail detection algorithms. Among the most widely used are the Severe Hail Index (SHI), Probability of Severe Hail (POSH), and Maximum Expected Size of Hail (MESH) (Witt et al., 1998). The SHI estimates hail severity using Z_H observations weighted by temperature-dependent growth considerations. POSH converts SHI values into probabilities of severe hail occurrence, while MESH provides an estimate of maximum expected hail size at the surface. These products have become widely used within operational forecasting environments and form the basis of many contemporary hail warning procedures.

More development led to hydrometeor classification algorithms (HCAs) which combine multiple polarimetric radar variables, including Z_H, Z_{DR}, (K_{DP}), copolar correlation coefficient (ρ_{HV}), and environmental temperature, to estimate the dominant hydrometeor type within each radar sampling volume. Modern fuzzy logic HCAs assign membership scores to various hydrometeor classes using empirically derived or physically based relationships between these radar observables and expected parti-

cle characteristics (Park et al., 2009). Although HCAs have substantially improved operational identification of hail, rain, graupel, and mixed-phase precipitation, their performance can degrade in regions containing melting hail because the radar signatures evolve rapidly as particles melt, shed water, and change shape. These processes may produce overlapping polarimetric signatures among hydrometeor classes, making accurate classification particularly challenging within the melting layer and beneath intense hail cores.

More recently, the Multi-Radar Multi-Sensor (MRMS) framework has combined observations from numerous radar systems to generate gridded hail products over large geographic regions (Smith et al., 2016). MRMS-based algorithms incorporate multiple sources of information and provide improved spatial consistency relative to single-radar approaches. These products have become increasingly important for operational forecasting, climatological studies, and severe weather verification.

Despite substantial advances, significant challenges remain. Radar observations are fundamentally indirect measurements of precipitation populations. Retrievals depend upon assumptions regarding PSDs, particle density, maximum hail size, and hydrometeor composition. Uncertainty in these characteristics can lead to uncertainty in hail retrievals, particularly in storms containing complex mixtures of rain, graupel, and hail (Carlin et al., 2016). Furthermore, many retrieval algorithms were developed using limited observational datasets and may not fully capture the variability observed among hail-producing storms.

These limitations highlight the continuing importance of direct observations and physically based numerical modeling. Radar observations provide unparalleled spatial and temporal coverage, but their interpretation ultimately depends upon understanding the microphysical populations responsible for the observed signatures. Modern hail research increasingly seeks to integrate direct observations, radar measurements, and

numerical simulations within a unified framework (Ryzhkov et al., 2013a,b; Dawson et al., 2010; Carlin and Ryzhkov, 2025). Such an approach provides the most promising pathway for improving hail detection algorithms and advancing understanding of hail-producing storms.

1.5 Numerical Modeling of Hail and Radar Signatures

While observational studies provide essential information regarding hail populations and storm structure, observations alone cannot fully resolve the processes responsible for hail growth and evolution. Hailstones experience complex trajectories through convective storms, encountering changing thermodynamic conditions, liquid water contents, and airflow patterns throughout their lifetimes. Many of these processes occur on spatial and temporal scales that are difficult to observe directly. Numerical modeling therefore provides an important complementary tool for investigating hail microphysics and interpreting observations.

Early hail models focused primarily on individual particle trajectories (Foote, 1984, e.g.). These models tracked idealized hail embryos through prescribed storm environments and calculated growth through the collection of supercooled liquid water. Such studies demonstrated that hail size depends strongly upon residence time within favorable growth regions and highlighted the importance of updraft strength, liquid water content, and environmental temperature. These models provided many of the foundational concepts that continue to influence hail research today.

As computational capabilities increased, more sophisticated cloud models became available (Rasmussen and Heymsfield, 1987; Ryzhkov et al., 2020). Bulk microphysical parameterizations represented hydrometeor populations using characteristic PSDs

and predicted quantities such as mass mixing ratio and number concentration. These approaches provided computational efficiency and therefore became widely adopted in numerical weather prediction and storm-scale simulation models.

Most bulk schemes assume that hydrometeor populations follow prescribed exponential or gamma PSDs. While such assumptions simplify the representation of cloud microphysics, they also introduce uncertainty because observed hail populations often exhibit substantial variability. Therefore, model results may depend strongly upon the assumed distribution parameters and maximum particle size.

Bin microphysical models provide a more detailed alternative. Rather than assuming a fixed functional form, bin schemes explicitly predict the evolution of particle concentrations across multiple size categories. This approach allows PSDs to evolve naturally in response to growth, melting, collision, and breakup processes. Although computationally expensive, bin models provide valuable insight into the evolution of hail populations and have played an important role in evaluating simpler bulk parameterizations (Khain et al., 2000).

One of the recurring themes in numerical hail studies is the importance of melting. Hail growth receives considerable attention because it determines maximum particle size aloft, but the subsequent evolution of hail below the freezing level can be equally important. As hailstones descend through warmer air, they undergo melting, shedding, and eventual transformation into rain. These processes alter PSDs while simultaneously modifying the surrounding thermodynamic environment.

Melting hail contributes to cooling through latent heat absorption and may enhance downdraft development through both thermodynamic and precipitation-loading effects (Srivastava, 1987; Rasmussen and Heymsfield, 1987). Numerous modeling studies have demonstrated that hail melting can significantly influence storm evolution, particularly in environments characterized by relatively dry sub-cloud layers. The radar signatures

associated with melting hail differ substantially from those of dry hail owing to water coating, drop shedding, and changes in particle shape during descent (Carlin and Ryzhkov, 2019).

The increasing availability of polarimetric radar observations motivated the development of radar forward operators capable of converting model output into synthetic radar observables. Forward operators use assumptions regarding particle size, shape, density, orientation, and dielectric properties to calculate radar variables such as Z_H, Z_{DR}, and K_{DP}. These calculations provide a direct connection between numerical simulations and radar observations and allow investigators to evaluate microphysical assumptions using remotely sensed data.

Modern numerical models now simulate the coupled evolution of hail microphysics, thermodynamics, and polarimetric radar signatures by explicitly representing particle growth, melting, shedding, and sedimentation while simultaneously calculating the corresponding radar variables using electromagnetic scattering calculations. These physically based modeling frameworks provide an important bridge between in situ aircraft observations and remotely sensed radar measurements, allowing the effects of particle size, shape, orientation, dielectric properties, and environmental conditions on polarimetric signatures to be investigated under controlled conditions.

Despite these advances, substantial uncertainties remain. Observed hail particle size distributions are derived from finite sampling volumes and must subsequently be represented using analytical distributions before they can be incorporated into numerical models. Additional uncertainty arises from estimating the upper tail of the distribution, particularly the maximum hail diameter, which strongly influences simulated radar variables. These uncertainties motivate the present study, which combines reprocessed T-28 aircraft observations, a one-dimensional cloud model, and polarimetric radar observations to evaluate how uncertainty in observed hail populations propagates

into simulated radar signatures.

Chapter 2

T-28 Dataset and Observations

The observational dataset utilized in this research was collected using the South Dakota School of Mines and Technology (SDSMT) armored T-28 research aircraft, shown in Figure 2.1. From the 1960s up until its formal retirement in 2005, the T-28 served as one of the primary platforms for in situ investigations of severe convective storms, providing direct measurements of hail particle populations, thermodynamic conditions, and storm kinematics that cannot be obtained through remote sensing alone (Foote, 1984; Heymsfield et al., 2023a). Unlike weather radar, which infers hydrometeor properties from electromagnetic scattering, aircraft observations directly sample the particles within the storm environment. These measurements therefore provide an essential observational foundation for understanding hail growth and for evaluating numerical models and radar retrieval techniques.



Figure 2.1: Photo of the T-28 Armored plane in 2001, courtesy of the Digital Library of South Dakota.

Originally manufactured as a military trainer aircraft, the T-28 was extensively modified for severe weather research through the addition of reinforced armor plating, impact-resistant windows, and specialized scientific instrumentation (NCAR/EOL, 2026). These modifications enabled repeated penetrations of intense convective storms containing large hail while maintaining stable operation within environments that would be inaccessible to conventional research aircraft. Over several decades, the aircraft participated in numerous field campaigns investigating hail growth, cloud microphysics, and storm dynamics, producing one of the most comprehensive collections of in situ hail observations currently available (Heymsfield et al., 2023a).

Table 2.1: Summary of the T-28 hail dataset used in this study.

Characteristic	**Value**
Observation years	1995–2003
Research flights	13
Particle size distributions	171
Aircraft	SDSMT T-28 storm-penetrating aircraft
Particle probe	Modified 1D optical array Hail Spectrometer
Detector array	128 photodiodes
Sampling interval	$\sim$10 s ($\sim$1 km flight distance)
Sampling volume	$\sim$100 m^3 per PSD ($\sim$10 m^3 s^{-1})
Flight altitude	4.1–6.2 km MSL
Particle diameter range	$\sim$1–50 mm
Diameter bin spacing	0.9 mm
Measured variables	PSDs, altitude, pressure, temperature, latitude, longitude, and vertical velocity

A broader summary of the reprocessed T-28 dataset used in this study is provided in Table 2.1. The dataset consists of 171 PSDs collected during 13 research flights between 1995 and 2003. PSDs were generated at approximately 10-s intervals during storm penetrations, with aircraft sampling altitudes ranging from 4.1 to 6.2 km MSL.

The observations utilized in this thesis span eleven research flights conducted during

the VORTEX, TCAD, STEPS, JPOLE/TELEX, and CHILL-TEX field programs. These campaigns sampled a diverse range of severe convective storms across the central United States under varying environmental conditions. Table 2.2 summarizes the flights included in the present study.

Flight #	Date	Campaign	Start (UTC)	End (UTC)
668	1995/06/22	VORTEX	23:28:25	23:45:05
670	1995/06/27	VORTEX	21:27:17	21:55:57
728	1999/06/11	TCAD	21:10:22	21:10:52
729	1999/06/12	TCAD	00:24:56	00:25:46
754	2000/06/11	STEPS	22:08:22	22:15:12
757	2000/06/22	STEPS	23:51:51	23:57:41
761	2000/06/29	STEPS	23:13:23	23:42:23
798	2003/05/16	JPOLE/TELEX	18:38:29	18:55:29
803	2003/06/01	JPOLE/TELEX	20:43:10	20:43:30
819	2003/07/29	CHILL-TEX	19:40:02	19:45:02
820	2003/07/30	CHILL-TEX	21:11:43	21:25:43

Table 2.2: T-28 research flights included in this study. Flight start and end times correspond to the first and last observations contained within the processed dataset.

2.1 Dataset Reprocessing

The observations used throughout this study are derived from a comprehensive reprocessing of the historical T-28 hail dataset conducted by Dr. Aaron Bansemer using the SODA-2 (SDSMT Optical Array Probe Data Analysis) software package (Bansemer, 2022). Although the original observations have supported numerous investigations of hail microphysics, advances in optical array probe processing, particle reconstruction algorithms, and image quality control motivated a complete reanalysis of the archived raw particle imagery. The resulting dataset provides more accurate particle sizing, improved quality control, and a substantially expanded set of microphysical variables while maintaining consistency across all research flights.

The reprocessing began with the archived raw images collected by the SDSMT hail spectrometer during each research flight. The spectrometer operated on 10 s intervals, capturing information on hail sized from 1-50 mm with a 0.9 mm bin width. Individual particle images were reconstructed using updated image-processing algorithms capable of identifying particle boundaries, removing artifacts, and correcting for partial particle images that commonly occur during high-speed aircraft sampling. Additional quality-control procedures removed ambiguous detections while improving estimates of particle dimensions throughout the observed size spectrum (Bansemer, 2022).

One of the primary outcomes of the reprocessing effort was a set of PSDs for every observation time. In addition to particle concentration, the processed dataset includes particle diameters, bin boundaries, aircraft position, altitude, pressure, temperature, vertical velocity, and numerous auxiliary variables describing the observed hail populations.

Because the entire observational archive was reprocessed using a common methodology, measurements collected during different field campaigns can be compared directly without introducing inconsistencies associated with earlier processing techniques. The resulting dataset therefore represents the most comprehensive and internally consistent version of the historical T-28 observations currently available.

Beyond improving the consistency of the observational archive, the reprocessing effort also produced revised estimates of the exponential PSD parameters describing the observed hail populations. Previous analyses of the historical T-28 observations established empirical relationships between the exponential intercept parameter (N_0) and slope parameter (Λ) that have subsequently been used to characterize hail PSDs in numerical modeling studies (Field et al., 2019; Heymsfield et al., 2023b). Note that the observations from the Hail Spectrometer directly measures discrete particle counts within fixed diameter bins over a finite sampling volume. These observations constitute

the measured PSD.

To provide a compact analytical description suitable for model initialization, the measured PSD is fit with an exponential distribution characterized by N_0 and Λ. This fitted distribution smooths the observed spectrum while preserving its overall structure, but the fitting process introduces additional uncertainty because a single analytical function cannot perfectly reproduce every measured PSD. Nonetheless, the updated processing performed by Dr. Aaron Bansemer provides revised PSD parameter estimates derived directly from the reprocessed particle observations, allowing each observed distribution to be represented more accurately while preserving the variability present within the aircraft observations.

2.2 T-28 PSDs

To characterize each observed hail distribution, an exponential PSD was fitted to the observed concentrations using nonlinear least-squares regression. The exponential form is given by

$$N(D) = N_0 e^{-\Lambda D}, \tag{2.1}$$

where $N(D)$ denotes the particle concentration at diameter D, N_0 is the intercept parameter, and Λ is the slope parameter (Marshall and Palmer, 1948). Although more complex gamma distributions can provide additional flexibility, the exponential representation provides a robust description of the observed hail populations while requiring only two fitted parameters. This simplified representation also facilitates direct comparisons among observations and provides a consistent framework for estimating characteristic hail sizes throughout the dataset.

Figure 2.2 illustrates representative PSDs together with the corresponding exponen-

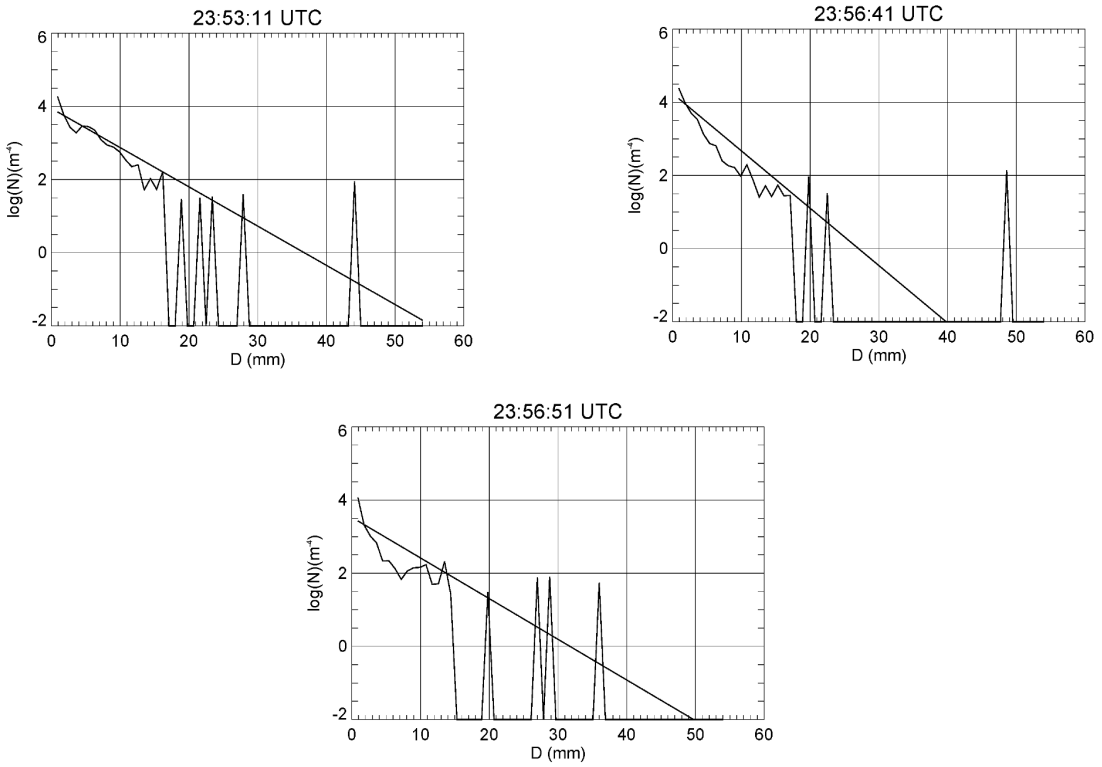


Figure 2.2: Examples of observed hail PSDs obtained from the reprocessed T-28 dataset. The observed particle concentrations are shown together with the corresponding exponential fits used to characterize each distribution.

tial fits. The fitted exponential distribution provides a compact mathematical description of the observed hail population while reducing sensitivity to sampling variability in individual diameter bins. These fitted PSDs form the basis for the first of the three maximum hail size estimates examined in this study.

Figure 2.3 summarizes the statistical characteristics of the reprocessed T-28 hail observations utilized in this study. Panel (a) shows the ensemble-mean PSD, while panel (b) quantifies the frequency with which particles of each diameter were observed among all measured PSDs. Together, these panels illustrate not only the average shape of the observed hail size distribution but also the sampling frequency of each size class, providing insight into the observational constraints on the upper tail of the PSD.

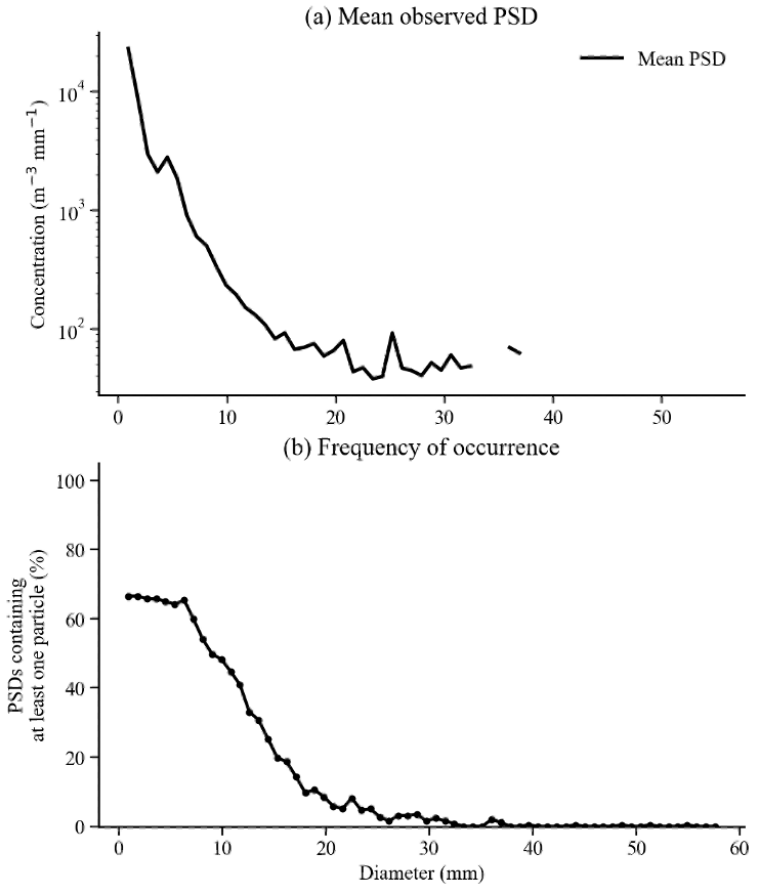


Figure 2.3: (a) Mean observed hail particle size distribution (PSD) computed by averaging all 257 T-28 PSD observations. (b) Frequency of occurrence of each diameter bin, expressed as the percentage of observed PSDs containing at least one particle within that size class.

The frequency of occurrence decreases rapidly with increasing particle diameter. While nearly two-thirds of PSDs contained particles smaller than approximately 5 mm, fewer than 10% contained particles larger than approximately 20 mm, and particles exceeding 35 mm were observed in fewer than 2% of all PSDs. If the observed PSDs closely followed ideal exponential distributions, particles within the smallest diameter bins would be expected in nearly every observation. Instead, the occurrence frequency plateaus near 65–67%, indicating that many observed PSDs contained no particles within the smallest measurable size classes. This behavior reflects the finite sampling

volume of the T-28 observations and the substantial variability among individual hail populations, demonstrating that the measured PSDs depart from idealized continuous exponential distributions.

The gradual decline in occurrence frequency toward larger diameters also produces a long, low-frequency tail extending to nearly 60 mm. Because hailstones of this size occur at extremely low concentrations, the presence or absence of only one or two particles within an individual sampling interval can determine whether a diameter bin is populated. Consequently, the upper tail of the observed PSD is increasingly influenced by stochastic sampling of rare particles, increasing the uncertainty associated with fitted PSD parameters and maximum hail size estimates.

These considerations motivate the sensitivity experiments performed in this study. Rather than assuming a single estimate of maximum hail size, three independent methods were used to define $D_{\max}$ while retaining the fitted exponential PSD parameters. This approach allows the influence of uncertainty in the upper tail of the hail distribution to be quantified while preserving the observed variability contained within the reprocessed T-28 dataset.

2.2.1 Comparison with Previous PSD Parameterizations

Previous analyses of the historical T-28 observations demonstrated that exponential hail PSDs could be represented by an empirical relationship between the intercept parameter (N_0) and slope parameter (Λ). Based on the original processing of the T-28 observations, Heymsfield et al. (2023b) reported the median relationship

$$N_0 = 125\Lambda^{3.68}, \tag{2.2}$$

which has since been deduced as a representative parameterization of observed hail

PSDs.

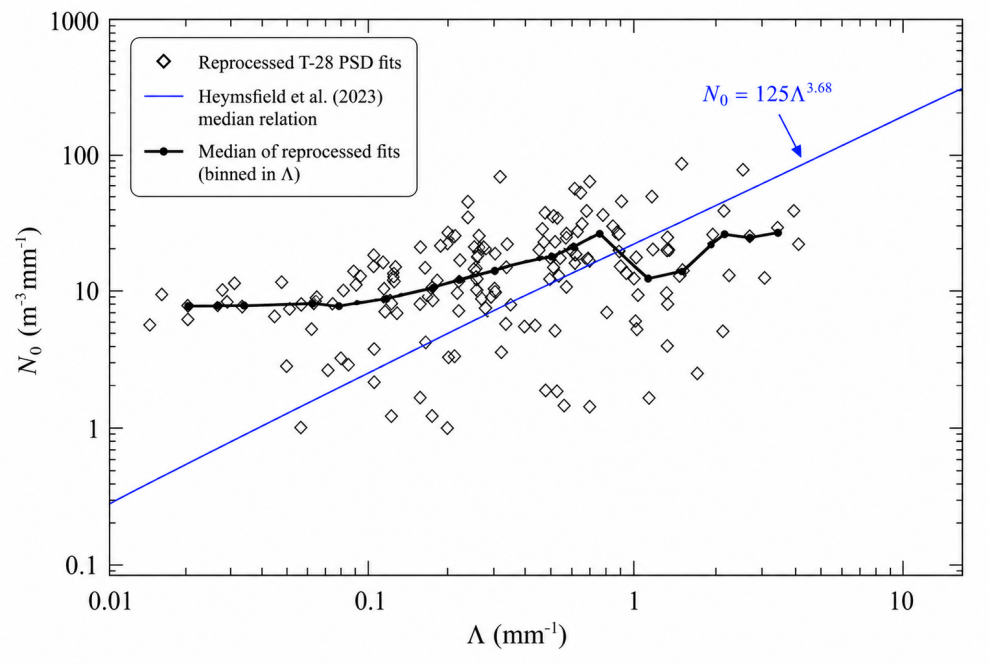


Figure 2.4: Comparison of exponential particle size distribution (PSD) parameters derived from the reprocessed T-28 dataset with the median N_0–Λ relationship reported by Heymsfield et al. (2023b). Open diamonds denote the fitted exponential intercept (N_0) and slope (Λ) parameters for individual PSDs obtained from the reprocessed observations. The blue line represents the median relationship, $N_0 = 125\Lambda^{3.68}$, derived from the original T-28 dataset, while the black line shows the median of the reprocessed observations computed within bins of Λ.

Figure 2.4 compares the exponential parameters obtained from the reprocessed T-28 dataset with the median relationship given by Eq. (2.2). Although the revised observations exhibit considerable scatter, they no longer follow the previously proposed median relationship across the full range of observed slope parameters. Instead, the updated PSDs span a substantially broader range of intercept parameters, reflecting the increased variability resolved by the reprocessed observational dataset.

The differences shown in Figure 2.4 illustrate that the updated processing modifies not only individual PSDs but also the statistical relationship between the fitted exponential parameters describing the observed hail populations. Because these fitted

parameters provide the initial conditions for the numerical simulations performed in this study, the revised dataset establishes a new observational foundation for evaluating the evolution of hail PSDs and their associated radar signatures.

2.3 Maximum Hail Size Estimation

Maximum hail diameter ($D_{\max}$) is among the most commonly reported quantities in both observational and operational hail studies because it provides a simple measure of the largest hailstones present within a storm. However, defining $D_{\max}$ from an observed PSD is not straightforward. Sampling limitations, finite particle concentrations, and uncertainty in the distribution tail may all produce different estimates of the largest physically representative hailstone (Field et al., 2019; Heymsfield et al., 2023b).

To investigate the sensitivity of subsequent numerical simulations to the definition of maximum hail size, three independent, physically motivated definitions of $D_{\max}$ were calculated from every observed PSD. These approaches represent different interpretations of the largest characteristic hailstone contained within the observed spectrum and provide the basis for the sensitivity experiments performed.

2.3.1 Fitted Maximum Diameter

The first estimate, referred to throughout this study as the fitted $D_{\max}$, is obtained directly from the exponential PSD shown in Eq. (2.1). Rather than identifying the single largest observed particle, the fitted distribution provides a continuous representation of the hail population. The fitted maximum diameter is defined as the largest connected diameter for which the exponential fit remains physically representative of the observed particle concentrations. Because this estimate is derived from the fitted distribution rather than an isolated observation, it is generally less sensitive to sampling variability

within the distribution tail. Shown below in Figure 2.5 is an annotated version of an example raw PSD to denote the fitted $D_{\max}$ estimation for a representative PSD.

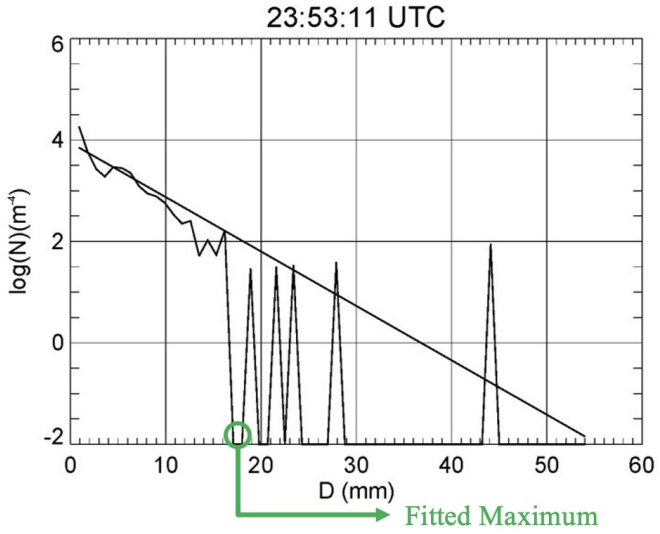


Figure 2.5: Visual representation of fitted $D_{\max}$ assessed from the raw PSDs in the T-28 Dataset.

2.3.2 Maximum Observed Diameter

The second estimate corresponds to the maximum observed hail diameter contained within each PSD. This approach simply identifies the largest individual hailstone measured by the aircraft and therefore requires no assumptions regarding the underlying distribution shape. Because the estimate depends upon a single observation, it may be sensitive to sampling variability, particularly for distributions containing relatively few large hailstones. A visualization to see how maximum observed $D_{\max}$ corresponds to changes in comparison to the fitted $D_{\max}$ is shown in Figure 2.6

2.3.3 Ulbrich Maximum Diameter

The third estimate follows the characteristic hail diameter proposed by Ulbrich (1983), in which the maximum hail size is related to the exponential slope parameter according

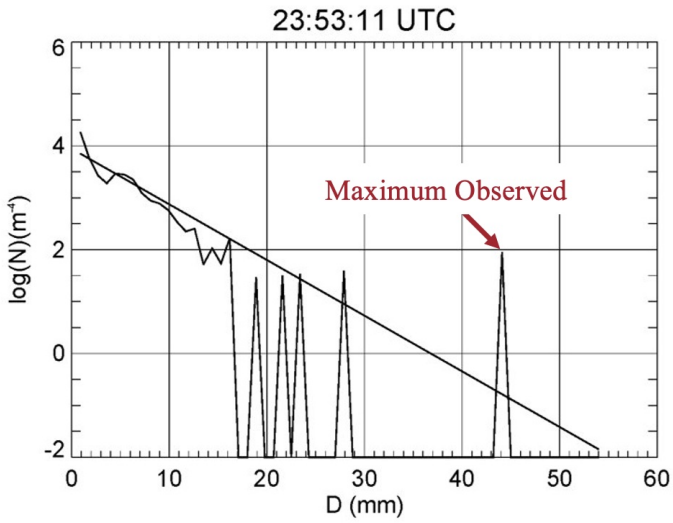


Figure 2.6: Example of the maximum observed $D_{\max}$ value obtained from the raw PSDs of the T-28 Dataset.

to

$$\Lambda_h D_{\max} = 7.9. \tag{2.3}$$

This relationship provides an estimate of the largest characteristic hailstone implied by the fitted exponential distribution and has been widely used in studies employing exponential PSDs. Unlike the previous two methods, the Ulbrich estimate depends entirely upon the fitted slope parameter and therefore reflects the overall shape of the observed PSD rather than individual particle measurements.

Figure 2.7 summarizes the distributions of the three $D_{\max}$ estimation methods computed for all PSDs included in the reprocessed T-28 dataset. Although all three methods produce estimates spanning a similar range of hail sizes, systematic differences are evident. The fitted $D_{\max}$ values are generally concentrated over a narrower range of diameters, whereas the maximum observed and Ulbrich/Atlas methods exhibit broader distributions and extend to larger hail sizes. These differences reflect the distinct approaches used to estimate the largest representative hailstone from an observed PSD.

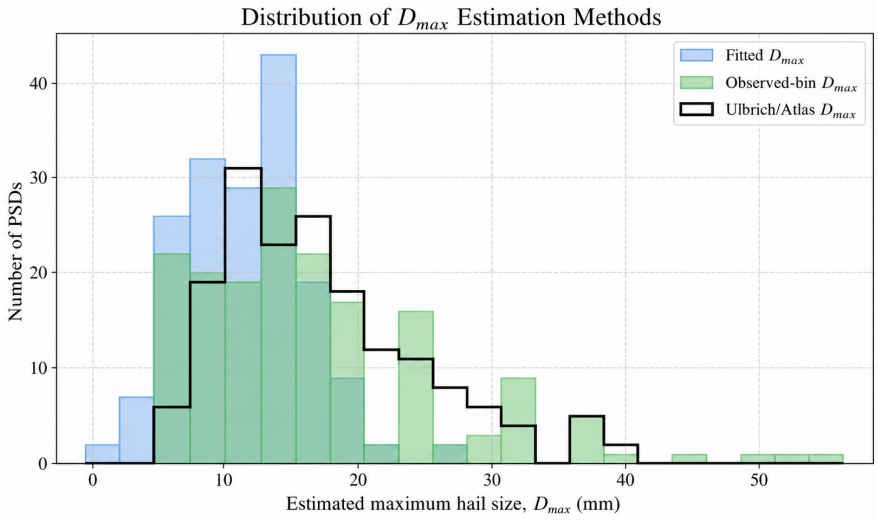


Figure 2.7: Histograms of the fitted $D_{\max}$, maximum observed $D_{\max}$, and Ulbrich $D_{\max}$ estimates computed from all reprocessed T-28 PSDs included in this study.

The overlap among the three distributions demonstrates that the methods are broadly consistent while simultaneously highlighting that the choice of $D_{\max}$ definition may influence the prescribed initial hail population. Because the present study seeks to evaluate the sensitivity of numerical simulations to the definition of maximum hail size, each estimation method is retained independently and used to initialize separate sets of model simulations.

To isolate the influence of the maximum hail size on the simulated radar signatures, the exponential hail PSD parameters (N_0 and Λ_h) were held constant for each experiment while only the prescribed upper truncation diameter ($D_{\max}$) was varied. Thus, the fitted, maximum observed, and Ulbrich-based $D_{\max}$ simulations differed only in the largest hailstone permitted within the analytical PSD, allowing the sensitivity of the model results to the assumed maximum hail size to be evaluated independently of changes in the PSD shape.

Chapter 3

Description of 1D Cloud Model

The numerical simulations presented throughout this study are performed using the one-dimensional spectral bin downburst model developed by Carlin and Ryzhkov (2025). The model was originally designed to investigate the evolution of melting hail and the associated development of convective downdrafts through coupled representations of cloud microphysics, thermodynamics, and atmospheric dynamics. In addition to predicting the evolution of the hail particle population, the model computes the environmental response to melting and evaporation while simultaneously producing synthetic polarimetric radar variables. This combination provides a physically consistent framework for relating observed hail PSDs to both the thermodynamic evolution of the storm environment and the corresponding radar signatures.

Although the physical formulation of the model remains unchanged from the original implementation, key modifications were developed for the present study to facilitate application to the historical T-28 observational archive. These adaptations include initialization using ERA5 atmospheric reanalysis data and direct ingestion of reprocessed aircraft-derived PSDs. The following sections first describe the physical basis of the numerical model before discussing the methodological adaptations implemented for this research.

3.1 Model Overview and Physical Basis

The simulations performed in this study utilize a one-dimensional cloud model originally developed to investigate the evolution of melting hail populations and their impacts on the surrounding environment. Unlike fully three-dimensional cloud-resolving models, which explicitly simulate storm dynamics across large computational domains, one-dimensional models focus on the vertical evolution of hydrometeor populations within a prescribed atmospheric profile. Although simplified relative to more complex numerical models, one-dimensional approaches provide substantial advantages for sensitivity studies because they isolate microphysical processes while maintaining relatively modest computational requirements.

The 1D model developed by Dr. Jacob Carlin (NOAA National Severe Storms Laboratory) traces its heritage to a series of investigations examining hail melting, downdraft generation, and radar signatures associated with severe convective storms. Previous studies demonstrated that the thermodynamic effects of melting hail can substantially modify the environment below the freezing level through latent cooling and precipitation loading. These processes influence downdraft development, alter hydrometeor trajectories, and affect the radar signatures ultimately observed by operational weather radar systems. Consequently, understanding the evolution of hail populations during descent is essential for interpreting both surface hail observations and radar-derived hail products.

Figure 3.1 gives an example of a portion of the outputted variables available from the model (Carlin and Ryzhkov, 2025). A major strength of the model is its ability to simulate the evolution of observed hail PSDs rather than relying exclusively upon idealized assumptions regarding hail populations. Traditional modeling studies frequently initialize simulations using prescribed exponential or gamma PSDs charac-

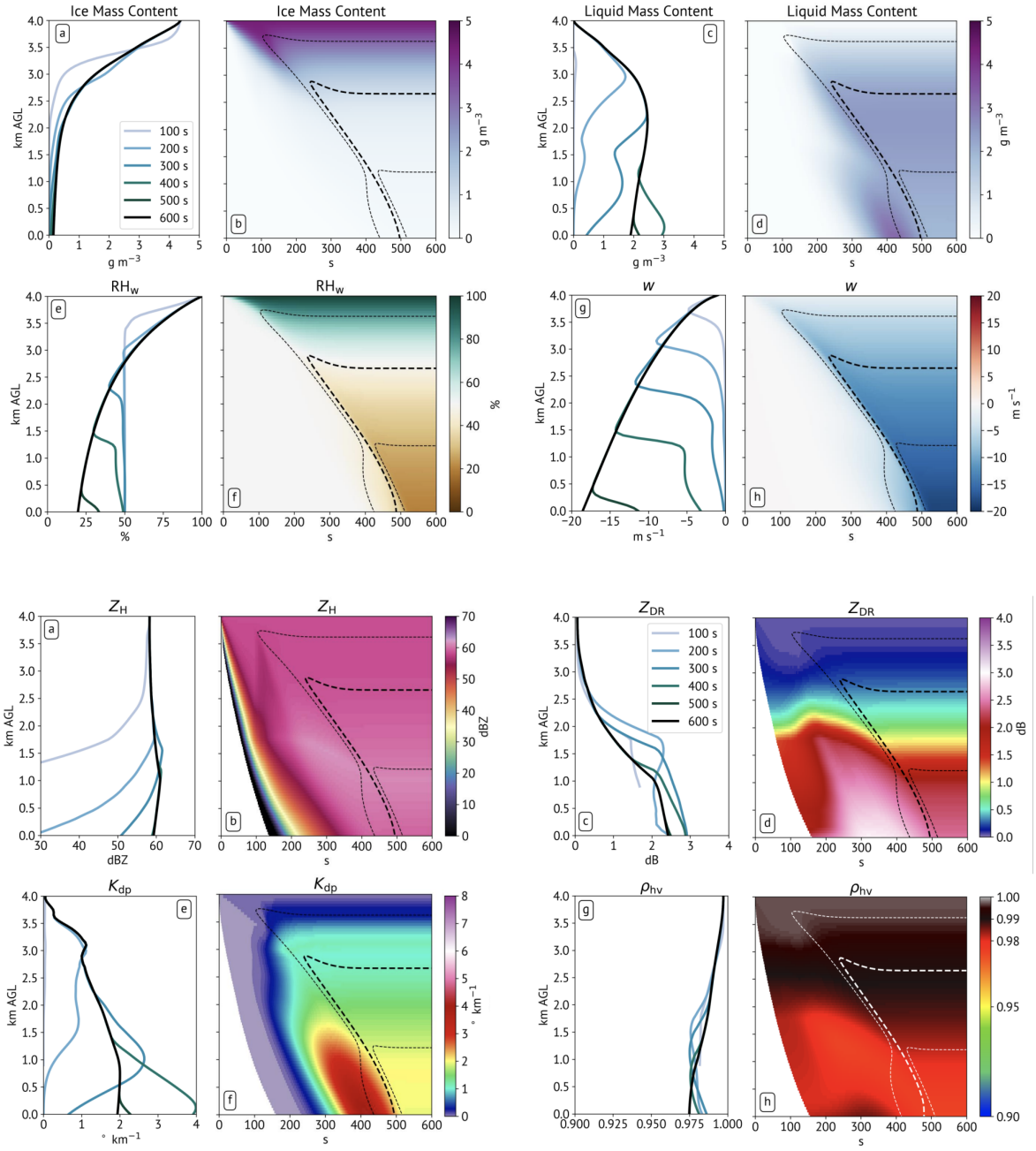


Figure 3.1: Evolution of simulated microphysical variables (top) and corresponding polarimetric radar variables (bottom) during the melting of hail in a one-dimensional downdraft model. The left panel shows the evolution of ice mass content, liquid mass content, relative humidity with respect to water, and vertical velocity, while the right panel shows simulated Z_H, Z_{DR}, K_{DP}, and copolar correlation coefficient (ρ_{hv}). Figures adapted from *Carlin and Ryzhkov (2025)* with permission.

terized by representative parameters. While useful for theoretical investigations, such approaches may not adequately capture the substantial variability observed among real hail-producing storms. By contrast, the present study utilizes PSDs derived directly from T-28 observations, thereby providing observationally constrained initial conditions for numerical simulations.

The model domain extends vertically through the lower troposphere and is initialized using atmospheric profiles derived from ERA5 reanalysis data. Environmental temperature, pressure, humidity, and wind conditions are prescribed at the beginning of each simulation and evolve in response to interactions with the descending hail population. Because the model incorporates the thermodynamic impacts of melting, evaporation, and sublimation, environmental conditions may be modified substantially during the course of a simulation, particularly in regions characterized by significant hail concentrations.

Within the model framework, hail particles are represented through discretized size bins that collectively describe the evolving PSD. Each size category is allowed to undergo microphysical evolution through processes such as melting, evaporation, sublimation, and sedimentation. As particles descend through the atmosphere, their mass, diameter, and concentration may change in response to the surrounding environmental conditions. The cumulative effects of these processes determine the evolution of the hail population and ultimately influence both surface precipitation characteristics and radar observables.

An important feature of the model is the explicit calculation of thermodynamic tendencies associated with hail melting. Melting requires latent heat and therefore cools the surrounding environment. When substantial hail concentrations are present, this cooling may generate negative buoyancy and contribute to downdraft formation. The model therefore provides a framework for examining interactions between hail

microphysics and storm thermodynamics, an aspect of severe convective storms that has received considerable attention in previous studies.

The present study utilizes the model in a series of experiments designed to examine how observed hail PSDs influence radar signatures and environmental evolution. Particular emphasis is placed upon the sensitivity of simulated results to assumptions regarding maximum hail size and PSD structure. Because maximum hail diameter remains one of the most uncertain characteristics of observed hail populations, understanding its influence on modeled radar variables represents a primary objective of this work.

Although the model does not explicitly simulate the full three-dimensional dynamics of severe convective storms, its relative simplicity provides important advantages. The reduced computational cost allows large numbers of simulations to be performed using observationally derived PSDs, thereby facilitating statistical analyses that would be impractical using more computationally intensive cloud-resolving models. Furthermore, the model serves as an effective bridge between direct observations and radar interpretations by providing a physically based framework through which observed hail populations may be examined.

3.2 Numerical Framework

The melting of individual hailstones is determined from coupled heat and mass transfer equations that account for conductive heat exchange, latent heat associated with melting, and evaporative cooling of meltwater. Because melting, evaporation, and sublimation modifies both particle mass and diameter, terminal fall velocities are continuously updated throughout the simulation. The resulting changes in particle sedimentation directly influence precipitation loading and the transport of condensed water through

the atmospheric column.

The environmental response is computed by solving the conservation equations governing heat, moisture, and momentum. Cooling associated with melting and evaporation modifies atmospheric buoyancy, while the cumulative weight of the hydrometeor population contributes to downward acceleration through precipitation loading. Together, these processes determine the evolution of vertical air motion throughout the simulation and permit explicit calculation of downburst intensity.

3.2.1 Radar Forward Operator

In addition to predicting the evolution of the hail population and atmospheric state variables, the model incorporates a polarimetric radar forward operator based on the framework of Ryzhkov et al. (2013a,b). At each model time step, the evolving PSD is converted into synthetic radar variables, including Z_H, Z_{DR}, and K_{DP}. These simulated radar observations provide a direct connection between the modeled hail population and the quantities routinely observed by operational weather radar, allowing comparisons between modeled microphysical evolution and radar signatures.

Direct comparison between numerical model output and radar observations requires transforming simulated microphysical fields into radar-observable quantities. This transformation is performed using a radar forward operator, which applies electromagnetic scattering calculations to the modeled hydrometeor size distributions to compute synthetic polarimetric radar variables. Rather than comparing particle concentrations or mixing ratios directly with radar observations, the forward operator produces (Z), (Z_{DR}), and (K_{DP}), allowing simulated storms to be evaluated in the same observational framework as weather radar measurements (Ryzhkov et al., 2013a; Dawson et al., 2010).

The radar forward operator implemented in this study follows the electromagnetic

scattering framework described by Ryzhkov et al. (2013a), as incorporated into the one-dimensional melting model of Ryzhkov et al. (2013a) and updated by Carlin and Ryzhkov (2025). At each model time step and vertical level, the simulated PSD, $N(D)$, is combined with the physical characteristics of each hydrometeor, including particle diameter, density, meltwater fraction, and shape. These properties determine the particle dielectric constant and geometry, which are used in T-matrix electromagnetic scattering calculations to compute the complex forward- and back-scattering amplitudes for horizontally and vertically polarized radiation. The resulting scattering amplitudes are integrated over the PSD together with angular moments describing the particle orientation (canting angle) distribution to obtain the bulk radar variables.

In general, the polarimetric radar variables can be expressed as integrals of the form

$$X = \int N(D)\, F(D, \epsilon, \mathbf{s})\, A(\theta)\, dD, \tag{3.1}$$

where $N(D)$ is the PSD, F represents the T-matrix-computed scattering amplitudes as functions of particle diameter D, complex dielectric constant ϵ, and particle shape $\mathbf{s}$, and $A(\theta)$ denotes the angular moments describing the particle orientation distribution. Z_H is obtained from the integrated backscattering cross sections, Z_{DR} from the ratio of the horizontally and vertically polarized backscattered powers, and K_{DP} from the difference between the forward-scattering amplitudes at horizontal and vertical polarization. Consequently, the simulated radar observables depend jointly on the evolving PSD, the electromagnetic scattering characteristics of individual melting hailstones, and their orientation within the radar sampling volume (Ryzhkov et al., 2013a,a; Carlin and Ryzhkov, 2025).

Because hailstones frequently exceed the Rayleigh scattering limit at S-band wavelengths, particularly as diameters approach several centimeters, the forward operator

employs a two-layer T-matrix rather than relying solely on the Rayleigh approximation. The scattering solution accounts for the changing dielectric properties of melting hailstones, including the transition from dry ice to water-coated particles and eventually fully melted raindrops. These evolving dielectric characteristics modify the relative horizontal and vertical backscattering amplitudes and the differential forward-scattering phase, producing the enhanced Z_H, elevated Z_{DR}, and increased K_{DP} that are characteristic of melting hail (Ryzhkov et al., 2013a). Unlike observational radar retrievals, which infer hydrometeor characteristics from measured radar variables, the forward operator follows the opposite approach by predicting radar signatures from known particle properties. This approach provides a physically consistent framework for evaluating model performance because differences between simulated and observed radar variables can be directly related to the underlying assumptions governing the modeled PSDs and microphysical evolution.

3.2.2 Representation of Hail Microphysics

The one-dimensional cloud model employed in this study explicitly simulates the descent and thermodynamic evolution of hail through the atmosphere. Rather than representing the hail population using a single bulk variable, the model discretizes the PSD into a series of 200 diameter bins, allowing the evolution of each size class to be calculated independently. At every model time step, the number concentration within each diameter bin is conserved while the masses of ice, liquid water, and entrained air are prognosed separately. These quantities determine the particle diameter, bulk density, terminal fall velocity, meltwater fraction, and thermodynamic state, all of which evolve in response to melting, evaporation, sublimation, water shedding, and vertical transport (Ryzhkov et al., 2013a). The separate treatment of ice, liquid water, and air is particularly important for low-density hail. Small hailstones often contain

substantial internal air voids, reducing their bulk density relative to solid ice.

During the initial stages of melting, liquid water preferentially infiltrates these pore spaces before a continuous external water layer develops. Only after the internal air volume becomes saturated does excess meltwater accumulate on the particle surface, eventually forming a torus, which is a liquid-water layer characteristic of melting hail. This evolution modifies the particle density, effective dielectric properties, and scattering behavior, making the separate prediction of the ice, water, and air components essential for accurately simulating polarimetric radar variables (Ryzhkov et al., 2013a,a). The collection of predicted number concentrations across the 200 diameter bins defines the PSD at each model level. Because each size bin evolves independently, the model explicitly resolves the continuous evolution of the hail size spectrum throughout the melting layer rather than diagnosing it from bulk quantities (Ryzhkov et al., 2013a; Carlin and Ryzhkov, 2025).

The thermodynamic evolution of each hailstone is determined from the local atmospheric conditions and the particle energy budget. As hail descends below the freezing level, sensible heat transferred from the surrounding air is used initially to warm the ice particle to the melting temperature. Once the particle reaches 0°C, additional energy is consumed through latent heating associated with melting, producing a liquid water layer that progressively surrounds the remaining ice core. The model continuously updates the ice mass, liquid water fraction, and particle diameter throughout this process, allowing the physical properties of each hailstone to evolve in response to the ambient temperature, humidity, and pressure profiles (Ryzhkov et al., 2013a).

During the descent of melting hail, the model works through various microphysical processes. Evaporation of meltwater reduces the total liquid water content under sufficiently dry environmental conditions, while sublimation removes ice mass when particles remain below the melting temperature in subsaturated air. The model also

represents water shedding once the liquid coating surrounding a hailstone exceeds the amount that can be retained by surface tension and aerodynamic forces. Excess liquid water is removed from the hailstone and transferred to the rainwater field, reducing the liquid mass of the melting hailstone while increasing the ambient rainwater content. Rather than explicitly predicting the size spectrum of the shed drops, the model assumes that the shed water follows a prescribed, fixed raindrop size distribution.

This simplification neglects potential variability in the sizes of shed drops arising from differences in hailstone size, meltwater thickness, or environmental conditions, but provides a computationally efficient representation of the transfer of liquid water from melting hail to the rain field (Ryzhkov et al., 2013a). The redistribution of liquid water through shedding alters the partitioning of mass between hail and rain and therefore affects the simulated dielectric properties and polarimetric radar variables. These interacting processes modify particle size, mass, density, and liquid water fraction simultaneously, producing realistic transitions from dry hail aloft to partially melted hail and eventually rain near the surface (Ryzhkov et al., 2013a; Dawson et al., 2010).

As melting continues, hailstones may also undergo breakup. When the remaining ice core becomes sufficiently small relative to the surrounding liquid water, the particle can no longer maintain its structural integrity, causing it to fragment into multiple smaller particles. In the model, the resulting fragments are redistributed among the hail and rain size distributions according to prescribed parameterizations rather than being explicitly resolved. Breakup therefore modifies both the hail and rain PSDs by increasing the concentration of smaller particles while reducing the number of large melting hailstones, influencing the subsequent evolution of the simulated polarimetric radar variables (Ryzhkov et al., 2013a).

Particle motion is governed by the balance between terminal fall velocity and the ambient vertical air motion. Terminal fall speeds vary with particle size, density, and

meltwater fraction, allowing larger hailstones to descend more rapidly than smaller particles while remaining responsive to environmental updrafts or downdrafts. In the present study, prescribed environmental soundings provide the thermodynamic structure through which the hail descends, while the model optionally includes dynamically calculated vertical air motion that evolves in response to evaporative cooling and precipitation loading. The interaction between particle fall speed and vertical air motion determines the residence time of hail within the melting layer and therefore strongly influences the degree of melting experienced before reaching the surface (Ryzhkov et al., 2013a; Carlin and Ryzhkov, 2025).

Although the model captures the primary physical processes governing the descent of melting hail, several simplifying assumptions are required to maintain computational efficiency. The simulations are performed within a one-dimensional vertical framework that neglects horizontal transport and assumes horizontally homogeneous environmental conditions. Hydrometeor interactions are represented through parameterized microphysical relationships rather than explicit particle-scale collisions or three-dimensional airflow around individual hailstones. Despite these simplifications, the model reproduces the dominant thermodynamic and microphysical processes responsible for the evolution of melting hail and provides a physically consistent framework for examining their associated polarimetric radar signatures.

3.2.3 Model Assumptions and Limitations

As with any numerical model, the one-dimensional hail model employed in this study relies on a series of simplifying assumptions that balance physical realism with computational efficiency. These assumptions allow the dominant thermodynamic and microphysical processes governing hail melting to be represented while maintaining sufficiently low computational expense to perform large numbers of simulations across a

range of environmental conditions. The resulting simulations are therefore intended to isolate the primary controls on hail evolution rather than reproduce every aspect of an observed storm.

The model assumes a one-dimensional, vertically varying atmosphere in which all thermodynamic variables depend only on height. Horizontal variability in temperature, moisture, and wind is neglected, and hydrometeors are assumed to descend through a horizontally homogeneous environment. This framework excludes processes such as horizontal advection, storm-scale circulation, turbulent mixing, and interactions with neighboring convective cells. Although these processes influence the evolution of hail within real thunderstorms, the one-dimensional formulation isolates the effects of vertical thermodynamic structure and microphysical evolution, allowing the influence of individual environmental parameters to be more clearly identified (Ryzhkov et al., 2013a; Carlin and Ryzhkov, 2025).

The initial hail PSD represents another important modeling assumption. Each simulation begins with a prescribed PSD derived from aircraft observations, and the subsequent evolution of the hail population depends directly on these initial conditions. Any uncertainty associated with the observed PSD, including sampling limitations of the largest hailstones or uncertainty in fitted distribution parameters, propagates through the simulation and influences the modeled radar variables. While the reprocessed T-28 dataset provides substantially improved estimates of hail size distributions relative to earlier versions of the dataset, the simulations remain dependent upon the quality and representativeness of the available in situ observations.

The model explicitly predicts the evolution of the hail size spectrum while representing unresolved particle-scale processes, including shape evolution, meltwater redistribution, water shedding, fragmentation, and orientation, using physically based parameterizations. Individual particle collisions, aggregation, fragmentation, and ir-

regular variations in particle shape are not explicitly resolved. Instead, each size bin represents the average behavior of a population of particles with similar diameters and thermodynamic properties. This approach substantially reduces computational cost while preserving the dominant processes controlling the evolution of the PSD.

The radar forward operator likewise incorporates several assumptions regarding hydrometeor scattering properties. Electromagnetic scattering calculations depend upon prescribed particle geometry, density, dielectric properties, and meltwater distribution The forward operator assumes smooth spheroidal hailstones with prescribed axis ratios and idealized orientation distributions. In contrast, natural hailstones are frequently irregular, possess rough surfaces and internal air cavities, and may develop asymmetric meltwater coatings during melting (Knight and Knight, 1973). These departures from the assumed particle geometry introduce uncertainty into the simulated polarimetric radar variables., particularly for large, partially melted hailstones whose scattering behavior becomes increasingly complex (Bringi and Chandrasekar, 2001; Ryzhkov et al., 2013a).

Furthermore, Dry hailstones are represented using prescribed spheroidal shapes with specified axis ratios, while melting hailstones are parameterized as water-coated spheroids whose dielectric properties and geometry evolve as the liquid-water fraction increases. Particle orientation is likewise prescribed through an idealized canting-angle distribution rather than being predicted dynamically. Consequently, the simulated polarimetric radar variables depend not only on the modeled microphysical evolution, but also on the assumed particle shape, orientation, and meltwater distribution. These assumptions are expected to have the greatest influence on Z_{DR} and K_{DP}, whereas Z_H remains more strongly controlled by particle size and dielectric constant.

Despite these limitations, the one-dimensional model provides an effective framework for investigating the physical relationships between hail microphysics and polari-

metric radar observations. By explicitly representing the dominant thermodynamic and microphysical processes governing hail descent while minimizing computational complexity, the model allows for the systematic evaluation of how PSDs, environmental conditions, and vertical air motion influence the resulting radar signatures. The simulations presented in this study should therefore be interpreted as physically consistent representations of the principal processes controlling melting hail rather than exact reproductions of individual storms.

3.3 Adaptations for the Present Study

Although the physical formulation of the one-dimensional downburst model remained unchanged, several methodological adaptations were implemented to facilitate application of the model to the historical T-28 observational archive. These modifications were designed to provide a consistent and reproducible framework for initializing simulations using observed hail PSDs together with representative environmental conditions. The principal developments include automated initialization using ERA5 atmospheric reanalysis, direct integration of the reprocessed T-28 PSD database, and an automated workflow for large-scale batch execution. These adaptations preserve the underlying physics of the original model while extending its application to a unique observational dataset.

3.3.1 Environmental Ingest Using ERA5

The original implementation of the one-dimensional downburst model was designed to initialize simulations using observed atmospheric soundings. When representative proximity soundings are available, this approach provides an appropriate description of the environmental thermodynamic profile. Application of the model to the historical

T-28 dataset, however, introduced several practical limitations. The aircraft observations span eleven research flights conducted between 1995 and 2003, during which many severe storms occurred between scheduled radiosonde launches or at considerable distances from the nearest upper-air observing station. As a result, any archived soundings found were not consistently representative of the thermodynamic environment immediately surrounding the sampled storm.

To provide a consistent environmental initialization for every aircraft observation, the model was modified to ingest atmospheric profiles derived from the European Centre for Medium-Range Weather Forecasts (ECMWF) ERA5 atmospheric reanalysis. ERA5 provides hourly global analyses of atmospheric state variables on a regular spatial grid and has become widely used for retrospective analyses of historical weather events because of its temporal consistency and comprehensive spatial coverage.

For each T-28 observation, the aircraft latitude, longitude, date, and observation time were extracted from the reprocessed dataset described in Chapter 2. These quantities were used to identify the nearest ERA5 analysis in both space and time. Atmospheric temperature, relative humidity, and geopotential height, were subsequently extracted from the corresponding pressure levels and interpolated onto the vertical grid required by the numerical model.

Because ERA5 provides geopotential height referenced to mean sea level, surface geopotential fields were additionally used to convert each profile to height above ground level (AGL). This conversion ensured consistency between the atmospheric initialization and the model's vertical coordinate system while preserving the observed thermodynamic structure surrounding each aircraft observation. The resulting workflow allowed every simulation to be initialized using an internally consistent environmental profile without requiring manual selection of proximity soundings.

3.4 Simulation Configuration

Simulations were integrated for 600 s runs to ensure the environment achieves steady-state. These runs updated at 2 s time intervals using a fixed height grid spacing of 200 m and a model top of 4 kilometers. At each time step, the model predicts the evolving hail PSD together with the corresponding thermodynamic and dynamic response of the surrounding atmosphere.

Chapter 4

Analysis of the PSD Data and Simulated Profiles

The results presented in this chapter evaluate how the reprocessed T-28 PSD observations influence simulated polarimetric radar profiles and downdraft evolution. The analysis focuses on three connected aspects of the simulations: the sensitivity of modeled polarimetric radar variables to the prescribed hail PSD, the influence of vertical velocity field updates on simulated radar profiles, and the comparison of the model output with independent radar observations.

The first portion of this chapter will examine the full suite of model simulations using all available T-28 PSDs. These simulations are used to determine whether the reprocessed observations produce physically reasonable vertical profiles of Z_H, Z_{DR}, and K_{DP}. The second portion evaluates the role of maximum hail diameter ($D_{\max}$) by comparing simulations initialized with different definitions of the upper limit of the hail PSD. The remainder examines the effect of vertical velocity field updates by comparing simulations performed with and without feedback between the evolving hydrometeor population and the vertical air motion.

4.1 Simulated Radar Profiles from the Full T-28 Dataset

The analyses presented in this section focus on the simulated radar variables at the conclusion of the 600-s integration period. At this time, the model will have achieved steady-state, allowing sufficient interaction between the hydrometeors and the surrounding atmosphere to produce mature vertical profiles of Z_H, Z_{DR}, and K_{DP}.

Collectively, these three radar variables provide complementary information regarding the evolution of melting hail. Z_H is primarily sensitive to the total scattering power of the hydrometeor population and is therefore dominated by the largest hailstones within the PSD. Z_{DR} provides information regarding particle shape and the degree of melting through differences between horizontally and vertically polarized backscatter. In contrast, K_{DP} is primarily controlled by the concentration of anisotropic liquid hydrometeors along the radar propagation path and therefore responds strongly to changes in liquid water content and particle number concentration. Evaluating these variables simultaneously provides a physically complete description of the melting process, allowing the respective influences of particle size, particle geometry, and hydrometeor concentration to be examined independently.

Figure 4.1 presents the mean vertical profiles of Z_H, Z_{DR}, and K_{DP} computed from the complete set of T-28 simulations. Five separate experiments are shown. Three simulations were initialized using the fitted, maximum observed, and Ulbrich definitions of $D_{\max}$ described in Chapter 2, while two additional simulations compare model integrations performed with and without vertical velocity field updates, denoted as "$w_{opt} = True$" and "$w_{opt} = False$", respectively. Because all simulations employ identical numerical parameters and environmental data from the same archive, differences

among the profiles primarily reflect changes in the prescribed hail PSD or the treatment of the evolving downdraft.

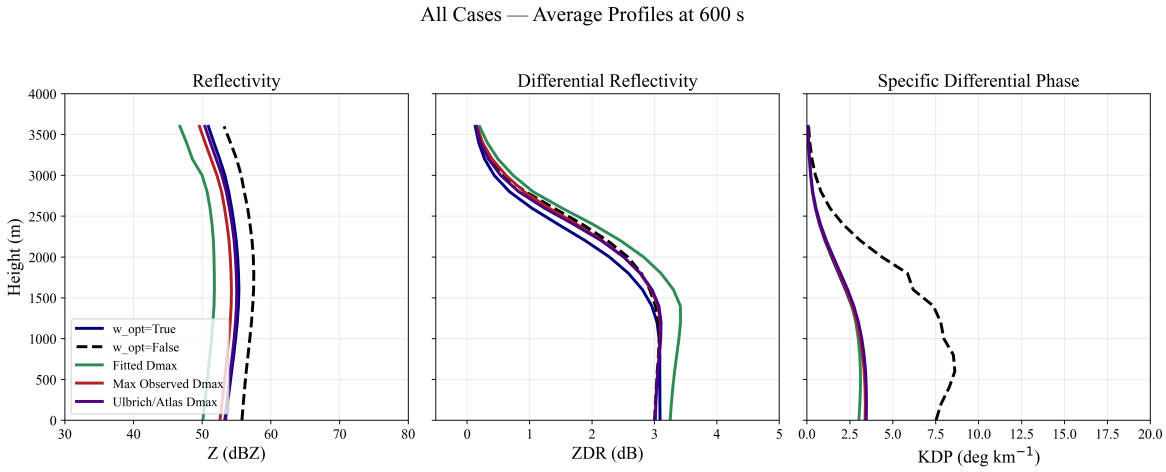


Figure 4.1: Mean vertical profiles of simulated horizontal reflectivity (Z_H), differential reflectivity (Z_{DR}), and specific differential phase (K_{DP}) after 600 s of model integration for all T-28 simulations. Profiles are shown for the three $D_{\max}$ estimation methods together with simulations performed with and without vertical velocity field updates.

The modeled Z_H profiles exhibit remarkably similar vertical structures despite the different initialization methods. In all experiments, Z_H remains relatively large throughout the lower 4 km of the atmosphere, indicating that substantial concentrations of large melting hydrometeors persist as the hail population descends. Z_H generally increases toward lower altitudes before reaching a broad maximum near the surface, consistent with the continued presence of large melting hailstones together with increasing liquid water content. Similar vertical structures have been reported in previous spectral microphysical simulations of melting hail, where the competing effects of decreasing particle diameter and increasing dielectric constant produce relatively modest changes in Z_H throughout the melting layer (Ryzhkov et al., 2013b).

Although the overall profile shapes are nearly identical, systematic differences among the three $D_{\max}$ initialization methods are apparent. Simulations initialized using the fitted $D_{\max}$ consistently produce slightly lower Z_H values than simulations initialized

using either the maximum observed or Ulbrich $D_{\max}$ estimates. This behavior follows directly from the strong dependence of radar reflectivity upon particle diameter. Because Z_H is proportional to approximately the sixth power of particle diameter in the Rayleigh scattering regime, relatively few large hailstones dominate the bulk radar signal. Consequently, even slight differences in the prescribed upper limit of the PSD produce measurable changes in simulated Z_H. However, the relatively small separation among the three curves indicates that the overall Z_H structure is governed not only by the largest hailstones but also by the concentration and shape of the broader PSD.

An important result is that the three $D_{\max}$ initialization methods remain substantially more similar than might be expected given the strong dependence of radar reflectivity upon particle diameter. Although extending the upper tail of the PSD introduces larger hailstones capable of contributing disproportionately to Z_H, these particles represent only a very small fraction of the total particle population. The bulk radar signature therefore continues to be governed by the complete PSD rather than by a single estimate of the largest observed particle. This finding suggests that uncertainty associated with defining $D_{\max}$ contributes less to the simulated radar variability than the natural differences among the observed hail PSDs themselves. In other words, accurately characterizing the overall PSD appears to be more important than selecting one particular definition of the maximum hail diameter.

The simulated Z_{DR} profiles exhibit a distinctly different behavior. Unlike Z_H, which is primarily controlled by particle size, Z_{DR} depends strongly upon particle shape, orientation, and liquid water fraction. Dry hailstones generally produce relatively small Z_{DR} because their nearly spherical geometry results in similar horizontal and vertical scattering characteristics. As melting progresses, however, liquid water accumulates preferentially around the hailstone surface while shed drops are introduced into the surrounding particle population. Both processes increase the nonsphericity of the scat-

tering particles and enhance Z_{DR}.

This physical evolution is evident throughout Figure 4.1. Values of Z_{DR} remain relatively small near the upper portion of the modeled domain, where melting is limited, before increasing steadily toward the lower atmosphere as the melting process progresses. The largest values occur within the warmest portion of the model domain where water-coated hailstones and shed liquid drops become increasingly abundant. Similar behavior has been documented in both observational and theoretical investigations of melting hail, including the spectral simulations of Ryzhkov et al. (2013a,b), which demonstrated that melting significantly increases Z_{DR} while maintaining relatively large Z_H values characteristic of hail-producing storms.

The gradual increase in Z_{DR} through the melting layer also demonstrates that Z_{DR} is responding primarily due to the change of the bulk dielectric constant caused by the increase of the water fraction caused by melting. As hailstones melt, the accumulation of liquid water and the production of shed drops increase the asymmetry of the hydrometeor population, enhancing the differential scattering between the horizontal and vertical polarizations. Because these processes occur progressively throughout the descent of the hailstones, the resulting increase in Z_{DR} represents a physically consistent indicator of melting intensity rather than a direct measure of hail size alone.

The response of K_{DP} differs substantially from both Z_H and Z_{DR}. Whereas Z_H is dominated by the largest particles within the size distribution and Z_{DR} is primarily controlled by particle shape and liquid water fraction, K_{DP} is fundamentally a measure of the integrated phase shift produced by anisotropic liquid hydrometeors along the radar propagation path. As a result, K_{DP} responds strongly to both particle concentration and the amount of liquid water contained within the melting population. Previous theoretical investigations have consistently shown that K_{DP} is among the most sensitive polarimetric variables for diagnosing mixed-phase precipitation because relatively

small changes in particle concentration or liquid water content can produce substantial changes in differential phase (Ryzhkov et al., 2013a,b; Kumjian et al., 2018).

The simulated profiles shown in Figure 4.1 are consistent with these theoretical expectations. In all experiments, K_{DP} remains relatively small near the upper portion of the model domain where the hail population consists primarily of frozen particles with limited liquid water content. As melting progresses during descent, the accumulation of liquid water on the hailstone surface together with the production of shed drops increases the differential propagation phase experienced by the transmitted radar pulse. It can be noted that K_{DP} increases steadily toward lower altitudes, producing the characteristic enhancement associated with melting hail. The overall profile shape agrees closely with previous numerical simulations of melting hail reported by Ryzhkov et al. (2013b), demonstrating that the reprocessed T-28 PSDs produce physically realistic evolution of the melting layer.

Although all three $D_{\max}$ initialization methods produce similar overall K_{DP} structures, the magnitude of the phase shift differs systematically among the simulations. The fitted $D_{\max}$ initialization generally produces the largest K_{DP} values, whereas the maximum observed and Ulbrich definitions produce somewhat smaller phase shifts throughout much of the modeled layer. Unlike Z_H, these differences cannot be attributed solely to the largest hailstones within the PSD. Instead, they reflect subtle differences in the concentration of melting particles and the amount of liquid water generated during descent. Because K_{DP} depends upon the cumulative contribution of all anisotropic liquid hydrometeors within the radar sampling volume, modifications to the overall particle spectrum influence the simulated phase response more strongly than the Z_H response.

Unlike Z_H, which is dominated by the relatively small number of the largest hailstones, K_{DP} integrates the cumulative contribution from the entire melting hydrome-

teor population. Thus, modest changes in particle concentration produce measurable differences in differential phase. This distinction explains why the fitted $D_{\max}$ initialization produces larger values of K_{DP} despite only minor changes in Z_H. The result emphasizes that concentration-sensitive radar variables respond to the complete PSD rather than to the upper tail alone, highlighting the importance of accurately representing the observed particle spectrum when simulating polarimetric radar signatures.

While the mean profiles summarize the overall behavior of the simulation set, they necessarily obscure the considerable variability among individual T-28 observations. Figure 4.2 therefore presents the same radar variables together with shaded envelopes representing the spread among all modeled cases. Rather than illustrating only the average response, these profiles demonstrate the range of radar signatures that can result from the diversity of hail PSDs observed by the T-28 aircraft.

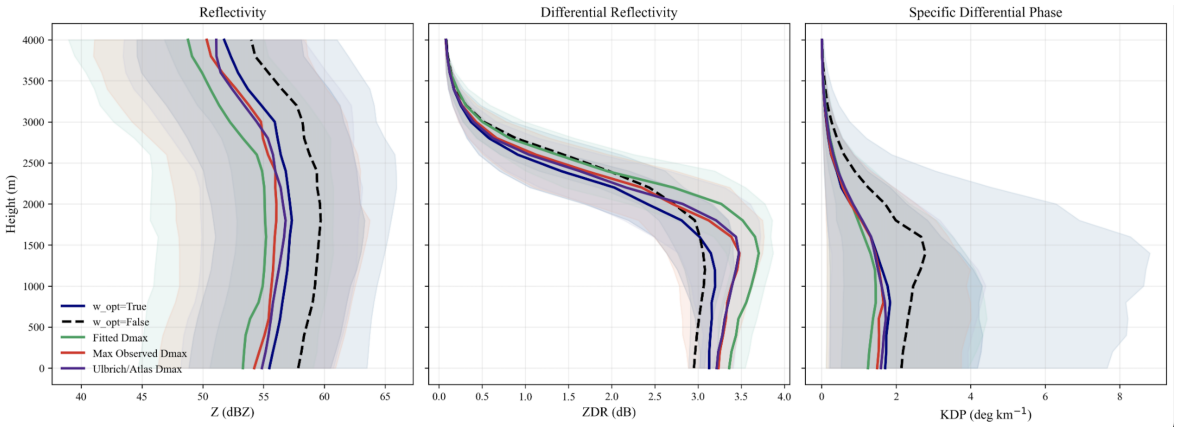


Figure 4.2: Mean simulated vertical profiles of Z_H, Z_{DR}, and K_{DP} after 600 s together with the variability among all modeled T-28 simulations. Shaded regions denote the spread among individual simulations for each experiment.

Several important features become evident once the variability among simulations is considered. First, the spread in Z_H is substantially larger than suggested by the mean profiles alone. Individual simulations span nearly 20 dB at some heights, illustrating the wide range of hail populations represented within the reprocessed T-28 dataset.

This variability reflects differences in both the observed PSDs and the environmental conditions used to initialize the model. Despite this broad range of Z_H values, the mean profiles remain remarkably consistent, indicating that the underlying microphysical evolution follows similar pathways across the complete observational dataset.

The variability in Z_{DR} exhibits a different structure. Near the upper portion of the modeled layer, where melting remains limited, relatively little spread is present among the simulations. As particles descend into progressively warmer air, however, the spread increases substantially. This behavior reflects the increasing sensitivity of Z_{DR} to melting rate, particle shape, and the production of liquid water. Because these processes depend on both the initialized PSD and the surrounding thermodynamic environment, individual storms naturally produce a broader range of Z_{DR} values within the lower portion of the melting layer.

The greatest variability occurs in K_{DP}. In particular, simulations performed without vertical velocity field updates occupy the upper envelope of the distribution throughout much of the lower atmosphere. This result immediately suggests that processes beyond particle size alone influence the simulated phase response. While the initialized hail PSD establishes the available hydrometeor population, subsequent evolution of the atmospheric flow field modifies the concentration of melting particles within each model layer. The resulting concentration changes produce systematic differences in K_{DP} that are considerably larger than those observed in either Z_H or Z_{DR}.

Overall, these simulated profiles are consistent with the expected physical behavior of the radar variables. Z_H exhibits the greatest sensitivity to the assumed maximum hail size because of its strong weighting toward the largest particles, whereas K_{DP} changes comparatively little because it remains governed primarily by the concentration of smaller melting hydrometeors. The relatively modest changes in Z_{DR} further suggest that variations in particle shape and dielectric evolution are less sensitive to the chosen

$D_{\max}$ definition than the total scattering power represented by Z_H.

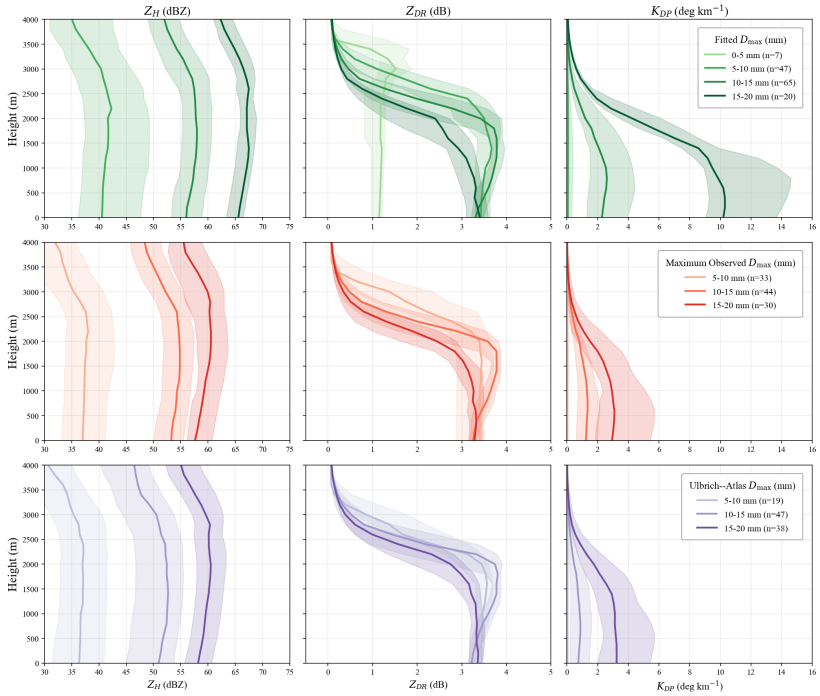


Figure 4.3: Median simulated vertical profiles of horizontal reflectivity (Z_H), differential reflectivity (Z_{DR}), and specific differential phase (K_{DP}) after 600 s of model integration, grouped by 5-mm $D_{\max}$ bins for each $D_{\max}$ estimation method. Rows correspond to the fitted, maximum observed, and Ulbrich–Atlas $D_{\max}$ definitions, respectively. Solid curves denote median profiles within each bin, and shaded regions indicate the interquartile range across simulations.

4.1.1 Closer Examination of $D_{\max}$ Estimations

Since these ensemble-average profiles indicate relatively small differences among the three $D_{\max}$ estimation methods, additional structure emerges when the simulations are stratified by estimated maximum hail size. Figure 4.3 shows median profiles of Z_H, Z_{DR}, and K_{DP} grouped into 5-mm $D_{\max}$ bins for each estimation method. This binning separates storms with smaller and larger initialized hail populations and reveals sensitivities that are partially hidden when all simulations are averaged together.

The Z_H profiles show the clearest monotonic response to increasing $D_{\max}$. Across

all three estimation methods, larger $D_{\max}$ bins produce systematically larger values of Z_H throughout much of the model depth. This behavior is consistent with the strong dependence of Z_H on particle diameter. Because Z_H is weighted heavily toward the largest hydrometeors, small changes in the concentration of large hailstones can produce substantial changes in Z_H. The fitted and maximum observed $D_{\max}$ methods show particularly clear separation among the hail-size bins, indicating that the upper tail of the PSD strongly influences the modeled Z_H profile.

The Z_{DR} response differs from Z_H. Larger hail-size bins do not simply produce larger Z_{DR}. Instead, the largest hail classes often exhibit lower or delayed Z_{DR} enhancement compared with smaller hail classes. This behavior is physically reasonable because larger hailstones melt more slowly and may remain more nearly spherical or irregular while descending through the modeled layer. Smaller hailstones melt more rapidly, producing water-coated particles and shed liquid drops higher in the column, which enhances Z_{DR} earlier during descent. Thus, the vertical placement and magnitude of the Z_{DR} maximum provide information about melting rate and liquid water production rather than maximum hail size alone.

The strongest sensitivity appears in K_{DP}, especially for the largest $D_{\max}$ bins. The fitted $D_{\max}$ method produces the largest values of K_{DP} in the 15–20 mm bin, with enhanced values extending through the lower portion of the modeled layer. This response reflects the concentration of liquid water produced as larger hailstones melt and shed mass during descent. Unlike Z_H, which is dominated by the largest particles, K_{DP} responds to the cumulative concentration of anisotropic liquid and melting hydrometeors within the radar sampling volume. As larger hailstones shed water, liquid mass is transferred from the fast-falling hail population into slower-falling raindrops, increasing liquid water residence time and enhancing the simulated differential phase.

The K_{DP} enhancement in the largest hail bins also highlights an important modeling

consideration. Because the model updates all species using a common time step, water shed from rapidly descending hailstones is transferred into the rain category, where particles fall more slowly and may accumulate within the column. This process is physically consistent with enhanced liquid water production during hail melting, but it may also amplify near-surface K_{DP} if shed water remains concentrated for too long. Therefore, the largest-bin K_{DP} values should be interpreted as evidence of strong sensitivity to meltwater production, while also motivating future refinement of the drop-shedding and sedimentation treatment.

The largest simulated K_{DP} values may also resemble the behavior documented "SPLASH" storms, where unusually large concentrations of small melting hail produce exceptionally high specific differential phase despite only modest changes in reflectivity. Such environments have been shown to produce substantial overestimation when conventional $R(K_{DP})$ rainfall relationships are applied.

Overall, Figure 4.3 demonstrates that the importance of $D_{\max}$ depends on how the simulations are analyzed. When all cases are averaged together, differences among $D_{\max}$ estimation methods appear relatively modest. When simulations are grouped by hail-size bin, however, systematic differences in Z_H, Z_{DR}, and K_{DP} become much clearer. This result suggests that $D_{\max}$ uncertainty is most important for interpreting storms containing the largest hailstones, where small differences in the upper tail of the PSD can produce large changes in radar variables, especially Z_H and K_{DP}.

Figures 4.1, 4.2, and 4.3 show that the simulated radar response depends on both the bulk PSD population and the estimated upper tail of the distribution. Ensemble-average profiles suggest that the three $D_{\max}$ methods produce broadly similar radar structures, but binning the simulations by $D_{\max}$ reveals clear microphysical sensitivity within individual hail-size classes. The dominant conclusion is therefore not that $D_{\max}$ is unimportant, but that its influence becomes most apparent when the simulations

are interpreted by hail-size category rather than by bulk ensemble mean. Although modest differences in K_{DP} were observed among the three $D_{\max}$ experiments, these changes were substantially smaller than those observed for reflectivity. This behavior is physically expected because K_{DP} depends primarily on the concentration of smaller, oblate melting hydrometeors rather than the few largest hailstones that dominate radar reflectivity.

These findings agree with theoretical expectations. Modifying only the maximum hail diameter primarily alters the sparsely populated upper tail of the PSD while leaving the bulk of the distribution unchanged. Additionally, variables dominated by the largest particles, particularly Z_H, respond more strongly than variables such as K_{DP} that depend on the integrated contribution of the broader particle population. The following section examines how environmental thermodynamic variability further modifies these modeled radar signatures through its influence on downdraft intensity.

4.2 Environmental Controls on Vertical Velocity

To evaluate the importance of the environmental profile within the present simulations, the maximum modeled downdraft velocity obtained from each experiment was compared with the corresponding environmental lapse rate derived from the ERA5 initialization profiles. Figure 4.4 summarizes this relationship for all modeled cases. Each point represents an individual simulation initialized using an observed T-28 hail PSD together with its associated environmental sounding.

A clear relationship exists between the environmental lapse rate and the strength of the modeled downdraft. Simulations initialized within environments characterized by steeper lapse rates generally produce substantially stronger downward velocities than simulations initialized within more stable environments. Although considerable vari-

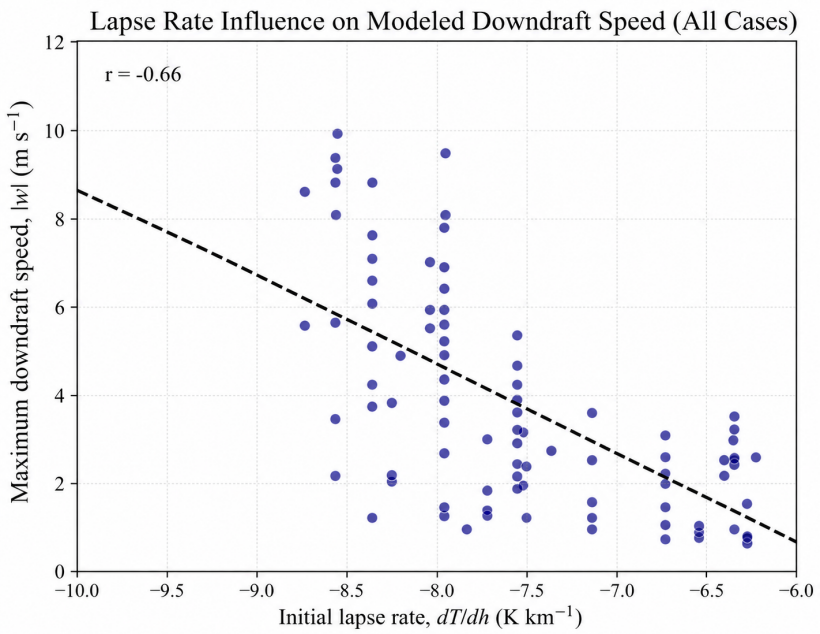


Figure 4.4: Relationship between the environmental lapse rate and the maximum modeled downdraft velocity for all simulations. The dashed line denotes the least-squares linear regression.

ability remains among individual cases, the overall trend indicates that environmental instability exerts a dominant influence on the magnitude of the modeled downdraft.

This behavior is physically expected. Steeper lapse rates reduce the static stability of the atmosphere, allowing negatively buoyant air generated through melting and evaporation to accelerate more readily toward the surface. In contrast, environments possessing weaker lapse rates provide greater resistance to vertical parcel motion, thereby limiting the downward acceleration even when identical hail PSDs are introduced into the model. Moreover, the efficiency with which melting hail generates a downdraft depends not only upon the characteristics of the hydrometeor population but also upon the thermodynamic structure through which that population descends.

The importance of lapse rate in severe convective storms has long been recognized within the severe storms literature. This relationship is also consistent with the environments known to favor severe hail production over the central United States.

Numerous observational studies have demonstrated that steep mid-level lapse rates associated with elevated mixed layers promote both intense updrafts and the development of large hail by increasing convective instability and supporting prolonged hail growth (e.g., Johns and Doswell, 1992; Rasmussen and Blanchard, 1998). The present simulations demonstrate that these same thermodynamic environments continue to influence storm evolution after hail formation has occurred. Once hail begins to descend through the melting layer, steep lapse rates enhance the downward acceleration of negatively buoyant air generated through melting and evaporation, producing stronger modeled downdrafts. Thus, the environmental lapse rate influences both the formation of large hail and its subsequent descent toward the surface.

Although the correlation is not perfect, this is not unexpected. The modeled downdraft represents the combined influence of numerous interacting processes, including melting rate, evaporation, precipitation loading, particle concentration, and environmental humidity. As a result, lapse rate alone cannot fully explain the variability in maximum downdraft velocity. Nevertheless, the significant negative relationship indicates that thermodynamic stability remains one of the primary controls governing downdraft evolution within the complete T-28 simulation dataset. The remaining scatter likely reflects differences in the initialized PSDs together with case-to-case variability in moisture profiles and melting efficiency.

4.3 Influence of Vertical Velocity Field Updates

Among the sensitivity experiments performed in this study, the inclusion of vertical velocity field updates produced the largest changes in the simulated polarimetric radar variables. While modifications to the initialized PSD altered the magnitude of the radar profiles, allowing the downdraft to evolve dynamically changed the manner in which

melting hydrometeors were distributed throughout the atmospheric column. These differences were most apparent in K_{DP}, while comparatively smaller changes were observed in Z_H and differential Z_H (Z_{DR}). This behavior suggests that storm dynamics influence concentration-dependent radar variables more strongly than those dominated by the largest hydrometeors.

Unlike the previous sensitivity experiments, which examined uncertainty associated with the initialized hail PSD, this comparison isolates the role of the evolving airflow. Both sets of simulations were initialized using identical environmental conditions and identical hail PSDs. The only difference between the two experiments was whether the vertical velocity field was permitted to evolve in response to melting, evaporation, and precipitation loading. Any differences between the resulting radar profiles therefore reflect the influence of storm dynamics rather than differences in the initialized microphysics.

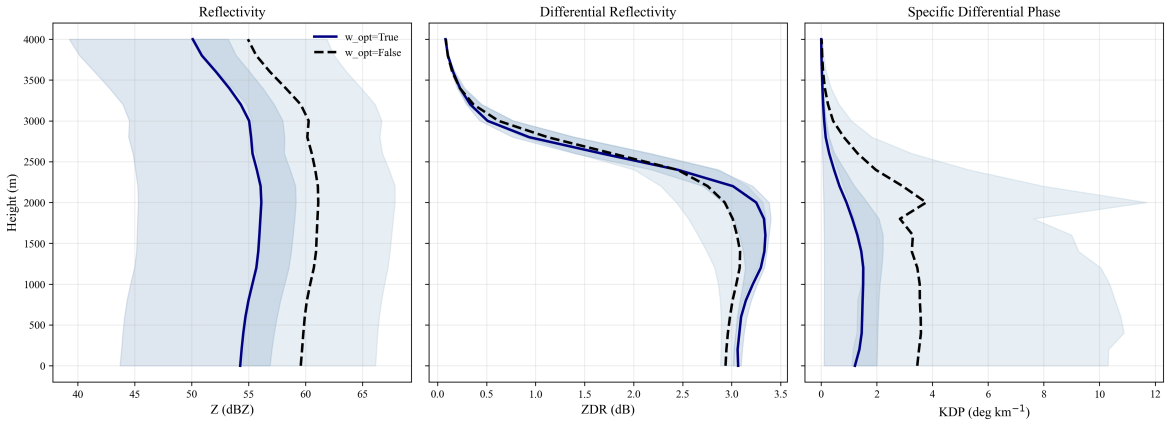


Figure 4.5: Comparison of simulated radar profiles after 600 s for simulations performed with and without vertical velocity field updates for the 29 June 200 case. Profiles are shown for horizontal reflectivity (Z_H), differential reflectivity (Z_{DR}), and specific differential phase (K_{DP}).

The influence of vertical velocity field updates is immediately evident in the modeled radar profiles. Z_H changes relatively little between the two simulations. Throughout

much of the modeled layer, differences remain within only a few decibels despite the development of substantially stronger downdrafts. This weak response indicates that the bulk Z_H continues to be controlled primarily by the largest melting hailstones rather than by modest changes in particle concentration. Although fewer particles occupy a given model layer as downward motion increases, the largest hailstones continue to dominate the radar backscatter, limiting the overall change in Z_H.

The response of Z_{DR} is somewhat larger but remains comparatively modest. Simulations including vertical velocity field updates generally produce slightly smaller values of Z_{DR} throughout the lower portion of the melting layer. This reduction reflects subtle differences in the melting history of the hydrometeor population. As downward motion increases, hailstones spend less time within each layer of the atmosphere before descending into warmer air. The resulting decrease in residence time limits the accumulation of liquid water on the particle surface and slightly reduces the asymmetry of the scattering population. Because Z_{DR} depends upon particle shape in addition to size, these changes produce measurable, although relatively small, reductions in Z_{DR}.

The largest response occurs in K_{DP}. Across nearly the entire melting layer, simulations including vertical velocity field updates produce systematically smaller values of K_{DP} than simulations performed without dynamical feedback. The separation between the two profiles is considerably larger than that observed for either Z_H or Z_{DR}, indicating that K_{DP} is substantially more sensitive to the evolving airflow than the remaining radar variables. This result is consistent across the full set of T-28 simulations and therefore represents a robust characteristic of the modeled melting process rather than the behavior of an individual case.

From an operational perspective, this result demonstrates that polarimetric radar signatures cannot always be interpreted solely in terms of microphysical evolution. Two storms possessing nearly identical hail PSDs aloft may produce measurably dif-

ferent values of K_{DP} if the storms differ substantially in their downdraft intensity. The present simulations therefore suggest that storm dynamics influence concentration-sensitive radar variables indirectly through their effect on the residence time and vertical distribution of melting hydrometeors. This distinction is particularly important when interpreting radar observations of mature hailstorms, where strong downdrafts frequently coexist with active melting.

The physical explanation for this behavior differs from the mechanisms controlling Z_H and Z_{DR}. Radar variables do not respond directly to vertical air motion. Instead, they respond to the evolving distribution of hydrometeors within the radar sampling volume. As the downdraft strengthens, particles descend more rapidly through the atmospheric column, reducing the amount of time that individual hailstones remain within any given model layer. For a fixed downward particle flux, shorter residence times produce lower particle concentrations. The total mass transported through the layer changes very little, but the instantaneous number of particles occupying that volume decreases.

This distinction is particularly important for K_{DP}. Unlike Z_H, which is heavily weighted toward the largest particles, K_{DP} depends upon the cumulative contribution of the entire melting hydrometeor population. A reduction in particle concentration therefore produces a nearly proportional reduction in differential phase. The simulations indicate that this concentration effect dominates the response of K_{DP} throughout the lower melting layer, explaining why the inclusion of vertical velocity field updates produces substantially smaller values despite relatively minor changes in the remaining radar variables.

The differing responses of the three radar variables provide insight into the relative importance of microphysical and dynamical processes within hail-producing storms. Z_H remains controlled primarily by the largest hailstones. Z_{DR} responds to the evolv-

ing geometry of melting particles and the production of liquid water. K_{DP}, however, integrates the effects of particle concentration throughout the radar sampling volume. Because storm dynamics modify concentration without substantially altering the largest hailstones, K_{DP} becomes the radar variable most sensitive to the evolving downdraft.

These results support the conceptual framework proposed by Carlin and Ryzhkov (2025), who demonstrated that storm dynamics influence polarimetric radar signatures indirectly through modifications to the hydrometeor population. The present simulations extend that work by applying the same physical framework to observed hail PSDs measured by the T-28 aircraft. Rather than relying upon idealized particle spectra, the concentration effect emerges naturally across a diverse collection of observed hail populations spanning multiple field campaigns and environmental conditions.

The simulated response to the evolving downdraft is likewise physically consistent. Increasing downward air motion reduces the local concentration of hydrometeors required to maintain a constant particle flux, producing modest reductions in concentration-sensitive radar variables. Because particle size itself changes comparatively little, the simulated decreases remain substantially smaller than those associated with changes in the assumed hail PSD. These results suggest that PSD uncertainty remains the dominant source of variability in the simulated radar signatures, while vertical transport primarily produces secondary modifications through changes in concentration.

4.3.1 Implications for Polarimetric Rainfall Estimation

The reduction in simulated K_{DP} associated with vertical velocity field updates has implications beyond the interpretation of melting hail alone. K_{DP} is widely used in operational quantitative precipitation estimation (QPE) because it is largely immune

to calibration errors, attenuation, partial beam blockage, and many of the uncertainties affecting reflectivity-based rainfall algorithms (Bringi and Chandrasekar, 2001; Ryzhkov et al., 2005). As a result, numerous operational and research applications estimate rainfall rate directly from K_{DP} or from blended relationships that combine K_{DP} with other polarimetric radar variables.

Radar rainfall estimation typically assumes that hydrometeor concentrations are determined by the PSD and fall speed in still air. However, in the presence of a downdraft, the relevant velocity is not simply the terminal fall speed, but the particle fall speed relative to the ground. For a steady particle flux, conservation of number concentration may be written schematically as

$$N(D)V_T(D) = N_w(D)\left[V_T(D) + w\right], \tag{4.1}$$

where $N(D)$ is the particle concentration in the absence of vertical air motion, $N_w(D)$ is the concentration in the presence of downdraft velocity w, and $V_T(D)$ is the terminal velocity of particles with diameter D. Solving for the concentration in the downdraft case gives

$$N_w(D) = N(D)\frac{V_T(D)}{V_T(D) + w}. \tag{4.2}$$

Thus, for positive downward velocity, the concentration of particles within a radar sampling volume is reduced even if the downward particle flux remains unchanged.

Many polarimetric rainfall algorithms estimate rainfall rate using empirical relationships of the form

$$R = aK_{DP}^{b}, \tag{4.3}$$

where R is rainfall rate and a and b are empirically determined coefficients. One

example currently used for rain mixed with hail is (Ryzhkov and Zrnić, 1996)

$$R(K_{DP}) = 44K_{DP}^{0.82}. \tag{4.4}$$

Because K_{DP} decreases when downdraft-induced concentration reductions occur, rainfall rates estimated from Eq. (4.4) may be biased low in regions of strong downdraft and melting hail.

Within the present simulations, however, changes in K_{DP} arise even though the initialized hail PSD remains unchanged. The reduction is instead produced by the evolving downdraft, which modifies the residence time and concentration of melting particles within each model layer. Since the magnitude of K_{DP} depends upon the integrated contribution of the hydrometeor population along the radar propagation path, decreases in particle concentration naturally produce smaller differential phase values. The simulated reduction in K_{DP} therefore reflects a dynamical response rather than a change in the intrinsic scattering characteristics of the hailstones themselves.

Both radar reflectivity in linear units and K_{DP} are directly proportional to hydrometeor concentration. Therefore, reductions in concentration produced by stronger downdrafts decrease both variables in a physically similar manner. The apparent difference in sensitivity arises because radar reflectivity is conventionally displayed on the logarithmic dBZ scale, whereas K_{DP} is reported in linear units. Consequently, relatively similar fractional decreases in concentration appear much larger in K_{DP} than in displayed reflectivity.

Figure 4.6 illustrates the conceptual relationship between downdraft evolution, particle concentration, K_{DP}, and rainfall estimation. As downward air motion strengthens, hydrometeors are transported more rapidly through the melting layer. The shorter residence time reduces the instantaneous particle concentration within the radar sampling

volume, decreasing the simulated value of K_{DP}. If conventional rainfall algorithms interpret this reduced differential phase without accounting for the evolving storm dynamics, the resulting rainfall estimate may also be reduced.

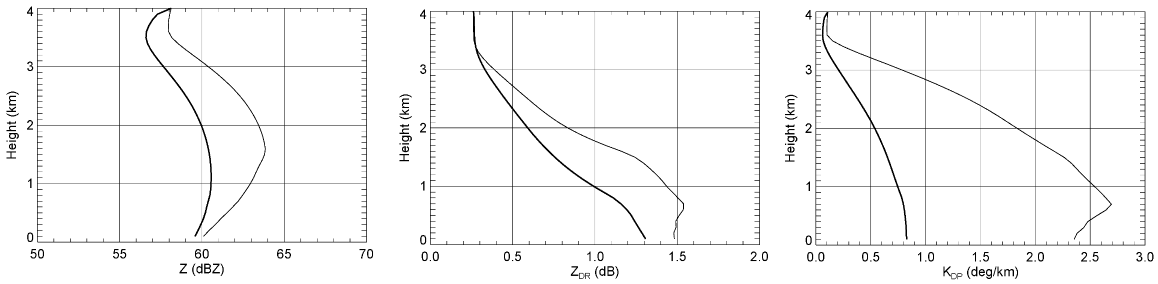


Figure 4.6: Illustration of the influence of downdraft velocity on K_{DP}-based rainfall estimation. The solid curve represents the particle size distribution and corresponding K_{DP} in the absence of vertical air motion ($w = 0$ m s^{-1}), while the thin line represents the same particle flux in the presence of a 20 m s^{-1} downdraft. Figure provided by Dr. Alexander Ryzhkov in tandem with this research avenue.

For the example shown in Figure 4.6, increasing the downdraft velocity from 0 to 20 m s^{-1} reduces the K_{DP}-based rainfall estimate from 88.5 to 37.6 mm h^{-1}, a factor of approximately 2.3. This example illustrates that the negative rainfall bias does not arise because the radar variable depends directly on vertical velocity. Instead, the bias arises because downdraft motion modifies the particle concentration that determines K_{DP}. This distinction is central to the interpretation of the simulations presented here: vertical velocity field updates alter radar variables through hydrometeor redistribution, not through the scattering calculation itself.

It is important to emphasize that these simulations do not demonstrate that operational rainfall algorithms are fundamentally incorrect. Rather, they suggest that an implicit assumption often made during radar rainfall estimation—that the observed hydrometeor concentration is independent of the evolving storm dynamics—may not always be satisfied in regions containing melting hail. During periods of strong downdraft development, the particle population sampled by the radar is continually redis-

tributed by the surrounding airflow. Although the total hydrometeor mass remains similar, the instantaneous concentration within an individual radar sampling volume decreases, reducing K_{DP} while leaving Z_H comparatively unchanged.

This distinction is particularly relevant within severe hail-producing storms, where melting, evaporation, precipitation loading, and strong downdrafts frequently occur simultaneously. In these environments, radar variables represent the combined response of both microphysical evolution and storm dynamics rather than the PSD alone. The present simulations indicate that neglecting the influence of vertical air motion may contribute to lower estimates of rainfall derived from K_{DP} during periods of intense melting. Quantifying the magnitude of this potential bias is beyond the scope of the present study; however, the simulations clearly demonstrate that storm dynamics influence concentration-sensitive radar variables through physically realistic mechanisms.

Although this result emerged from a one-dimensional modeling framework, the underlying physical mechanism is not unique to the present simulations. Any environment in which strong downdrafts modify the residence time of melting hydrometeors may experience similar changes in particle concentration. This finding suggests that future improvements in polarimetric rainfall estimation may benefit from accounting for dynamical processes in addition to traditional microphysical assumptions, particularly in storms producing large hail and intense downdrafts.

The importance of this result extends beyond rainfall estimation. Because K_{DP} is frequently incorporated into hail detection, hydrometeor classification, and quantitative precipitation estimation algorithms, changes in particle concentration associated with storm dynamics have the potential to influence multiple operational radar products simultaneously. These simulations therefore demonstrate that the evolving airflow should be considered alongside microphysical processes when interpreting polarimetric radar observations of severe convection.

Even though we are primarily focusing on the interpretation of melting hail, these findings have broader implications for operational radar applications. Because K_{DP} contributes to quantitative precipitation estimation, hydrometeor classification, and several radar-based hail detection algorithms, dynamical modifications to particle concentration may influence multiple operational products simultaneously. Future work should therefore investigate the extent to which vertical air motion can be incorporated into polarimetric retrieval algorithms designed for severe convective storms.

4.4 Discussion

The simulations presented in this chapter identify several processes that systematically modify the polarimetric radar signatures associated with melting hail. These include uncertainty in the initialized PSD, variability in the environmental thermodynamic profile, and feedback between the evolving downdraft and the hydrometeor population. An important question is whether these modeled behaviors are relevant to operational radar observations.

John Krause (CIWRO) developed one of the largest observational climatologies of polarimetric radar signatures associated with severe hail using 25,520 hail reports from 1,560 hail-producing storms observed by the WSR-88D network across the contiguous United States. Storms were grouped according to maximum reported hail diameter into four classes: Class 1 (1.0–3.5 cm), Class 2 (3.5–6.0 cm), Class 3 (6.0–10.0 cm), and Class 4 ($>$ 10 cm). This dataset, better illustrated in provides an observational benchmark describing how radar signatures evolve across a broad spectrum of hail-producing storms.

Unlike the present study, which investigates the physical evolution of melting hail using a one-dimensional numerical model, Krause's climatology represents an observa-

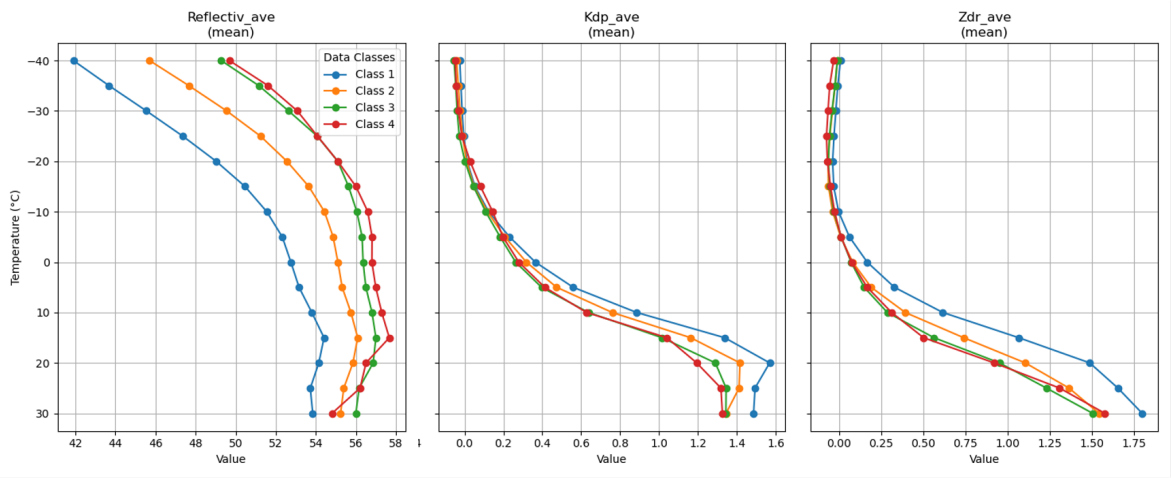


Figure 4.7: Mean vertical profiles of (a) reflectivity (Z_H) specific differential phase (K_{DP}), and (c) differential reflectivity (Z_{DR}) for four hail-size classes derived from the WSR-88D hail climatology provided with permission by Krause et al.

tional synthesis of thousands of naturally occurring hailstorms sampled by the WSR-88D radar network. The two datasets therefore provide complementary perspectives. The climatology documents the radar signatures commonly observed in hail-producing storms, whereas the numerical simulations presented here identify the physical mechanisms responsible for producing those signatures. This comparison is not here to serve as a direct validation dataset, but the climatology provides an operational context within which the modeled results can be interpreted.

While we are not making an attempt to reproduce Krause's climatology directly, we do gain good physical insight into the processes responsible for many of the observed radar characteristics. Krause's climatology shows that storms producing progressively larger hail generally maintain larger values of Z_H throughout the melting layer. The present simulations suggest that this behavior arises because Z_H continues to be dominated by the largest hailstones despite ongoing melting.

Likewise, increasing values of Z_{DR} toward lower levels are consistent with the modeled production of water-coated hailstones and shed liquid drops during melting. The

strongest connection occurs in K_{DP}. Krause's climatology documents enhanced K_{DP} in hail-producing storms, while the simulations presented here demonstrate that K_{DP} responds not only to melting but also to the concentration of hydrometeors within the radar sampling volume. The reduction in simulated K_{DP} produced by vertical velocity field updates indicates that storm dynamics may contribute to part of the variability observed among hail-producing storms.

An equally important outcome of the present study concerns the updated T-28 PSDs. Previous simulations initialized using the historical median relationship frequently underestimated near-surface K_{DP}, producing values smaller than those commonly observed in severe hailstorms. Initialization with the reprocessed T-28 dataset produces substantially larger and more realistic values of K_{DP}, together with improved representations of Z_H and Z_{DR}. This improvement emphasizes the importance of accurately characterizing the hail PSD when modeling polarimetric radar signatures.

Collectively, these results suggest that realistic simulation of polarimetric radar signatures requires more than an accurate scattering calculation. The initialized hail PSD, environmental thermodynamic structure, and evolving storm dynamics all contribute to the observed radar presentation. By combining reprocessed aircraft observations with a physically based downburst model, the present study provides a framework for interpreting the radar signatures documented in observational studies while identifying processes that may not be apparent from radar observations alone.

More broadly, these findings demonstrate that physically realistic simulation of polarimetric radar signatures requires accurate representation of both the hydrometeor population and the surrounding storm environment. Improvements introduced through the reprocessed T-28 PSD dataset provide more realistic initialization of the hail spectrum, while the inclusion of vertical velocity field updates captures the dynamical redistribution of melting hydrometeors throughout the atmospheric column.

Together, these developments produce simulated radar signatures that are more physically consistent with observations of severe hailstorms and establish a framework for future investigations into radar-based hail retrievals, quantitative precipitation estimation, and hydrometeor classification algorithms.

Chapter 5

29 June 2000 Case Study

A cornerstone of both results shown stems from the 29 June 2000 STEPS case in the T-28 dataset. This event provides a unique opportunity to evaluate the model because in situ measurements of the hail PSD were collected by the T-28 aircraft while the storm was simultaneously observed by the NCAR S-Pol polarimetric radar. Few severe hailstorms have been sampled with both detailed aircraft microphysical observations and high-quality polarimetric radar measurements, making this case one of the most comprehensive datasets available for evaluating physically based hail models.

5.1 Case Overview

The 29 June 2000 storm developed over the High Plains during the STEPS field campaign and produced severe hail while remaining within range of the NCAR S-Pol radar. During the mature stage of the storm, the T-28 aircraft sampled hail PSDs within the storm core, providing direct measurements of the hydrometeor population used to initialize the numerical simulations presented throughout this study. The availability of these observations eliminates the need to assume an idealized hail PSD and instead allows the model to be initialized using measurements collected directly from the storm under investigation. While vertical profile data were also sampled from this storm during the field campaign, we were unable to access these observations. Thus, to maintain consistency, environmental conditions were obtained from the ERA5 reanalysis, pro-

viding a thermodynamic profile representative of the storm environment at the time of the aircraft observations.

Because the aircraft and radar sampled the same storm, this case provides a direct connection between the observed hail microphysics and the resulting polarimetric radar signatures. Although the one-dimensional model cannot reproduce the complete three-dimensional evolution of the supercell, it is expected to capture the dominant microphysical processes controlling the evolution of melting hail below the freezing level. The comparison therefore focuses on the vertical structure of Z_H, Z_{DR}, and K_{DP}, rather than attempting to reproduce the full spatial structure of the storm.

Figure 5.1 presents the 1.5° elevation reflectivity scan collected by the S-Pol radar near the time of the aircraft observations. The location of the T-28 flight transect is shown along the core of the storm, illustrating that the aircraft sampled the storm while traversing the high-reflectivity core associated with the hail region. Peak reflectivity values exceeded 60 dBZ, indicating the presence of a mature hail-producing supercell capable of producing large hydrometeors. The aircraft observations obtained within this region therefore provide an appropriate initialization dataset for evaluating the numerical model under conditions representative of severe hail.

There are few datasets that exist in which detailed aircraft microphysical observations and high quality polarimetric radar observations were obtained simultaneously within the same severe hailstorm. The combination of the T-28 aircraft observations and NCAR S-Pol measurements provided us with a unique opportunity to evaluate the performance of the 1D model.

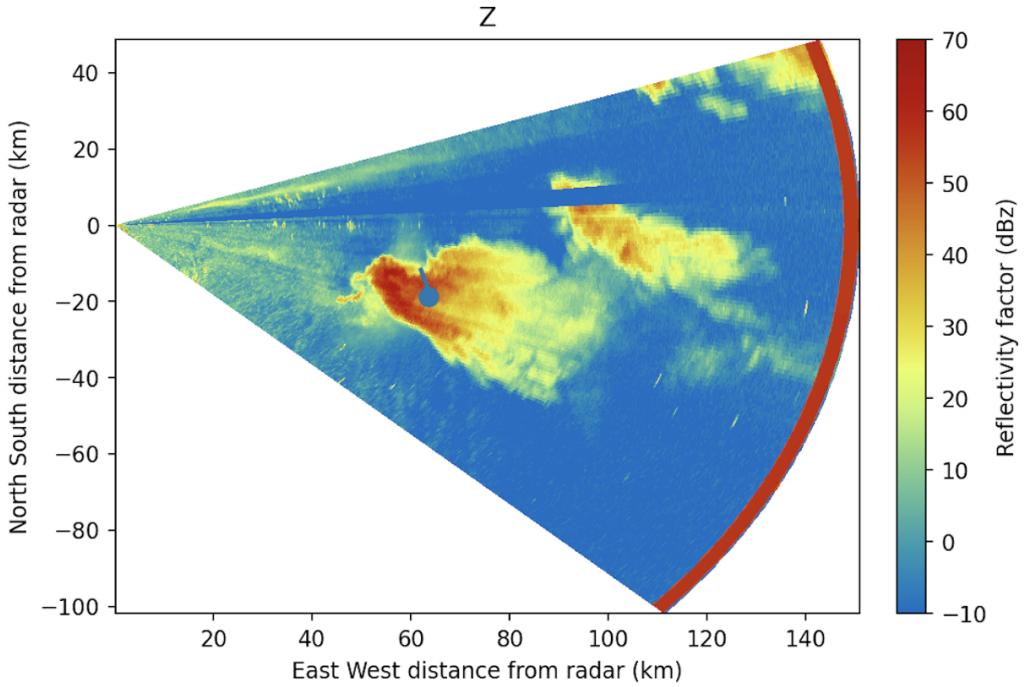


Figure 5.1: S-Pol 1.5° elevation reflectivity PPI collected at 23:37:52Z on 29 June 2000 during the STEPS field campaign. The blue line denotes the T-28 aircraft flight transect through the storm, while the marker indicates the approximate aircraft sampling location used to initialize the numerical simulations for the comparison in this chapter.

5.2 Comparison of Simulated and Observed Radar Profiles

To evaluate the ability of the numerical model to reproduce observed radar signatures, simulated vertical profiles of Z_H, Z_{DR}, and K_{DP} were compared with profiles derived from four consecutive S-Pol volume scans spanning the period of aircraft sampling. Because the T-28 observations occurred during a relatively short interval while the storm remained mature, the observed radar profiles exhibited only modest temporal variability.

Figure 5.2 compares the simulated radar profiles with those derived from the four S-Pol volume scans. Instead of attempting to reproduce every small-scale fluctuation

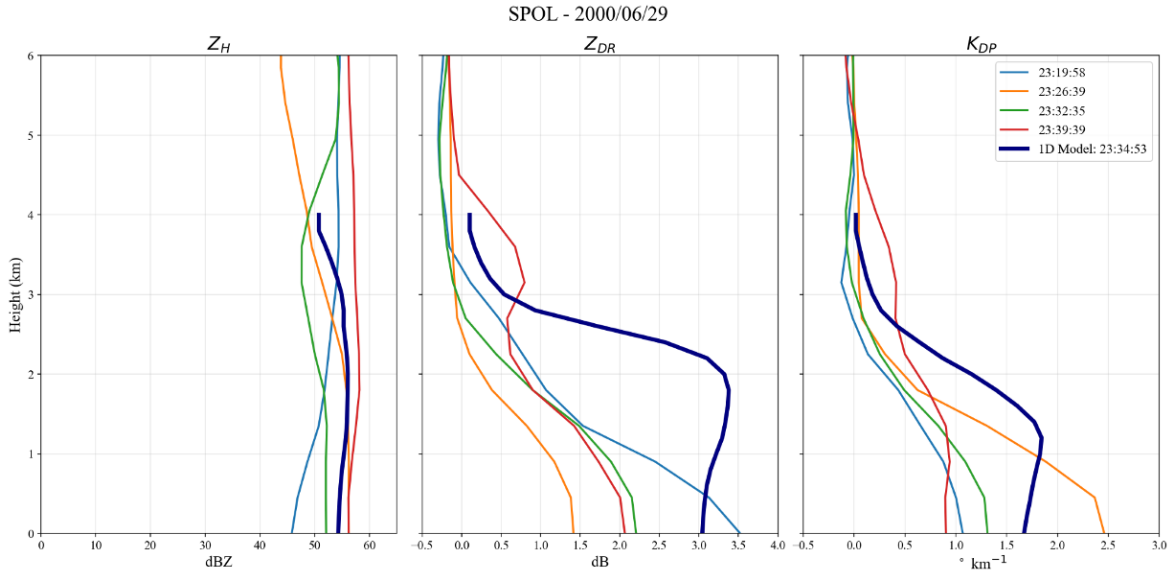


Figure 5.2: Comparison between observed S-Pol vertical profiles and the simulated radar variables from the one-dimensional downburst model for the 29 June 2000 STEPS supercell. Colored curves represent four successive S-Pol volume scans spanning the aircraft sampling period, while the bold navy curve denotes the model simulation initialized using the T-28 PSD measured at 23:34:53 UTC. Profiles are shown for horizontal reflectivity (Z_H), differential reflectivity (Z_{DR}), and specific differential phase (K_{DP}). The comparison emphasizes the overall vertical structure and magnitude of the radar variables rather than exact point-by-point agreement.

present within the radar observations, the comparison focuses on the overall magnitude and vertical evolution of each radar variable. Given the simplified one-dimensional representation of the atmosphere, agreement should be evaluated in terms of the dominant physical trends governing the melting hail layer as opposed to exact point-by-point correspondence.

To facilitate comparison with the one-dimensional model output, vertical profiles of the polarimetric radar variables were derived from a sequence of S-Pol plan position indicator (PPI) scans collected during the 29 June 2000 STEPS supercell. Because S-Pol performs a series of low-to-high elevation scans rather than directly measuring a vertical column, an objective procedure was developed to reconstruct representative vertical profiles from the available observations.

For each radar volume, the aircraft flight transect shown in Figure 5.1 was used as the reference location for sampling. NCAR S-Pol observations were obtained from successive plan position indicator (PPI) volume scans collected during the 29 June 2000 STEPS field campaign. Individual elevation scans separated by less than 120 s were grouped into complete radar volume scans, with the midpoint of each volume used as the representative observation time. Each volume was interpolated onto a three-dimensional Cartesian grid extending from the surface to 18 km AGL. A fixed storm-centered analysis region (40 km $\times$ 40 km) was defined using the location of the primary hail core identified from representative radar volumes. Within this region, the reflectivity core was tracked upward by identifying the maximum reflectivity within 8 km of the previously identified core at each successive height.

Radar variables were then averaged within a 3-km radius of the tracked core to construct representative vertical profiles of Z_H, Z_{DR}, and K_{DP}. Reflectivity was averaged in linear units prior to conversion back to dBZ, whereas the remaining polarimetric variables were averaged directly. Finally, a three-level vertical smoothing filter was applied to reduce small-scale sampling variability while preserving the overall vertical structure of the storm.

This approach was selected because a fixed vertical column or a profile extracted along the aircraft flight path may not adequately represent the evolving hail core within a dynamically changing supercell. By tracking the radar-defined storm core through each volume scan, the analysis follows the principal hail-producing region while minimizing contamination from surrounding precipitation and allowing meaningful comparisons between the modeled and observed vertical evolution of the polarimetric radar variables. Although these profiles do not represent a point-for-point comparison with the T-28 observations, they provide a physically representative characterization of the storm's dominant hail core.

Discussion

Because the aircraft-derived PSDs and the S-Pol radar observations were not perfectly collocated in space and time, I intend to evaluate agreement in profile structure and magnitude rather than provide a point-by-point model verification. The observed and modeled maximum values of Z_H, Z_{DR}, and K_{DP} were compared together with the altitudes at which these maxima occurred.

The simulated Z_H profile reproduced the overall magnitude and vertical structure of the observed S-Pol profiles. Throughout most of the melting layer (approximately 1-4 km AGL), the modeled Z_H remained between 53 and 56 dBZ, which falls within the envelope of the four observed radar profiles. The largest differences occurred above approximately 4 km AGL, where the modeled Z_H was 2-4 dBZ lower than the strongest observed profile, and below approximately 1 km AGL, where the model remained near 54 dBZ while the observations ranged from approximately 46 to 58 dBZ.

The relatively small vertical gradient in both the modeled and observed Z_H profiles is consistent with theoretical expectations for melting hail. Because Z_H is weighted by the sixth moment of the PSD, the largest hailstones continue to dominate the returned power despite ongoing melting. This behavior indicates that the largest hailstones, which dominate Z_H because of the approximate D^6 dependence of backscattered power, experience comparatively little reduction in size throughout much of the melting layer. Although smaller hailstones melt more rapidly and the overall particle concentration evolves continuously, these changes contribute relatively little to the bulk Z_H while the largest hailstones remain largely intact.

With Z_{DR}, the model was able to capture the overall increase toward the surface observed by S-Pol, but exhibited larger values through much of the melting layer. Above approximately 3 km AGL, both the modeled and observed profiles remained

below approximately 0.5 dB, indicating predominantly dry or only weakly melting hail. Between approximately 2 and 3 km AGL, however, the modeled profile increased rapidly to values near 2.5-3.0 dB, whereas the observed profiles generally remained below 1 dB. Below approximately 1.5 km AGL, the modeled Z_{DR} remained near 3 dB, while the observed values ranged from approximately 1.5 to 3.5 dB.

The increase in Z_{DR} below the melting layer is consistent with the expected evolution of melting hail as liquid water accumulates on particle surfaces and increases particle oblateness. The positive bias in the modeled profile between 2 and 3 km AGL suggests that one or more assumptions governing the electromagnetic scattering calculations may not fully represent the physical characteristics of melting hail. In particular, the model assumptions regarding retained meltwater, particle nonsphericity, and the orientation distribution of melting hailstones all influence the simulated polarimetric variables. While the effects of meltwater retention and particle shape are reasonably well understood, the evolution of hailstone orientation during melting remains poorly constrained, introducing additional uncertainty into the simulated radar signatures.Despite this difference in magnitude, both the modeled and observed profiles indicate that melting is the dominant process governing the evolution of particle shape beneath the freezing level.

The modeled K_{DP} reproduced the overall increase toward lower altitudes observed by S-Pol but exhibited a smoother vertical structure than the individual radar profiles. Above approximately 3 km AGL, both the modeled and observed values remained near 0 km^{-1}, indicating relatively little contribution from liquid, non-spherical hydrometeors. Between approximately 1.5 and 3 km AGL, the modeled profile increased steadily to values near 1.0 km^{-1}, remaining within the range of the observed profiles. The largest differences occurred below approximately 1.5 km AGL, where the modeled K_{DP} remained near 1.7–1.9 km^{-1} while the observed values ranged from approximately

1.0 to 2.5 km^{-1}.

The overall agreement in profile structure indicates that the model realistically captures the production of liquid water associated with hail melting. Because K_{DP} is particularly sensitive to the concentration and orientation of anisotropic melting hydrometeors, the smoother modeled profile likely reflects the prescribed particle shape, orientation distribution, and meltwater parameterizations used by the forward operator. In contrast, the observed profiles include additional variability arising from spatial heterogeneity within the storm and from the poorly constrained orientation and tumbling behavior of melting hailstones, both of which can substantially modify the differential propagation phase.

Although the model reproduces the overall evolution of the observed radar variables, several factors limit the degree of agreement that can reasonably be expected between the modeled and observed profiles. The aircraft PSD represents a localized in situ sample, whereas each radar profile represents a much larger sampling volume. Temporal displacement between the aircraft observation and radar volume scan, spatial variability within the hail core, uncertainty in the upper tail of the particle size distribution, and assumptions within the one-dimensional model may all contribute to the remaining differences. Furthermore, due to concerns of instrument icing, later PSDs past 23:40Z are to be considered with caution. Therefore, the timesteps used in this analysis is constrained to this limit. The comparison should therefore be interpreted as an evaluation of whether the modeled profiles reproduce the observed range and vertical evolution of the radar variables, rather than as a deterministic reconstruction of the observed storm.

The simulated Z_H profile reproduces the overall magnitude of the observed S-Pol measurements throughout much of the modeled layer. Z_H remains between approximately 50 and 60 dBZ, consistent with the presence of large melting hailstones within

the storm. Although individual radar profiles exhibit modest variability associated with the evolving storm structure, the simulated values remain well within the range sampled by the observations. The relatively weak vertical gradient in both the modeled and observed profiles indicates that large hailstones continue to dominate the radar backscatter throughout much of the melting layer, despite ongoing melting and mass loss.

The agreement in Z_H is particularly encouraging because the model was initialized using a single aircraft-derived PSD rather than through tuning to match the radar observations. The ability to reproduce observed Z_H using independently measured hail PSDs suggests that the reprocessed T-28 dataset provides physically realistic estimates of the hail size spectrum for use in numerical simulations.

The relatively weak vertical gradient exhibited by both the observed and simulated Z_H profiles suggests that large hailstones remain the dominant contributors to radar backscatter throughout much of the modeled melting layer. Because Z_H is approximately proportional to the sixth power of particle diameter, even a small concentration of large melting hailstones dominates the radar return. Melting then goes on to reduce particle mass without producing a corresponding decrease in Z_H until substantial fragmentation or complete melting occurs. This behavior is consistent with the relatively uniform Z_H observed throughout the lower portion of the hail core by S-Pol.

The ability of the simulation to reproduce this nearly constant Z_H profile using an independently measured aircraft PSD provides confidence that the updated T-28 PSD dataset contains realistic information regarding the upper tail of the hail size spectrum. This result is particularly encouraging because no adjustment of the PSD was performed to improve agreement with the radar observations.

The comparison of Z_{DR} demonstrates that the model captures the principal characteristics of hail melting while also highlighting the limitations associated with the

one-dimensional framework. Both the observed and simulated profiles exhibit increasing Z_{DR} toward lower levels, reflecting the progressive development of water-coated hailstones and the production of shed liquid drops during melting. The model generally produces larger peak values than those observed by S-Pol, particularly between approximately 1.5 and 3 km AGL. This positive bias likely reflects the simplified treatment of particle orientation and the absence of three-dimensional mixing processes that broaden the observed hydrometeor population. Nevertheless, the model successfully reproduces the overall vertical structure expected during the melting of large hail.

The evolution of Z_{DR} reflects changes in particle shape and phase rather than particle size alone. As hailstones descend through the melting layer, liquid water accumulates preferentially around the particle surface while continual shedding of meltwater produces increasingly oblate raindrops. These processes increase the difference between the horizontally and vertically polarized radar returns, producing the gradual increase in Z_{DR} observed toward lower levels.

Although the simulated profile generally exceeds the observed values, the height of the increasing Z_{DR} signal is reproduced reasonably well. This agreement suggests that the modeled onset of melting and subsequent production of liquid water occur within a physically realistic portion of the storm. Remaining differences likely reflect the simplified treatment of particle orientation and the absence of turbulent mixing and horizontal variability that broaden the observed hydrometeor population.

K_{DP} exhibits the greatest variability among the observed radar profiles and also represents the most demanding test of the numerical model. As demonstrated in Section 4.3, K_{DP} responds strongly to changes in particle concentration and residence time within the melting layer. The simulated profile reproduces the observed increase in K_{DP} below approximately 3 km while remaining within the envelope defined by the four radar volume scans. Although differences in peak magnitude remain, particularly

near the lowest model levels, the comparison indicates that the numerical framework captures the dominant physical processes governing the evolution of differential phase in melting hail. Considering the simplified one-dimensional representation of the storm and the inherent spatial variability sampled by the radar, the level of agreement is encouraging.

Among the three radar variables, K_{DP} provides the most stringent evaluation of the numerical model because it responds primarily to the concentration of liquid water and melting hydrometeors rather than simply the presence of large hailstones. As demonstrated in Chapter 4, K_{DP} is particularly sensitive to changes in particle concentration resulting from melting, water shedding, and vertical transport. Consequently, successful reproduction of the observed K_{DP} profile requires that these processes evolve realistically within the model.

The simulated profile reproduces the observed increase in K_{DP} below approximately 3 km while remaining within the envelope defined by the four S-Pol volume scans. The magnitude of the peak differs somewhat from the observations, particularly near the lowest model levels, but the overall structure is captured well. Considering that the simulation was initialized from a single aircraft-observed PSD and does not explicitly resolve storm dynamics, the agreement suggests that the dominant microphysical processes governing differential phase are represented realistically.

This result is particularly significant because Chapter 4 demonstrated that K_{DP} exhibits the greatest sensitivity to uncertainty in $D_{\max}$ and to modifications of the vertical velocity field. Agreement with the observed profile therefore provides independent support for the physical interpretation developed throughout the statistical analyses, namely that changes in meltwater production and hydrometeor concentration exert a substantially greater influence on K_{DP} than on either Z_H or Z_{DR}.

The comparison presented in this chapter demonstrates that physically realistic

polarimetric radar signatures can be reproduced using PSDs measured directly within the storm, without empirical adjustment of either the initial PSD or the radar operator. Although the one-dimensional framework cannot reproduce every aspect of a complex three-dimensional supercell, it successfully captures the dominant vertical evolution of Z_H, Z_{DR}, and K_{DP} associated with melting hail.

More importantly, the agreement between the modeled and observed radar profiles provides an independent evaluation of the physical relationships identified throughout Chapter 4. The sensitivity of Z_H, Z_{DR}, and particularly K_{DP} to variations in hail PSDs and melting processes is not merely a consequence of the numerical model, but is supported by comparison with research-quality polarimetric radar observations collected during one of the most comprehensively observed severe hailstorms available. This validation therefore strengthens confidence in the broader conclusions of this thesis and supports the application of physically based hail melting models for improving the interpretation of polarimetric radar observations and future hail retrieval algorithms.

Chapter 6

Summary and Conclusions

Hail remains one of the most difficult hydrometeor species to characterize using weather radar because its observed polarimetric signatures are governed not only by particle size but also by melting, particle orientation, water shedding, environmental conditions, and vertical air motion. Although numerous radar-based hail detection algorithms have been developed over the past several decades, many rely on empirical relationships between radar products and surface hail reports, providing only indirect information on the physical evolution of hail within the storm (Witt et al., 1998). The primary objective of this thesis was to investigate how observed hail PSDs evolve during melting and how this evolution influences the simulated polarimetric radar variables.

This research combined in situ observations collected by the T-28 research aircraft to initialize a physically based one-dimensional hail melting model. These observed PSDs were represented using exponential fits derived from aircraft measurements collected during severe hailstorms. Model output was then coupled with a polarimetric radar forward operator to simulate reflectivity (Z_H), Z_{DR}, and K_{DP}. A comprehensive suite of simulations was performed to evaluate the influence of maximum hail size estimation, environmental thermodynamic structure, and vertical velocity field updates on the resulting radar signatures. Finally, the simulated radar profiles were evaluated using research-quality S-Pol observations collected during the 29 June 2000 STEPS supercell.

The results demonstrate that observed hail PSDs produce realistic polarimetric radar signatures without empirical adjustment of either the PSD or the radar forward

operator. While differences remain between the one-dimensional simulations and the observed storm owing to the simplified model framework, the primary vertical structures of Z_H, Z_{DR}, and K_{DP} were reproduced successfully. The observed evolution of the polarimetric variables throughout the melting layer was consistent with the increasing liquid-water fraction within melting hailstones, which increases the effective dielectric constant and dominates the evolution of Z_{DR} and K_{DP}. These results support the use of physically based hail melting models as an effective framework for interpreting polarimetric radar observations.

The choice of maximum hail size estimation method influences the simulated radar signatures, although the magnitude of this influence depends upon the radar variable being considered. Ensemble-average profiles showed relatively modest differences among the fitted, maximum observed, and Ulbrich–Atlas $D_{\max}$ methods. However, when the simulations were grouped according to hail-size bins, substantially larger differences became apparent. Z_H increased systematically with increasing hail size owing to the strong sixth-power dependence of radar backscatter on particle diameter. Z_{DR} exhibited more complex behavior, reflecting changes in melting rate and liquid water production rather than hail size alone. K_{DP} showed the greatest sensitivity to hail size, particularly for the largest hail classes, demonstrating that relatively small changes in the upper tail of the PSD can substantially modify the simulated polarimetric radar signatures.

These findings suggest that uncertainty in $D_{\max}$ becomes increasingly important for storms containing large hail, where small differences in the PSD produce disproportionately large changes in radar observables.

Among the environmental variables examined, lapse rate exerted the strongest influence on simulated downdraft magnitude. Cases characterized by steeper environmental lapse rates consistently produced stronger downdrafts, reflecting the enhanced

development of negative buoyancy during hail melting and evaporative cooling. Relative humidity influenced the simulations to a lesser degree, modifying the efficiency of evaporative cooling and melting but not fundamentally altering the relationship between thermodynamic instability and downdraft intensity.

By updating the vertical velocity field throughout the simulation produced measurable changes in the simulated radar variables. Z_H exhibited only modest sensitivity because the dominant radar scatterers remained the largest melting hailstones. Z_{DR} showed moderate reductions associated with changes in melting evolution. The largest response occurred in K_{DP}, where reduced hydrometeor concentration associated with stronger downward particle transport produced systematically lower K_{DP} values.

Although downdrafts reduce linear reflectivity through decreased hydrometeor concentration, this reduction has relatively little impact on operational rainfall estimation because reflectivity-based rainfall relations are generally avoided in hail. Reflectivity is heavily weighted toward the largest hailstones and therefore does not reliably represent rainfall rate in mixed-phase precipitation.

These results demonstrate that vertical air motion modifies radar signatures indirectly through changes in hydrometeor concentration rather than through the scattering calculations themselves. On the other hand, neglecting vertical air motion may introduce systematic biases when interpreting polarimetric radar observations within regions of intense downdraft.This result indicates that environmental thermodynamic structure plays a greater role in determining downdraft magnitude than the initial hail PSD itself. Consequently, environmental information obtained from numerical weather prediction models or observed soundings may provide valuable constraints for interpreting radar signatures associated with melting hail.

Comparison with S-Pol observations collected during the 29 June 2000 STEPS supercell demonstrated that the updated PSDs reproduce the principal vertical structure

of the observed radar variables. Although the simplified one-dimensional framework cannot capture the full complexity of a three-dimensional supercell, the agreement between the simulated and observed profiles supports the physical realism of the modeled melting processes.

Because the simulations were initialized directly from aircraft observations collected independently of the radar data, this comparison allowed us to put a lot of trust into the one-dimensional model. The successful reproduction of the observed radar signatures therefore strengthens confidence in the broader statistical relationships identified throughout this study.

There is a lot to learn surrounding the interpretation of polarimetric radar observations. These simulations demonstrate that identical radar signatures do not necessarily correspond to identical hail PSDs. Melting, water shedding, environmental thermodynamics, and vertical air motion all modify the radar variables simultaneously. Therefore, algorithms based solely upon instantaneous radar observations may not uniquely determine hail size without additional environmental information.

Additionally, the pronounced sensitivity of K_{DP} to both melting processes and vertical air motion suggests that K_{DP} contains valuable information regarding ongoing microphysical evolution within the storm. Rather than serving only as an estimator of rainfall rate, K_{DP} may provide insight into the evolution of melting hail and associated hydrometeor concentrations. Another finding suggests that physically based forward models provide an important bridge between aircraft observations and operational weather radar. By explicitly simulating the evolution of observed PSDs, these models provide a physically interpretable framework for understanding how radar signatures evolve during hail melting.

One of the more significant findings of this work concerns the potential influence of vertical air motion on polarimetric rainfall estimation. Conventional $R(K_{DP})$ relation-

ships implicitly assume that particle concentrations are governed solely by terminal fall speed. However, the simulations presented here demonstrate that downdrafts reduce the residence time of hydrometeors within the radar sampling volume, decreasing particle concentration while maintaining approximately the same downward particle flux.

Because K_{DP} depends strongly upon hydrometeor concentration, this reduction produces systematically smaller values of K_{DP} despite little change in the total hydrometeor mass flux. As illustrated in Chapter 4, neglecting this process may lead to underestimation of rainfall rates derived from conventional $R(K_{DP})$ relationships during storms containing intense downdrafts and melting hail.

6.1 Closing Thoughts

Seeing as the goal for this research was not to propose a new algorithm, the results suggest that future polarimetric quantitative precipitation estimation techniques may benefit from incorporating information describing vertical air motion or environmental thermodynamic conditions. Environmental lapse rate, in particular, exhibited a clear relationship with downdraft magnitude and therefore may provide useful supplementary information for correcting rainfall estimates in severe convective storms.

After sifting through all this data, I can leave you all with some ideas that have been tossed up in the air. A promising direction involves the development of inverse retrieval techniques capable of estimating hail PSDs aloft from observed polarimetric radar signatures. Recent efforts have continued to improve physically based representations of hail melting and associated radar signatures, suggesting that increasingly sophisticated forward models may support future retrieval algorithms capable of estimating hail characteristics aloft from polarimetric radar observations (Vagasky et al., 2025). I

would also infer such observations would also provide the independent datasets needed to develop and evaluate future inverse retrieval techniques capable of estimating hail PSDs aloft from polarimetric radar measurements.

The forward modeling framework utilized here demonstrates that changes in PSD produce systematic responses in Z_H, Z_{DR}, and particularly K_{DP}. Although these relationships are non-unique, combining polarimetric radar observations with environmental information may permit probabilistic estimation of the hail PSD prior to melting. By coupling physically based melting models with fully three-dimensional cloud-resolving models, we would obtain explicit representation of storm dynamics, hydrometeor recycling, and turbulent mixing while retaining the detailed microphysical treatment developed here. Such coupled modeling approaches have been identified as an important direction for advancing polarimetric radar interpretation (Ryzhkov et al., 2020). Such retrievals would represent a substantial advancement beyond current operational hail algorithms, which generally estimate only surface hail size or probability of severe hail.

It is worth pointing out that aircraft observations might not be the most feasible (or safe) way to obtain data. While I will refrain from suggesting field campaigns that warrant crews to barrel through damaging storms with severe turbulence, these kinds of observations remain essential for evaluating hail melting parameterizations and improving physically based radar retrievals. There are other ways though, particularly through emerging observational platforms designed specifically for hail microphysics (Soderholm et al., 2025).

I believe it would also be interesting to investigate the incorporation of environmental information directly into polarimetric radar algorithms. Because lapse rate exhibited a stronger influence on downdraft magnitude than relative humidity, environmental thermodynamic structure may provide a practical means of constraining the

expected evolution of melting hail and improving both hail detection and quantitative precipitation estimation. Perhaps some additional sensitivity testing could connect these pathways.

To close, this work demonstrates that physically based modeling initialized using in situ aircraft observations provides powerful insight for interpreting polarimetric radar observations of hail. Rather than relying solely upon empirical relationships between radar variables and hail occurrence, combining observed PSDs with physically based melting simulations permits the radar signatures to be interpreted in terms of the underlying microphysical processes governing hail evolution. There is much work to do ahead; however, I am confident in the minds of those who will go on to undertake the continuation of this research.

Reference List

Allen, J. T., M. K. Tippett, and A. H. Sobel, 2015: An empirical model relating u.s. monthly hail occurrence to large-scale meteorological environment. *Journal of Advances in Modeling Earth Systems*, **7 (1)**, 226–243, https://doi.org/10.1002/2014MS000397.

Amburn, S. A., and P. L. Wolf, 1997: Vil density as a hail indicator. *Weather and Forecasting*, **12 (3)**, 473–478, https://doi.org/10.1175/1520-0434(1997)012⟨0473:VDAAHI⟩2.0.CO;2.

Bansemer, A., 2022: System for oap data analysis (soda-2). Zenodo, https://doi.org/10.5281/zenodo.10914403.

Bringi, V. N., and V. Chandrasekar, 2001: *Polarimetric Doppler Weather Radar: Principles and Applications*. Cambridge University Press, Cambridge, United Kingdom, https://doi.org/10.1017/CBO9780511541094.

Brook, J. P., A. Protat, J. Soderholm, J. T. Carlin, H. McGowan, and R. A. Warren, 2021: Hailtrack—improving radar-based hailfall estimates by modeling hail trajectories. *Journal of Applied Meteorology and Climatology*, **60 (2)**, 237–254, https://doi.org/10.1175/JAMC-D-20-0087.1.

Browning, K. A., 1962: Cellular structure of convective storms. *Meteorological Magazine*, **91**, 341–350.

Browning, K. A., 1964: Airflow and precipitation trajectories within severe local storms which travel to the right of the winds. *Journal of the Atmospheric Sciences*, **21 (6)**, 634–639, https://doi.org/10.1175/1520-0469(1964)021⟨0634:AAPTWS⟩2.0.CO;2.

Carlin, J. T., and A. V. Ryzhkov, 2019: Estimation of melting-layer cooling rate from dual-polarization radar: Spectral bin model simulations. *Journal of Applied Meteorology and Climatology*, **58 (7)**, 1485–1508, https://doi.org/10.1175/JAMC-D-18-0343.1.

Carlin, J. T., and A. V. Ryzhkov, 2022: A one-dimensional model for melting hail and downdraft evolution. *Proceedings of the 40th Conference on Radar Meteorology*, American Meteorological Society.

Carlin, J. T., and A. V. Ryzhkov, 2025: What can polarimetric radar signatures of developing hail tell us about storm microphysics? *Journal of the Atmospheric Sciences*,

82 (10), https://doi.org/10.1175/JAS-D-25-0014.1.

Carlin, J. T., A. V. Ryzhkov, J. C. Snyder, and A. Khain, 2016: Hydrometeor mixing ratio retrievals for storm-scale radar data assimilation: Utility of current relations and potential benefits of polarimetry. *Monthly Weather Review*, **144 (8)**, 2981–3001, https://doi.org/10.1175/MWR-D-15-0423.1.

Changnon, S. A., 1999: Data and approaches for determining hail risk in the contiguous united states. *Journal of Applied Meteorology*, **38 (12)**, 1730–1739.

Cintineo, R. M., T. M. Smith, V. Lakshmanan, H. E. Brooks, and K. L. Ortega, 2012: An objective high-resolution hail climatology of the contiguous united states. *Weather and Forecasting*, **27 (5)**, 1235–1248, https://doi.org/10.1175/WAF-D-11-00151.1.

Crum, T. D., and R. L. Alberty, 1993: The wsr-88d and the wsr-88d operational support facility. *Bulletin of the American Meteorological Society*, **74 (9)**, 1669–1687.

Dawson, D. T., M. Xue, J. A. Milbrandt, and M. K. Yau, 2010: Comparison of evaporation and cold pool development between single-moment and multimoment bulk microphysics schemes in idealized simulations of tornadic thunderstorms. *Monthly Weather Review*, **138 (4)**, 1152–1171, https://doi.org/10.1175/2009MWR2956.1.

Doviak, R. J., and D. S. Zrnić, 1993: *Doppler Radar and Weather Observations*. 2nd ed., Academic Press, San Diego, California.

Field, P. R., A. J. Heymsfield, A. G. Detwiler, and J. M. Wilkinson, 2019: Normalized hail particle size distributions from the t-28 storm-penetrating aircraft. *Journal of Applied Meteorology and Climatology*, **58 (2)**, 231–245, https://doi.org/10.1175/JAMC-D-18-0118.1.

Fischer, J., and Coauthors, 2025: Hail trajectories in a wide spectrum of supercell-like updrafts. *Journal of the Atmospheric Sciences*, **82 (7)**, https://doi.org/10.1175/JAS-D-24-0222.1.

Foote, G. B., 1984: A study of hail growth utilizing observed storm conditions. *Journal of Climate and Applied Meteorology*, **23**, 84–101.

Greene, D. R., and R. A. Clark, 1972: Vertically integrated liquid water—a new analysis tool. *Monthly Weather Review*, **100 (7)**, 548–552, https://doi.org/10.1175/1520-0493(1972)100⟨0548:VILWNA⟩2.3.CO;2.

Heymsfield, A. J., A. Bansemer, and Coauthors, 2023a: Normalized hail particle size

distributions from in situ aircraft observations. *Journal of the Atmospheric Sciences*, or the final publication information if published.

Heymsfield, A. J., M. A. Cecchini, A. G. Detwiler, R. Honeyager, and P. R. Field, 2023b: Exploring the composited t-28 hailstorm penetration dataset to characterize hail properties within the updraft and downdraft regions. *Journal of Applied Meteorology and Climatology*, **62 (12)**, 1803–1826, https://doi.org/10.1175/JAMC-D-23-0030.1.

Khain, A., M. Ovtchinnikov, M. Pinsky, A. Pokrovsky, and H. Krugliak, 2000: Notes on the state-of-the-art numerical modeling of cloud microphysics. *Atmospheric Research*, **55 (3–4)**, 159–224, https://doi.org/10.1016/S0169-8095(00)00064-8.

Knight, C. A., and N. C. Knight, 1973: Conical hailstones. *Journal of the Atmospheric Sciences*, **30 (4)**, 750–751.

Knollenberg, R. G., 1970: The optical array spectrometer. *Journal of Applied Meteorology*, **9 (1)**, 86–103, https://doi.org/10.1175/1520-0450(1970)009⟨0086:TOAS⟩2.0.CO;2.

Kumjian, M. R., 2013a: Principles and applications of dual-polarization weather radar. part i: Description of the polarimetric radar variables. *Journal of Operational Meteorology*, **1 (19)**, 226–242, https://doi.org/10.15191/nwajom.2013.0119.

Kumjian, M. R., 2013b: Principles and applications of dual-polarization weather radar. part ii: Warm- and cold-season applications. *Journal of Operational Meteorology*, **1 (20)**, 243–264, https://doi.org/10.15191/nwajom.2013.0120.

Kumjian, M. R., A. V. Ryzhkov, V. M. Melnikov, and T. J. Schuur, 2018: Polarimetric radar observations of hail. *Meteorological Monographs*, **58**, 1.1–1.33.

Lawson, R. P., E. J. Jensen, R. H. Cormack, and A. B. Davis, 1993: The high-volume precipitation spectrometer (hvps): Design and performance. *Proceedings of the 27th International Conference on Radar Meteorology.*

Ludlam, F. H., 1958: The hailstorm. *Meteorological Magazine*, **87**, 97–120.

Macklin, W. C., 1963: The density and structure of ice formed by accretion. *Quarterly Journal of the Royal Meteorological Society*, **89**, 30–50.

Marshall, J. S., and W. M. Palmer, 1948: The distribution of raindrops with size. *Journal of Meteorology*, **5 (4)**, 165–166, https://doi.org/10.1175/1520-0469(1948)005⟨0165:TDORWS⟩2.0.CO;2.

Mason, B. J., 1971: *The Physics of Clouds*. 2nd ed., Oxford University Press, Oxford, United Kingdom.

NCAR/EOL, 2026: T-28 aircraft data archive. URL https://www.eol.ucar.edu/field_projects/t-28-aircraft-data-archive, accessed 30 June 2026.

Ortega, K., J. C. Snyder, and S. Waugh, 2025: A high-speed, high-resolution, dual-camera system to image hail and other large hydrometeors. *Bulletin of the American Meteorological Society*, https://doi.org/10.1175/BAMS-D-23-0221.1.

Ortega, K. L., J. M. Krause, and A. V. Ryzhkov, 2016: Polarimetric radar characteristics of melting hail. part iii: Validation of the algorithm for hail size discrimination. *Journal of Applied Meteorology and Climatology*, **55 (4)**, 829–848, https://doi.org/10.1175/JAMC-D-15-0203.1.

Park, H. S., A. V. Ryzhkov, D. S. Zrnić, and K.-E. Kim, 2009: The hydrometeor classification algorithm for the polarimetric wsr-88d: Description and application to an mcs. *Weather and Forecasting*, **24 (3)**, 730–748, https://doi.org/10.1175/2008WAF2222205.1.

Pruppacher, H. R., and J. D. Klett, 1997: *Microphysics of Clouds and Precipitation*. 2nd ed., Kluwer Academic Publishers, Dordrecht.

Rasmussen, R. M., and A. J. Heymsfield, 1987: Melting and shedding of graupel and hail. part i: Model physics. *Journal of the Atmospheric Sciences*, **44 (19)**, 2754–2763, https://doi.org/10.1175/1520-0469(1987)044⟨2754:MASOGA⟩2.0.CO;2.

Ryzhkov, A. V., M. R. Kumjian, S. M. Ganson, and A. P. Khain, 2013a: Polarimetric radar characteristics of melting hail. part i: Theoretical simulations using spectral microphysical modeling. *Journal of Applied Meteorology and Climatology*, **52 (12)**, 2849–2870, https://doi.org/10.1175/JAMC-D-13-073.1.

Ryzhkov, A. V., M. R. Kumjian, S. M. Ganson, and P. Zhang, 2013b: Polarimetric radar characteristics of melting hail. part ii: Practical implications. *Journal of Applied Meteorology and Climatology*, **52 (12)**, 2871–2886, https://doi.org/10.1175/JAMC-D-13-074.1.

Ryzhkov, A. V., M. Pinsky, A. Pokrovsky, and A. Khain, 2011: Polarimetric radar observation operator for a cloud model with spectral microphysics. *Journal of Applied Meteorology and Climatology*, **50 (4)**, 873–894, https://doi.org/10.1175/2010JAMC2363.1.

Ryzhkov, A. V., T. J. Schuur, D. W. Burgess, P. L. Heinselman, S. E. Giangrande,

and D. S. Zrnić, 2005: The joint polarization experiment: Polarimetric rainfall measurements and hydrometeor classification. *Bulletin of the American Meteorological Society*, **86 (6)**, 809–824, https://doi.org/10.1175/BAMS-86-6-809.

Ryzhkov, A. V., J. C. Snyder, J. T. Carlin, A. P. Khain, and M. Pinsky, 2020: What polarimetric weather radars offer to cloud modelers: Forward radar operators and microphysical/thermodynamic retrievals. *Atmosphere*, **11 (4)**, 362, https://doi.org/10.3390/atmos11040362.

Ryzhkov, A. V., and D. S. Zrnić, 1996: Assessment of rainfall measurement that uses specific differential phase. *Journal of Applied Meteorology*, **35 (11)**, 2080–2090, https://doi.org/10.1175/1520-0450(1996)035⟨2080:AORMTU⟩2.0.CO;2.

Ryzhkov, A. V., and D. S. Zrnić, 2019: *Radar Polarimetry for Weather Observations*. 1st ed., Springer Atmospheric Sciences, Springer, Cham, Switzerland, https://doi.org/10.1007/978-3-030-05093-1.

Smith, T. M., V. Lakshmanan, and Coauthors, 2016: Multi-radar multi-sensor (mrms) severe weather and aviation products. *Bulletin of the American Meteorological Society*, **97 (9)**, 1617–1630.

Soderholm, J. S., and Coauthors, 2025: Measuring hail-like trajectories and growth with the hailsonde. *Bulletin of the American Meteorological Society*, **106 (10)**, E2128–E2142, https://doi.org/10.1175/BAMS-D-24-0021.1.

Srivastava, R. C., 1987: A model of intense downdrafts driven by the melting and evaporation of precipitation. *Journal of the Atmospheric Sciences*, **44 (14)**, 1752–1773, https://doi.org/10.1175/1520-0469(1987)044⟨1752:AMOIDD⟩2.0.CO;2.

Testud, J., S. Oury, R. A. Black, P. Amayenc, and X. Dou, 2001: The concept of "normalized" distribution to describe raindrop spectra: A tool for cloud physics and cloud remote sensing. *Journal of Applied Meteorology*, **40 (6)**, 1118–1140, https://doi.org/10.1175/1520-0450(2001)040⟨1118:TCONDT⟩2.0.CO;2.

Ulbrich, C. W., 1983: Natural variations in the analytical form of the raindrop size distribution. *Journal of Climate and Applied Meteorology*, **22 (10)**, 1764–1775, https://doi.org/10.1175/1520-0450(1983)022⟨1764:NVITAF⟩2.0.CO;2.

Vagasky, H. C., and Coauthors, 2025: The sensitivity of falling hail to different melting and terminal velocity parameterizations and environmental conditions. *Monthly Weather Review*, **153 (11)**, https://doi.org/10.1175/MWR-D-24-0180.1.

Waldvogel, A., B. Federer, and P. Grimm, 1979: Criteria for the detection of hail

cells. *Journal of Applied Meteorology*, **18 (12)**, 1521–1525, https://doi.org/10.1175/1520-0450(1979)018⟨1521:CFTDOH⟩2.0.CO;2.

Wegener, A., 1911: *Thermodynamik der Atmosphäre*. J. A. Barth, Leipzig.

Witt, A., M. D. Eilts, G. J. Stumpf, J. T. Johnson, E. D. W. Mitchell, and K. W. Thomas, 1998: An enhanced hail detection algorithm for the wsr-88d. *Weather and Forecasting*, **13 (2)**, 286–303, https://doi.org/10.1175/1520-0434(1998)013⟨0286:AEHDAF⟩2.0.CO;2.

Zrnić, D. S., and A. V. Ryzhkov, 1999: Polarimetry for weather surveillance radars. *Bulletin of the American Meteorological Society*, **80 (3)**, 389–406, https://doi.org/10.1175/1520-0477(1999)080⟨0389:PFWSR⟩2.0.CO;2.